US Army Corps
of Engineers
Construction Engineering
Research Laboratory

CERL Technical Report 99/72
August 1999

# Piezoelectric Patch Sensors for Structural Integrity Monitoring of Composite-Upgraded Masonry and Concrete Structures

J. Berman, R. Quattrone, A. Averbuch, F. Lalande, H. Cudney, V. Raju, and G.L. Cohen

An acoustical impedance-based structural integrity monitoring technique employing piezoelectric (PE) patch sensor/actuators was used to detect real-time damage introduced to composite-upgraded wall test specimens. Concrete and brick masonry wall sections externally upgraded with fiber-reinforced polymer (FRP) composite materials were subjected to various stresses in a load test machine. During the tests, the wall sections were periodically interrogated via the PE sensor/actuators and electrical impedance measurements were made at various frequencies. When damage was present, the impedance vs frequency signature changed. Furthermore, there was a marked difference between the signature pattern for loading and for debonding of the composite upgrade or cracking of the concrete/masonry substrate.

This report includes details on the development of the impedance-based technique and documents a demonstration of the technology on a composite-upgraded pier at Norfolk, VA.

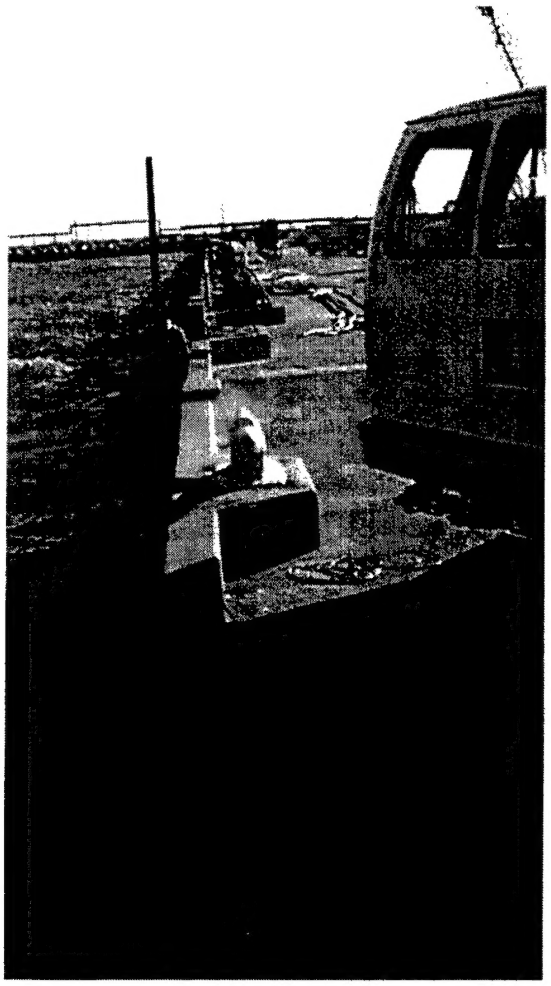

US Army Corps
of Engineers
Construction Engineering
Research Laboratory

CERL Technical Report 99/72
August 1999

# Piezoelectric Patch Sensors for Structural Integrity Monitoring of Composite-Upgraded Masonry and Concrete Structures

J. Berman, R. Quattrone, A. Averbuch, F. Lalande, H. Cudney, V. Raju, and G.L. Cohen

An acoustical impedance-based structural integrity monitoring technique employing piezoelectric (PE) patch sensor/actuators was used to detect real-time damage introduced to composite-upgraded wall test specimens. Concrete and brick masonry wall sections externally upgraded with fiber-reinforced polymer (FRP) composite materials were subjected to various stresses in a load test machine. During the tests, the wall sections were periodically interrogated via the PE sensor/actuators and electrical impedance measurements were made at various frequencies. When damage was present, the impedance vs frequency signature changed. Furthermore, there was a marked difference between the signature pattern for loading and for debonding of the composite upgrade or cracking of the concrete/masonry substrate.

This report includes details on the development of the impedance-based technique and documents a demonstration of the technology on a composite-upgraded pier at Norfolk, VA.

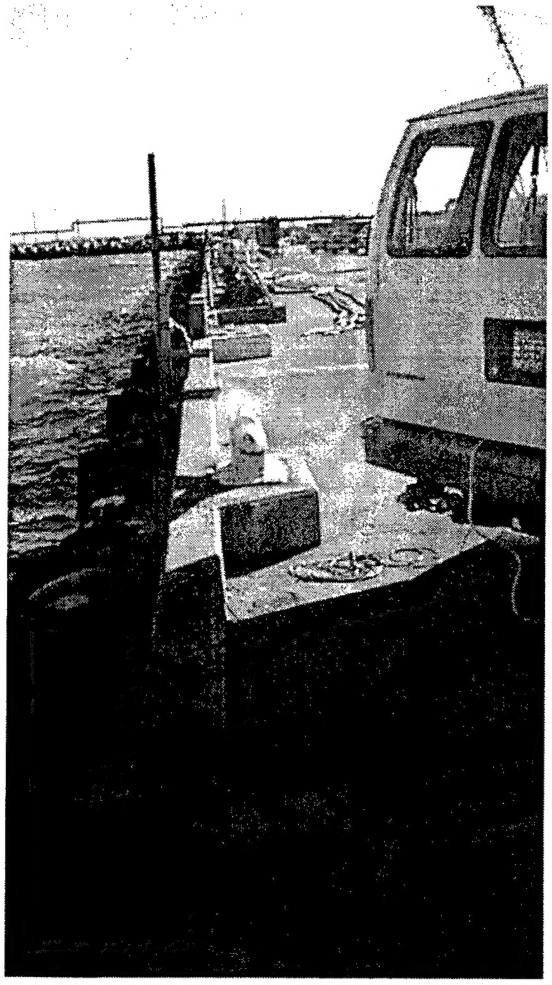

# Foreword

This research was conducted for the Directorate of Military Programs, Headquarters, U.S. Army Corps of Engineers, under Project 4A162784AT41, "Military Facilities Engineering Technology"; Work Unit FM-CM9, "Tagged Construction Elements." The technical monitor was Charles Gutberlet, Jr., CEMP-ED.

The work was performed by the Materials and Structures Branch (CF-M) of the Facilities Technology Division (CF), U.S. Army Construction Engineering Research Laboratory (CERL). The CERL Principal Investigator was Justin B. Berman. Dr. Ilker R. Adiguzel is Chief, CEERD-CF-M, and L. Michael Golish is Chief, CEERD-CF. The Technical Director of the Facility Acquisition and Revitalization Business Area is Dr. Alan W. Moore.

A portion of this work was performed under contract by Dr. H. Cudney and Dr. F. Lalande, Virginia Polytechnic Institute and State University, Center for Intelligent Systems and Structures (VPI & SU, CIMSS). V. Raju is affiliated with VPI & SU. Matching funds and manufacturing of all composite samples were provided by the Composites Institute, a Division of the Society of the Plastics Industry, Inc. The following Composites Institute Market Development Alliance companies assisted in this research: Owens-Corning, Granville, OH; Reichhold Chemicals, Inc., Research Triangle Park, NC; Clark Schwebel Tech-Fab Co., Anderson, SC; and Tonen Corp., Tokyo, Japan. Fyfe Co., LLC, San Diego, CA, also assisted in manufacturing composite walls.

The Director of CERL is Dr. Michael J. O'Connor.

# Contents

# List of Figures and Tables

## Figures

## Tables

# 1 Introduction

## Background

The U.S. Army maintains an aging inventory of 130,000 buildings and civil engineering structures that has a high-priority unfinanced backlog of maintenance and repair (BMAR) amounting to $4.6 billion. Seventy percent of these structures exceed 30 years in age, and 50 percent are more than 50 years old (U.S. Army Red Book*, FY 1996). Most of these aging military and civil structures fail to meet modern engineering codes and environmental standards. Structural elements in buildings and concealed or buried structures often degrade without being detected. For example, steel reinforcement in concrete structures can severely corrode before spalling becomes evident. Catastrophic failure may become imminent in masonry structures due to the effects of structural overload, which may be caused by changes in a building's function, or by seismic activity, high winds, and other environmental stressors. Just as the causes of excessive structural stress may not be immediately obvious, the locations of damage caused by those stresses also may be difficult to detect or predict.

As the Operations and Maintenance, Army (OMA) budget continues to shrink, there is a growing need to

- rehabilitate mission-critical facilities before structural degradation leads to catastrophic failures
- adapt, upgrade, and reuse buildings for new missions
- generally extend usable facility life while reducing life-cycle costs.

It is clear to many in the Army engineering community that old facilities with undetected structural deficiencies and environmental vulnerabilities cannot be relied upon to meet the evolving requirements of the Army mission:

* The formal title of the "Red Book" is *Directorates of Public Works Annual Summary of Operations* (Headquarters, Department of the Army [HQDA], published annually).

> "Aging infrastructure requires a focus on maintenance and rehabilitation." (Inland Navigation 1996)

> To meet the goals of reducing life-cycle costs and extending usable facility life, the Army must "be able to more quickly explore, evaluate and apply emerging and innovative technologies." (Coastal Navigation 1996)

Various emerging technologies offer new opportunities for improving Army facility performance. In the area of advanced materials, demonstration projects conducted by the Construction Engineering Research Laboratory (CERL), the Composites Institute, and other partners have shown that fiber-reinforced polymer (FRP) composite materials can successfully be substituted for internal steel rebar in reinforced concrete (GangaRao et al. 1995) and used as sheet pile (Lampo et al. 1997, 1998). FRP composite materials also have successfully been demonstrated in external upgrade applications to strengthen unreinforced masonry walls (Marshall, Sweeney, and Trovillion 1998).

Another promising technology is remote sensors, where applications such as roofing leak detection are being demonstrated. Such sensors are intended to detect facility damage at its earliest stages and create a record of it for easy access by maintenance personnel. Recent breakthroughs in the active tagging of composite materials (Quattrone, Berman, and White 1998) open innovative new possibilities for developing "smart" high-performance materials systems. For example, small, durable sensors might be developed to detect and identify structural damage at an early stage. Such sensors might even be integrated into composite materials to create self-monitoring high-performance structural members. Smart systems of this type could help to ensure that scarce OMA dollars are prioritized toward structures whose potential critical deficiencies are detected and verified early. "Self-inspecting" structures would enable engineers to solve impending structural problems before excessive degradation has occurred. Just as importantly, this type of smart system also could provide a nondestructive, labor-efficient means for documenting long-term structural performance.

The ultimate goal of structural integrity monitoring systems would be to provide early warnings of serious impending damage rather than reporting advanced degradation or failure after the fact. This type of technology would seem to offer a potentially huge return on investment, but several obstacles must be overcome before widespread implementation by the Army is likely.

First there is the question of composites performance and durability data. Even though these materials have been used in engineering for almost half a century,

long-term composite performance and durability data for structural applications are not yet available. Therefore, the civil engineering community has been reluctant to use composite materials in structural rehabilitation and modernization projects. To gain civil engineering (and Army) acceptance, short-term and long-term performance testing of existing composites must be completed in a variety of structural environments. Such testing must provide an understanding of (1) composite failure mechanisms and (2) inspection techniques needed for assessing fielded composite structural elements.

Another obstacle to acceptance arises from the vast inventory of composite fibers and matrices currently available. This 'overabundance of choice' creates much complexity in the selection of a composite materials system for a specific project. To address this complexity, a systematic approach is needed for purchasing, implementation, and evaluation of composite structural elements. Standardized inspection techniques, self-diagnosing structural composites, and advanced structural integrity monitors could provide the Army with a consistent and expedient means of safely implementing advanced composite structural materials.

In theory, "self-inspecting" structural elements could provide an elegant tool that would allow engineers to closely monitor composite structural integrity, but such an application presents its own unique challenges. The most significant of these is the inherent inapplicability of conventional modal analysis techniques to such a technology. Modal analysis techniques are by their nature not well suited for identifying incipient structural damage. One reason for this is that modal analysis techniques typically rely on low-order global modes to detect damage; using these techniques, material damage must be global in scale before a change in lower-order global modes and properties can be experimentally measured. Another serious limitation of modal analysis methods for self-diagnostic structural applications is the extreme sensitivity of the frequencies and modes to boundary conditions. In many structures (e.g., piers), changes in the mass and loading are a part of normal operation. Simulation of all possible normal usage changes and their effect on the modal parameters would be impossible to store so as to distinguish them from damage. Even under tightly controlled conditions using the same configuration in which the original data were acquired, it would be extremely difficult to reproduce modal testing results.

As an alternative, an impedance-based monitoring technique may be highly effective for detecting and qualitatively identifying incipient structural damage. The fundamental difference between modal techniques and impedance-based techniques lies in the frequency used to 'interrogate' the structure (i.e., to excite the structure and sense the magnitude and phase of resulting vibrations). The frequencies used in an impedance-based technique are much higher than those

typically used in modal analysis. To detect damage that does not yet produce any measurable change in a structure's global stiffness properties, it is necessary for the wavelength of excitation to be shorter than the characteristic length of the damage to be detected. Identifying damage before global structural integrity is compromised would be most useful as it would provide the desired early warning and allow sufficient time for repairs or upgrades.

## Objective

The objective of this work was to investigate and optimize the use of a new impedance-based sensor as a nondestructive evaluation technique for inspecting Army infrastructure for internal or external structural integrity problems.

## Approach

The material selected for this experiment was a lead zirconate titanate (PZT) ceramic that exhibits both direct and converse (i.e., bidirectional) piezoelectric effects. Piezoelectric (PE) actuator/sensor patches* measuring 1.25 x 1.25 x 0.01 in. were fabricated from this material, and electrodes for applying an electric field to each patch were formed by nickel plating both sides and soldering copper tabs to them. When bonded to a substrate, the patches provide an interface through which to acoustically excite a structure, typically in the high kilohertz (kHz) range, and simultaneously measure the structure's response. Several experiments were conducted, followed by an in situ demonstration of the sensor technology on a Navy pier that had previously been structurally upgraded with FRP composites. These experiments, documented in detail in the body of this report, comprised the following:

1. A protocol was developed to allow sequential monitoring of multiple PE sensors by a single computer-controlled impedance analyzer.
2. PE sensors were attached to test specimens, including a quarter-scale model bridge joint, and the area and magnitude of sensitivity were tested.
3. Damage metrics were conceived, applied to the collected data, and validated, and a damage index was developed.

* A single PE patch is used both to excite a structure and sense its response. Strictly speaking, these units are in fact *actuator/sensors*, but for purposes of brevity here they are in most cases referred to as "PE sensors."

4. A test was designed and conducted to determine whether the impedance-based monitoring technique could detect when and where a composite material has debonded from a masonry substrate.
5. Laboratory experiments were conducted to determine the best technique for bonding PE sensors to composite materials.
6. Tests were conducted to determine the size of the sensing area for composite materials, and to investigate the monitoring technique's specific sensitivity to composite debonding and delamination damage.
7. The technique was tested for its ability to detect incipient damage in small composite-reinforced masonry wall sections that were incrementally loaded to failure in a million-pound compression load frame.

As noted above, upon completion and analysis of the laboratory experiments, a demonstration of this structural monitoring technique was implemented at Norfolk (VA) Pier 11 on a section that had recently been structurally upgraded with FRP composite reinforcement fabric by the Naval Facilities Engineering Service Center (NFESC).

## Mode of Technology Transfer

The results of this work may have an impact on related Corps of Engineers Guide Specifications (CEGS) and other technical guidance. Findings could be incorporated into Technical Instruction (TI) 809-05 for composite upgrade inspection of unreinforced masonry walls. Also, the results of this work support the idea of testing the effectiveness of this technique to monitor weld cracking in steel structures.

## Nomenclature

| | |
|---|---|
| $d_{ij}$ | piezoelectric coupling tensor |
| $D_i$ | electric displacement tensor |
| $DM_1$ | average squares difference damage metric |
| $DM_2$ | statistical correlation damage metric |
| $E_j$ | electric field strength |
| i | complex number |
| n | number of data points in data set |
| $Q_{33}^{E}$ | complex Young's modulus of PE sensor at zero electric field |
| $S_i$ | strain tensor |

| | |
|---|---|
| $s_{ij}^{E}$ | elastic compliance tensor at zero electric field |
| $x_i$ | $i^{th}$ member of baseline impedance data set |
| $y_i$ | $i^{th}$ member of baseline questioned data set |
| Y | electrical admittance |
| $Z_{PE\ sensor}$ | mechanical impedance of the PE sensor sensor |
| $Z_s$ | mechanical impedance of the structure |
| $\alpha$ | PE sensor geometric constant |
| $\delta$ | PE sensor dielectric loss tangent |
| $\Delta\mu$ | difference between averages in two data sets |
| $\varepsilon_{ij}^{\sigma}$ | electrical permitivity tensor at zero stress |
| $\sigma_i$ | stress tensor |
| $\sigma_i$ | standard deviation of data set "i" |
| $\omega$ | frequency |
| $\mu_i$ | average of data set "i" |

## Units of Weight and Measure

U.S. standard units of measure are used throughout this report. A table of conversion factors for Standard International (SI) units is provided below.

| SI conversion factors | | |
|---|---|---|
| 1 in. | = | 25.4 cm |
| 1 ft | = | 0.305 m |
| 1 sq in. | = | 6.452 $cm^2$ |
| 1 sq ft | = | 0.093 $m^2$ |
| 1 cu in. | = | 16.39 $cm^3$ |
| 1 lb | = | 0.453 kg |
| 1 ton | = | 906 kg |
| 1 psi | = | 6.89 kPa |

# 2 Theoretical and Technical Overview of Impedance-Based Piezoelectric Sensing

## Constitutive Theory

The basis of the proposed technology is the property of *piezoelectricity*. A material is said to be piezoelectric when its mechanical impedance is coupled to its electrical impedance. In a piezoelectric material, a change in mechanical impedance causes a corresponding change in electrical impedance. Therefore, if physical damage causes a change in a material's mechanical impedance, the corresponding change in electrical impedance may be used to measure or characterize that physical damage. In other words, the electromechanical coupling property of PE materials theoretically makes it possible to detect physical damage by measuring changes in a material's electrical impedance.

Piezoelectricity comprises a direct effect and a converse effect. The *direct effect* is described by the generation of an electrical field in a material that is subjected to a mechanical stress. The *converse* effect is described by the generation of a mechanical strain when an electrical field is applied to that same material. For a linear piezoelectric material, Equations 1 and 2 (Crawley and Anderson 1990) can describe the direct and converse effects, respectively:

$$S_i = s_{ij}^E \sigma_j + d_{ij} E_j \qquad \text{[Eq 1]}$$

and

$$D_i = d_{ji} \sigma_j + \varepsilon_{ij}^\sigma E_j \qquad \text{[Eq 2]}$$

An impedance-based structural integrity monitoring system would use the PE sensor concurrently as both an actuator and a sensor. A PE sensor bonded onto a structure and driven by an alternating electrical field will excite the structure and induce vibrations (converse effect). The resulting vibrational response,

which is characteristic of the specific structure being evaluated, modulates the current flowing through the PE sensor (direct effect). This modulation is a function of the degree of mechanical interaction between the PE sensor and the structure over the frequency range of the applied current. In electrical terms, variation in the current modulates the electrical impedance.

Electrical impedance is defined as the ratio of the energized voltage to the resulting current. Mechanical impedance is defined as the ratio of an applied force to the resulting velocity of the body to which the force is applied. Electromechanical transducer materials such as piezoelectrics provide a means of coupling mechanical and electrical impedance. The piezoelectric property makes it possible to extract mechanical impedance information from a structure by measuring changes in its electrical impedance. Electrical impedance readings may be made with various commercially available impedance analyzers. With such analyzers, high-resolution amplitude and phase measurements can be made from 5 Hz to 13 MHz frequency range (Hewlett Packard 1983). The typical impedance analyzer can be operated manually or in various computer-controlled modes.

## The Proposed Application

The technique documented in this report uses small sensors made from a lead zirconate titanate (PZT) ceramic that exhibits a bidirectional PE effect. Electrodes for applying an electric field to the ceramic were formed by nickel-plating both sides and soldering copper tabs to them (Figure 1). These commercially available PE sensors (Piezo Systems, Inc., Cambridge, MA; Morgan Matroc, Inc., Bedford, OH) were used to mechanically excite the structure being monitored, typically in the high kilohertz (kHz) frequency range. At such high frequencies, structural response is dominated by local modes of oscillation. Incipient damage such as small cracks and delaminations produces measurable change in the material's mechanical impedance characteristics.

The use of high frequencies in this technique limits the size of the actuation/sensing area. The effects of excitation frequency, geometry, material properties, structural joints, etc., on the size of the actuation/sensing area is currently being researched. However, early observations indicate that for the PE patch systems used in these studies, the sensing area extends at a minimum of a 12 in. radius around the sensor. The limited size of the sensing area offers a practical way to isolate the effects of local damage from far-field changes in mass-loading, stiffness, and boundary conditions. Therefore, a structural monitoring technique based on bidirectional PE actuator/sensors could be highly useful in identifying

and tracking damage in specific areas where high structural integrity must be assured at all times (e.g., joints, load-bearing members, etc.).

The proposed impedance-based technique offers several advantages over modal analysis techniques:

1. It requires no special measurement equipment, relying instead on off-the-shelf high-frequency electrical impedance instrumentation.
2. The small size of the PE sensor (typically less than 1.5 in. square and 0.01 in. thick) allows for nondestructive installation on structural elements.
3. As noted above, this technique allows for the simultaneous actuation and sensing of structural response.
4. Electrical high-frequency excitation can be achieved at low input power.

**PIEZOELECTRIC PATCH ACTUATOR/SENSOR SPECIFICATIONS**

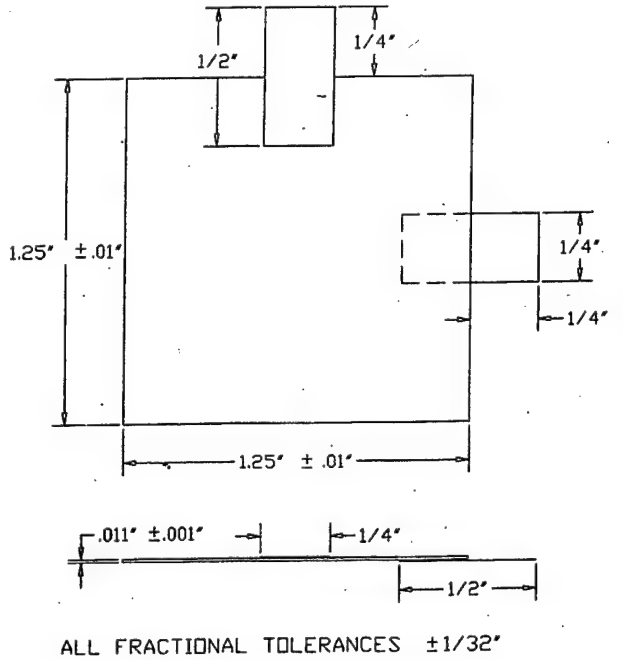


| | |
|---|---|
| **PATCHES** | |
| *Dimensions:* | 1.25 in. ± 0.01 in. length<br>1.25 in. ± 0.01 in. width<br>0.010 in. min. thickness<br>0.012 in. max. thickness |
| *Material:* | PZT-5A |
| *Curie Temperature* | 645 °F ± 20 °F |
| *Poled Direction:* | Through the thickness<br>(Positive side marked) |
| *Coating:* | Nickel |
| *Coating Thickness:* | 0.000050 in. min. thickness<br>0.000200 in. max. thickness |
| *Parallelism:* | 0.002 in. |
| | |
| **EDGE TABS** | (overlap ¼ in.) |
| *Dimensions:* | ½ in. ± 1/32 in. (length) |
| | ¼ in. ± 1/32 in. (width) |
| | 0.002 in. ± 0.001 in. (thickness) |
| *Material:* | Copper |
| *Solder Melting Point:* | 350 °F min.<br>400 °F max. |
| *Total Thickness of Patch with Edge Tab:* | 0.011 in. min. thickness<br>0.015 in. max. thickness |

(See attachment #1 for piezoelectric patch end-tab placement criteria.)

(Manufacturer must ensure that the piezoelectric properties of the patch are not damaged by heat from application of solder.)

**Figure 1. Diagram and specifications for PE patch actuator/sensor.**

5. The variation in electrical impedance of a PE sensor bonded to a structure is analogous to frequency response in modal analysis, but it has much higher resolution and is more easily obtained.
6. The use of high frequencies ensures that even minor (or incipient) damage produces a clear change in the structure's impedance/vibration characteristics.
7. The use of high frequencies results in a localization of the actuation/sensing area.

It is this last unique advantage — localization of the actuation/sensing area — that makes this technique practical for implementation in full-scale infrastructure. Because this technology is sensitive to structural damage (i.e., impedance changes) only in an area close to the sensor/actuator, it is possible to know with certainty that a change in impedance is due to damage. Therefore, localization by its nature rules out changes in far-field boundary conditions, mass loading, or other 'false positive' readings that may be attributable to normal use of the structure.

### *PE Sensor Electromechanical Principles*

The interaction between a PE sensor and a one-degree-of-freedom system can be qualitatively described by considering the PE sensor as a thin film bar undergoing axial vibration in response to a uniform applied alternating voltage (Figure 2). One end of the bar is fixed and the other end is connected to the external structure (Liang, Sun, and Rogers, April 1993).

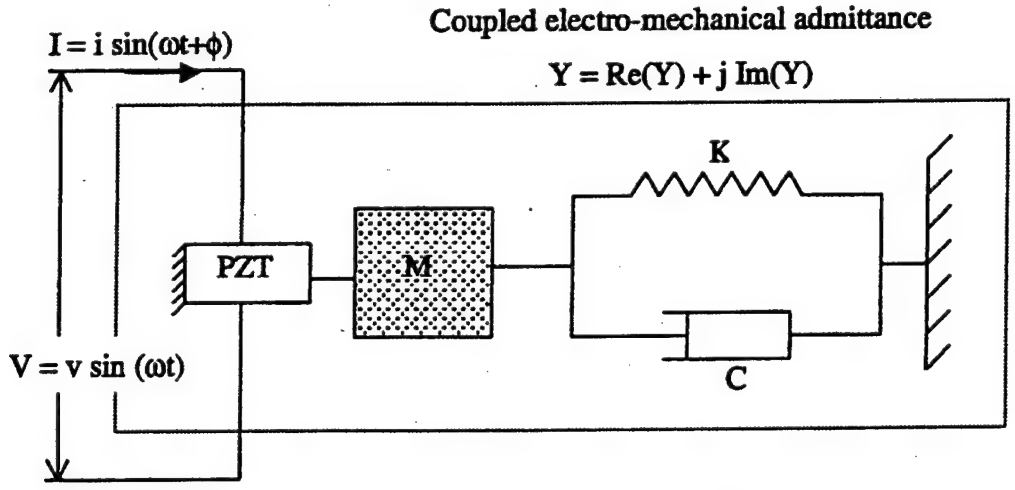


**Figure 2. Model representing a PE-driven dynamic structural system.**

The above assumption about interaction of the PE sensor at two discrete points is consistent with the mechanism by which forces are transferred from the bonded PE sensor actuator to the substrate structure (Crawley and Anderson

1990). Solving the wave equation for the PE sensor bar connected to an external mechanical point on the structure leads to the following equation for frequency-dependent electrical admittance (Sun et al., June 1994):

$$Y = i\omega\alpha\left[\varepsilon_{33}^{T}(1-i\delta) - \frac{Z_s(\omega)}{Z_s(\omega)+Z_{PZT}(\omega)}\cdot d_{33}^{2}Q_{33}^{E}\right] \qquad \text{[Eq 3]}$$

The first term in Eq 3 — the capacitive admittance of the free PE sensor — provides the baseline admittance of the system. The second term includes the mechanical impedance of both the PE sensor and the external structure. When a PE sensor is bonded onto a structure, its own impedance, $Z_{PE\ sensor}$ is fixed. Hence, it is $Z_s$, the external structure's impedance, that uniquely determines the contribution of the second term to the overall admittance. Because these peaks correspond to specific structural resonances, they constitute a unique signature of the dynamic behavior of the structure. Therefore, any later changes in the impedance signature are attributed to damage or a change in the structure.

In electrical terms, the impedance analyzer generates a sinusoidal voltage signal that is specified by the user (i.e., the frequency and peak root mean square [RMS] voltage). At a given frequency, the impedance analyzer measures the PE sensor steady state current magnitude and phase. These are translated into the equivalent real and imaginary impedance components. A frequency range can be specified so that admittance (or impedance) versus frequency curves can be established. The PE sensor sees the structure as a frequency-dependent boundary stiffness. Therefore, one can detect and measure any variation in electrical impedance over the entire frequency range that is due to both (1) the electrically capacitive nature of the PE sensor and (2) the interaction between the PE sensor and the host structure.

In terms of this capacitive contribution of the PE sensor, it is found that certain piezoelectric ceramic geometries are more favorable than others. For example, increasing the thickness of the PE sensor (bonded to the host structure) decreases the capacitive contribution of the PE sensor, and therefore decreases the height of the peaks in the impedance signature. On the other hand, an increase in the contact area of the PE sensor causes an increase in the sensor's capacitive contribution. This results in an increase in the height of the peaks in the impedance signature, which in turn implies greater dynamic interaction between the host structure and the PE sensor. Laboratory tests indicate that PE sensor plates as small as 0.50 in. square and 0.01 in. thick are sufficient for structural integrity assessment.

### *Damage Metrics*

While the impedance-versus-frequency-response plots provide qualitative information on structural integrity, damage metrics charts can provide a qualitative evaluation of the data. To compute a damage metric, data are first accumulated as a series of impedance-frequency pairs. The impedance analyzer does this automatically under computer control. An initial baseline data set $x_i$ is taken, which consists of impedance values over a fixed frequency range. Each subsequent data set $y_i$ is compared to this baseline set, and a numerical value referred to as the damage metric $DM_i$ is returned. The damage metric provides quantitative information that is useful in summarizing and comparing data sets. The damage metric also can be used to establish threshold criteria for a green/yellow/red light status system that indicates when a structure should be inspected, repaired, or removed from service.

#### Average Squares Difference Metric

One damage metric that can be used with this technology is the Average Squares Difference (ASD) method. The mathematical formulation for this metric simply comprises the average of the squared differences between the initial data set and each subsequent set. The ASD method is represented by the following:

$$DM_1 = \sum_{i=1}^{n} \left[ x_i - \left( y_i - \Delta\mu \right) \right]^2 \qquad \text{[Eq 4a]}$$

where

$$\Delta\mu = \mu_x - \mu_y \qquad \text{[Eq 4b]}$$

The ASD metric filters out vertical shifts in the curve. In other words, the ASD metric returns a zero when the two curves to be compared are (a) identical or (b) separated by a uniform vertical shift. However, if the vertical shift is not uniform (e.g., there are different vertical spacings at different frequencies), the ASD metric returns a non-zero value, indicating a difference between signatures. Using the ASD formulation, the greater the damage metric, the greater the difference between the baseline reading and the subsequent reading. There is no upper bounding on the value of the metric. When the ASD metric is interpreted with reference to the impedance-based monitoring technique, the larger the metric, the greater the damage or change in the integrity of the structure.

### Statistical Correlation Metric

Another damage metric that can be used is the Correlation Metric, which is based on the statistical correlation function. The mathematical formulation used in this damage metric is 1 minus the correlation function between the baseline and subsequent readings. If the baseline reading and the subsequent reading are identical, then the 1 minus correlation reading returns a metric of zero. The value range for the Correlation Metric is [0,2.0]. The correlation function returns the statistical correlation coefficient between the two data sets. The mathematical formulation is as follows:

$$DM_2 = 1 - \frac{Cov(X,Y)}{\sigma_x \cdot \sigma_y} \qquad \text{[Eq 5a]}$$

where

$$Cov(X,Y) = \frac{1}{n}\sum_{i=1}^{n}(x_i - \mu_x)(y_i - \mu_y) \qquad \text{[Eq 5b]}$$

In the current work, the metric calculated is one minus the correlation function, thereby ensuring that increasing damage or change in structural integrity produces a positive increase in the metric. The correlation metric also accounts for vertical shifts between data sets. Because the algorithm represented by Equations 5a and 5b provides a more accurate indicator of structural damage than the ASD metric, the Correlation Metric is used in most of the analysis that follows.

# 3 Development of the Procedure for Impedance-Based Testing

## Introduction

In this phase of the research, PE sensors were attached to various test specimens to identify the size of the area that can be monitored by a PE sensor and to determine its general degree of sensitivity. Also, the damage metrics (described in Chapter 2) were applied to the data collected, and were analyzed for validity.

The impedance-based technique was initially tested on a quarter-scale model of a bridge joint (Figure 3) to determine whether full-scale civil engineering structures might be successfully inspected using the impedance-based technique (Sun et al. June 1994).

## Bridge Joint Tests

Figure 3 shows the effects of minor structural defects in the model bridge joint, as detected by the PE sensors. Figure 4 shows the admittance measurements made as the result of loosening a single bolt near a PE sensor, and Figure 5 shows the measurements made as the result of loosening a more distant bolt of the same type. The change in the baseline electrical admittance measurements resulting from the nearby defect is significant, but the baseline measurement is unaffected by the distant defect. These results clearly show that (1) the high frequency used to excite the bridge joint model is very sensitive to minor change and (2) the actuation/sensing area of the PE sensor is limited to a small area. It can be seen that the localization of the sensing area provides a practical means of using impedance measurements to monitor specific critical elements of a structure. This finding suggests that it would be feasible to use impedance-based monitoring on large civil engineering structures.

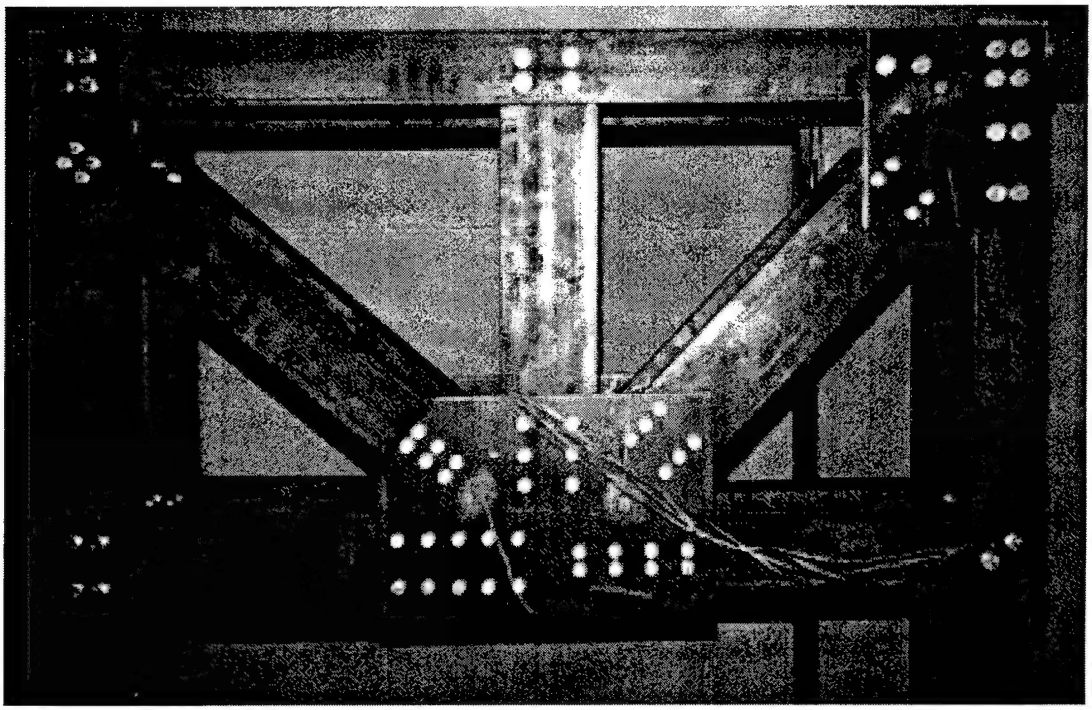

**Figure 3. Quarter-scale model of a bridge joint used in preliminary testing.**

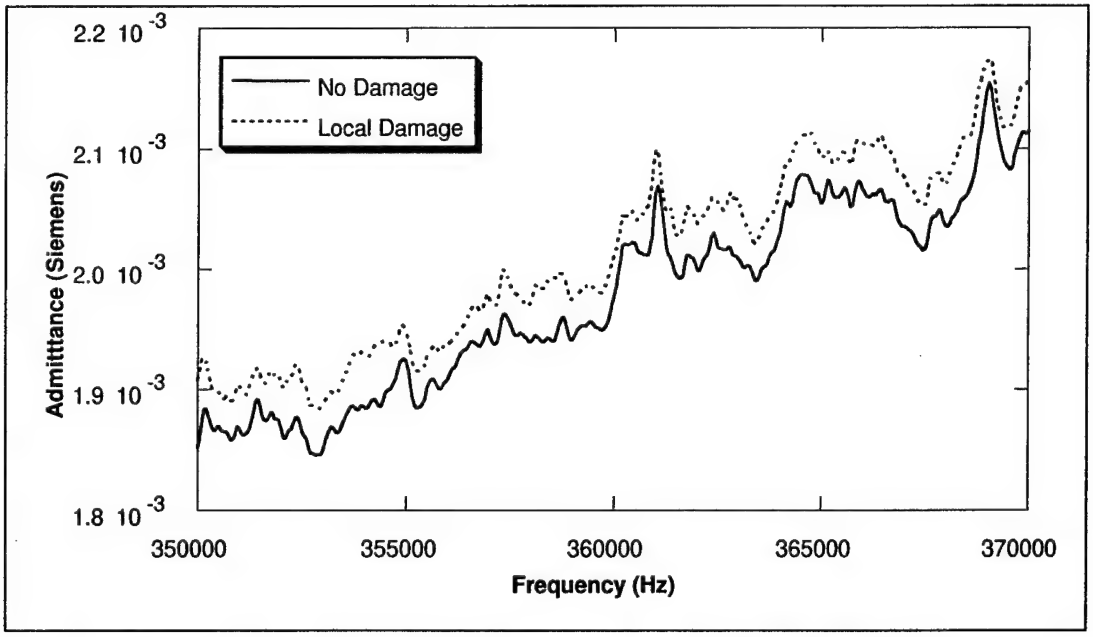


**Figure 4. Electrical admittance of PE sensor before and after one nearby bolt was loosened. The large variations in the measurements indicate presence of damage.**

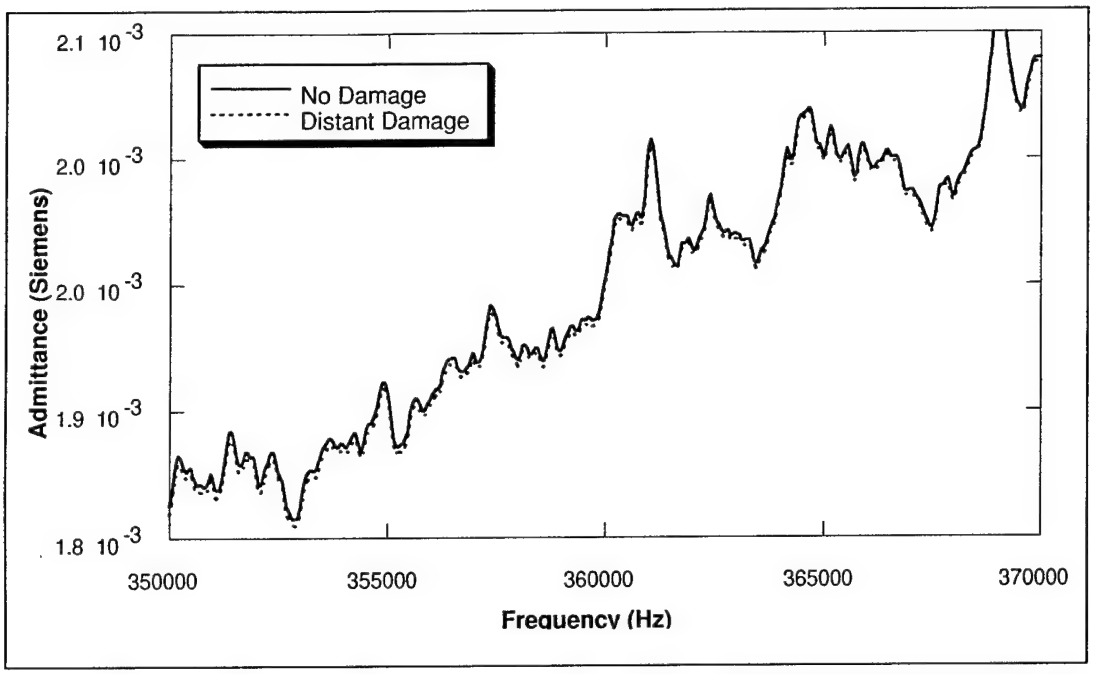


**Figure 5. Electrical admittance of PE sensor before and after one distant bolt was loosened. Note that the measurements are unchanged, indicating the localized nature of the sensing area.**

The damage metrics described in Chapter 2, as applied to the results of the model bridge joint tests, are shown in Figure 6. The damage index is the sum of the differences of the real admittance change, squared at each frequency step. The damage index is normalized to 100 percent with respect to local damage, it is used as the basis of comparison for all other damage measurements. This index provides a useful tool for rapid interpretation of structural monitoring data. It also can be used as the basis for damage threshold values that can be reported automatically as green/yellow/red light criteria for evaluation by appropriate personnel when corrective actions are necessary.

## Preliminary Debonding/Delamination Tests

The next experiment in this phase of the project was to test the impedance-based technique on a cracked aluminum substrate repaired with a high-strength composite repair patch (Figure 7) to determine whether the PE sensors could identify debonding and distinguish it from other defects.

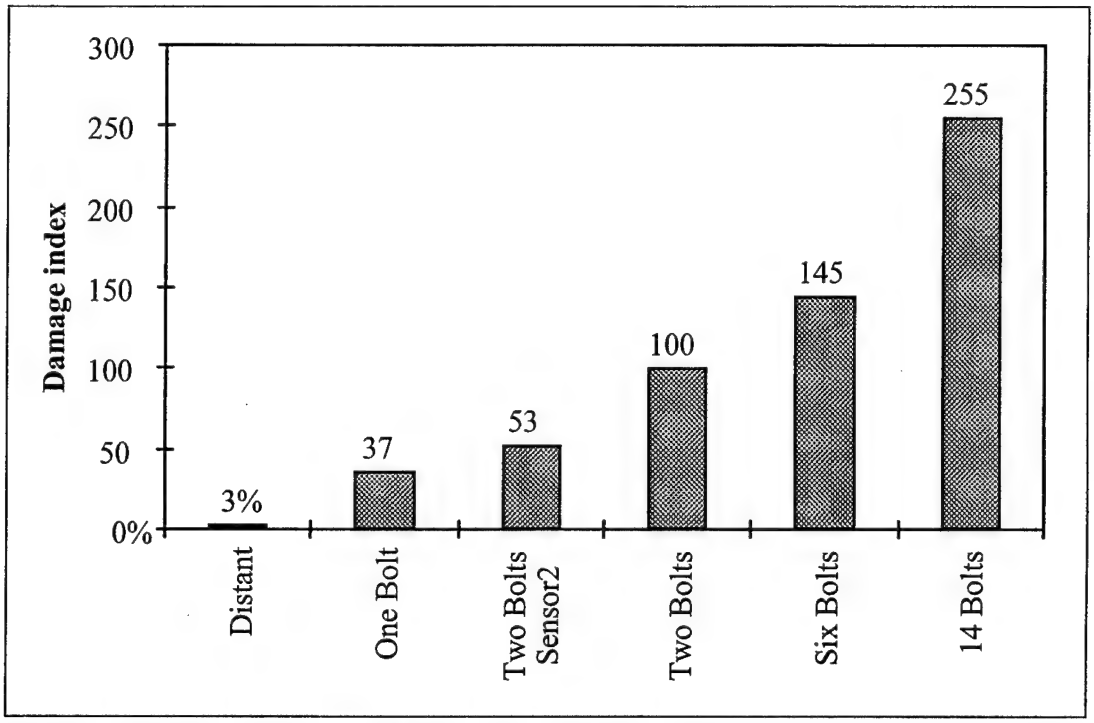


**Figure 6. Damage index for bolted bridge joint subjected to various local and distant alterations.**

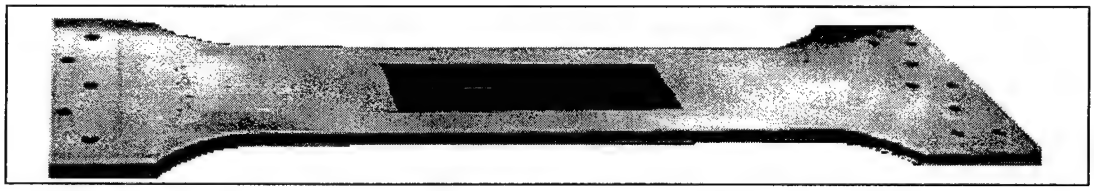

**Figure 7. Cracked aluminum dog-bone specimen repaired with graphite/epoxy composite patch.**

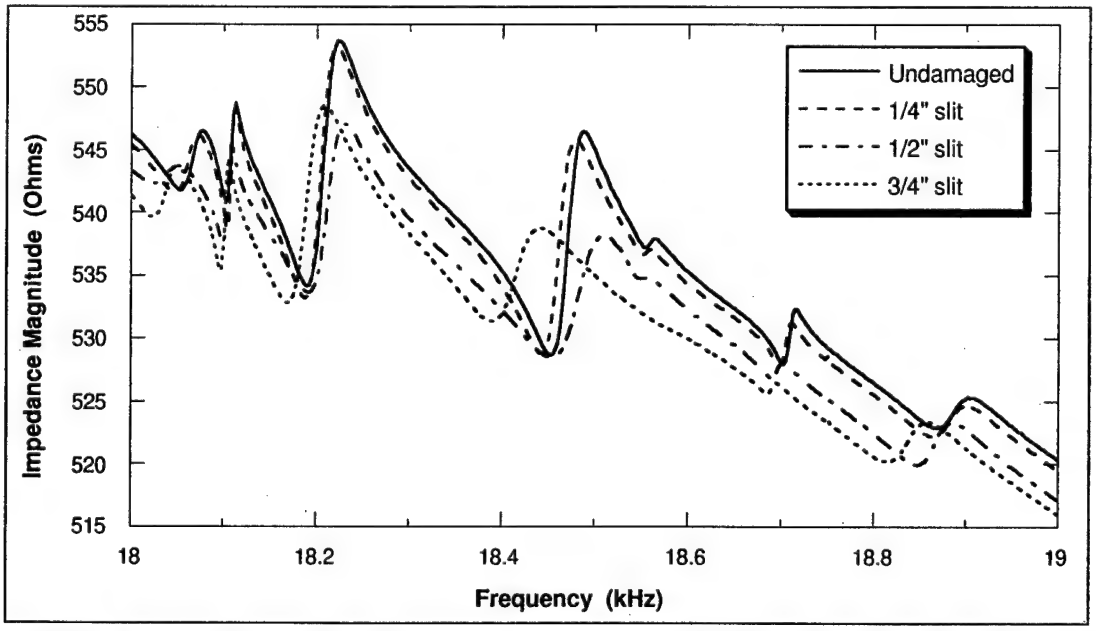


**Figure 8. Impedance graph clearly indicating debonds at edge of composite repair patch.**

In this experiment the debonding damage was created by forcing a flat screwdriver to depths of 0.25 in., 0.50 in., and 0.75 in. between the composite repair patch and the substrate. The resulting impedance measurements are shown in Figure 8 (previous page). It can be observed that the progressively deeper debonds produce clear variations in electrical impedance. Thus, the results of this test clearly show that the debonding of a composite repair material from an aluminum substrate can effectively be detected using PE sensors.

## Experiments for the Norfolk Pier Monitoring Demonstration

Laboratory experiments were performed to (1) study and optimize the quality of the bond between the PE sensor and the composite reinforcement material and (2) determine the effective range and sensitivity of the sensors to the debonding and delamination of graphite/epoxy composite upgrades from a concrete substrate. Bonding is of utmost importance because the PE actuation/sensing process depends on the effective electromechanical coupling of the sensor with the composite material being monitored. The results of these experiments were used to help determine how and where to bond the PE sensors to the test section of Norfolk Pier 11.

For these experiments, the Naval Facilities Engineering Service Center (NFESC) prepared one concrete block measuring 4 x 18 x 18 in. and another measuring 4 x 12 x 30 in., as shown in Figure 9 and Figure 10, respectively. Two 10 x 15 in. unidirectional plies of graphite reinforcement (0.009 in. thickness per ply) were bonded to the first block, and a single ply of reinforcement fabric measuring 10 x 28 in. was bonded to the second block.

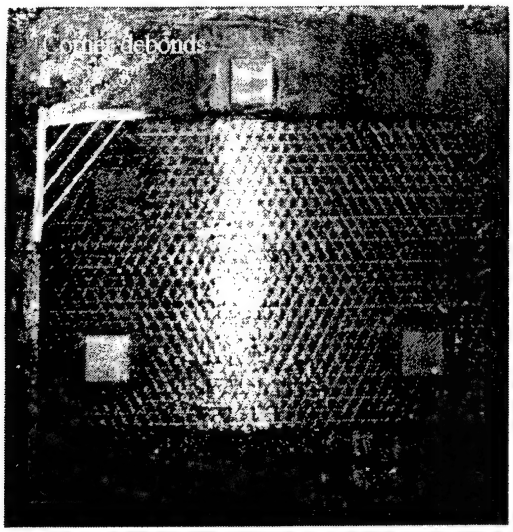

**Figure 9. Concrete block (4 x 18 x 18 in.) with two graphite/epoxy plies (0.018 x 10 x 15 in.).**

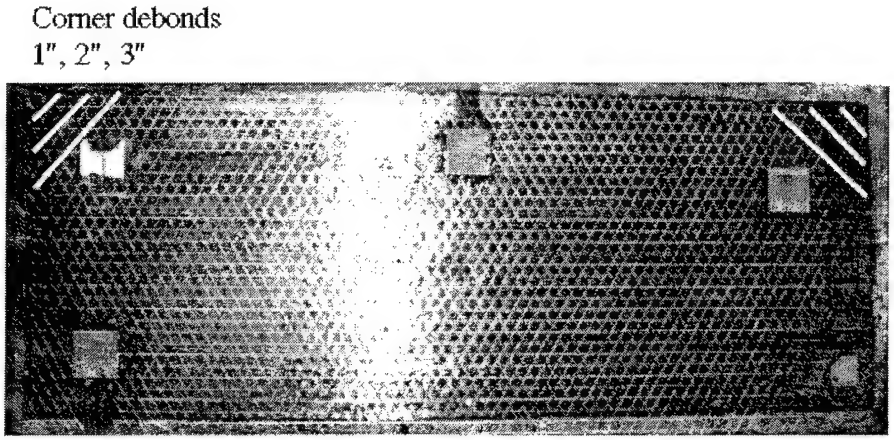


**Figure 10. Concrete block (4 x 12 x 30 in.) with single graphite/epoxy ply (0.009 x 10 x 28 in.).**

### *Bonding Experiment*

The first investigation using these two composite-reinforced concrete blocks was conducted to determine the best procedure for bonding the PE sensors to the graphite reinforcement. All tested bonding procedures are summarized in Table 1. First, a PE sensor was applied to the graphite reinforcement at the time of the lay-up, when the epoxy resin was still wet. In Case 1, no pressure was applied to the PE sensor while in Case 2, 5 psi pressure was applied to the top surface of the patch. Pressure helps to obtain better bond quality because it forces excess epoxy out from between the PE sensor and reinforcement material. In Case 3, a PE sensor was applied with no pressure after the resin had cured for 2 hours but was still sticky. In Cases 4 and 5 the sensor was bonded with pressure to the graphite after the lay-up had completely cured.

**Table 1. Procedures investigated for bonding PE sensors to graphite reinforcement.**

| | Bonding procedure | Bond quality |
|---|---|---|
| 1 | Applied to wet resin, no pressure applied. | **Poor**, thick layer of epoxy between PE sensor and graphite reduces actuation performance. |
| 2 | Applied to wet resin, pressure applied. | **Mediocre**, layer of epoxy is thinner, but actuation performance still not acceptable. |
| 3 | Applied after two hours of curing, no pressure applied. | **Poor**, thick layer of epoxy between PE sensor and graphite reduces actuation performance. |
| 4 | Applied after complete cure using cyano-acrylate adhesive, pressure applied. | **Acceptable**, layer of cyano-acrylate adhesive much thinner than epoxy, good actuation performance. |
| 5 | Applied after complete cure using cyano-acrylate adhesive, fiberglass mesh removed, pressure applied. | **Best**, thinnest layer of cyano-acrylate adhesive for optimum actuation performance. |

After the graphite reinforcement had completely cured for all five test cases, several impedance measurements were made to determine which procedure produced the optimal bond between PE sensor to the graphite reinforcement. In Cases 1 and 3, where no pressure was applied, the bond quality was found to be poor. The thick layer of epoxy between the PE sensor and the graphite acts to dampen — and therefore inhibit — electromechanical coupling between the sensor and the reinforcement fabric. In Case 2, where pressure was applied, the bond quality was better but not acceptable for the intended application. It can be seen, therefore, that the PE sensors will not function as intended when applied directly to the epoxy during lay-up of the composite reinforcement.

The bond quality in Cases 4 and 5 was greatly improved. In Case 4, where the PE sensor was bonded directly to the cured graphite with a cyano-acrylate adhesive, the resulting bonding layer was much thinner than in Cases 1 – 3. In Case 5 it was demonstrated that bond quality could be further improved by carefully sanding off the fiberglass mesh that is applied by the manufacturer to prevent the fibers in the unidirectional graphite reinforcement from separating during handling. This protective mesh creates pockets of excess epoxy between the sensor and the reinforcement, thereby reducing bond quality. Therefore, the bonding procedure used in Case 5 was selected for application in the full-scale demonstration at Norfolk Pier 11.

One other bonding procedure, in which the PE sensor would be embedded in the composite material, was considered but dismissed. It was determined that the embedding of PE sensors into the composite could create delamination problems. The bonding procedure investigated in Case 5, on the other hand, was shown to provide good actuation performance for nonintrusive damage detection.

One additional advantage of the chosen bonding procedure is that the sensors do not have to be installed at the same time the composite reinforcement is being laid up. Consequently, there is no urgency to install the PE sensors before the epoxy cures, so there is no need to have several people working on the wet reinforcement material simultaneously.

### *Sensing Area and Sensitivity*

To determine the size of the technology's sensing area and its sensitivity to debonding and delamination defects, the reinforcement fabric was deliberately debonded at various corners of the test blocks, as shown in Figures 7 and 8. Three levels of damage were induced: 1 in., 2 in., and 3 in. The impedance measurements before and after damage for both the single-ply and double-ply graphite reinforcement samples were inconclusive; the variations in impedance

measurements were very small. This lack of sensitivity to debonding and delamination damage can be attributed to the thinness of the graphite reinforcement material (0.009 in. and 0.018 in., respectively). When the graphite reinforcement is that thin, force transfer between the PE sensor/actuator and the graphite composite becomes very difficult. Evidently, when the composite material is so thin, the PE sensor/actuator propagated most of its signal *through* the composite and dissipated it into the concrete. It was hypothesized that this problem would subside as thicker reinforcement materials were used because the actuator signal would increasingly be transferred to the graphite rather than the stiff, dissipative concrete. Theoretical modeling was employed to determine that the thickness of the graphite reinforcement applied to Norfolk Pier 11 (0.120 in.) would be sufficient for use of the impedance-based technique.

In order to confirm this reinforcement-thickness hypothesis, further laboratory experiments were conducted. A 20-ply (0 degree/90 degree) graphite/bismaldeide composite plate measuring 2.5 x 11 in. was manufactured at the composite manufacturing laboratory, Virginia Polytechnic Institute and State University VPI & SU). The lay-up was to have a final thickness of 0.125 in. The composite plate was then glued to a concrete block using high-strength epoxy, as shown in Figure 11. A 1.25 x 1.25 in. PE sensor was bonded at one end of the graphite reinforcement, and debonds were induced at the opposite end. This damage was introduced across the entire 2.5 in. width of the laminate, at depths of 0.5, 1.0, 1.5, and 2.0 in.

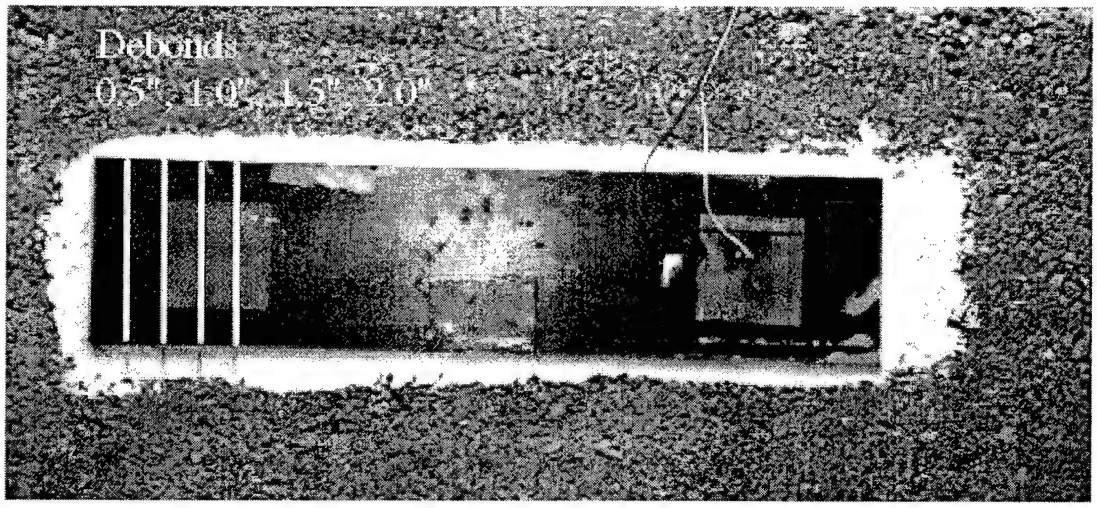


**Figure 11 . Concrete block with bonded graphite reinforcement, showing PE sensor at right.**

Impedance was measured for each level of damage over a frequency range of 30 – 240 kHz. The results for the 0.5 in. and 1.5 in. debonds from three different frequency ranges are shown in Figure 12, Figure 13, and Figure 14.

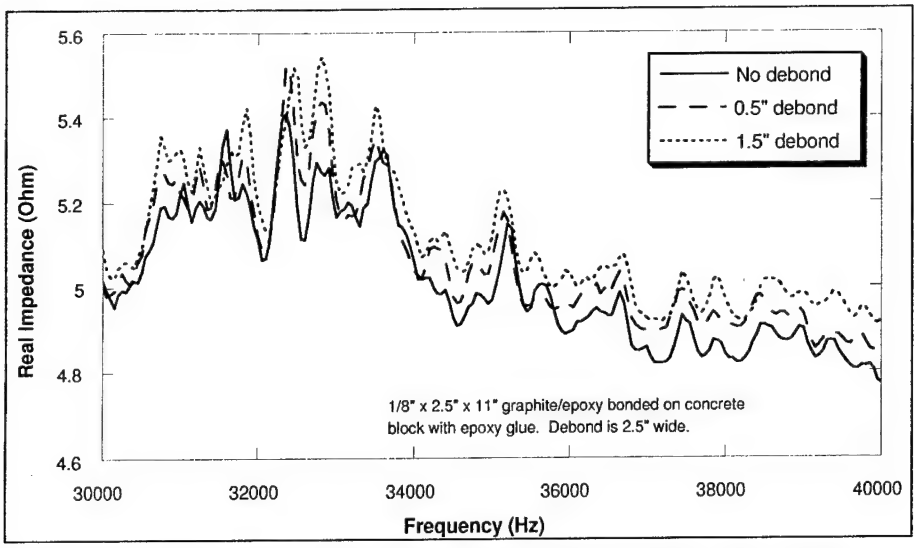


**Figure 12. Impedance measurements for debonded graphite at 30 – 40 kHz.**

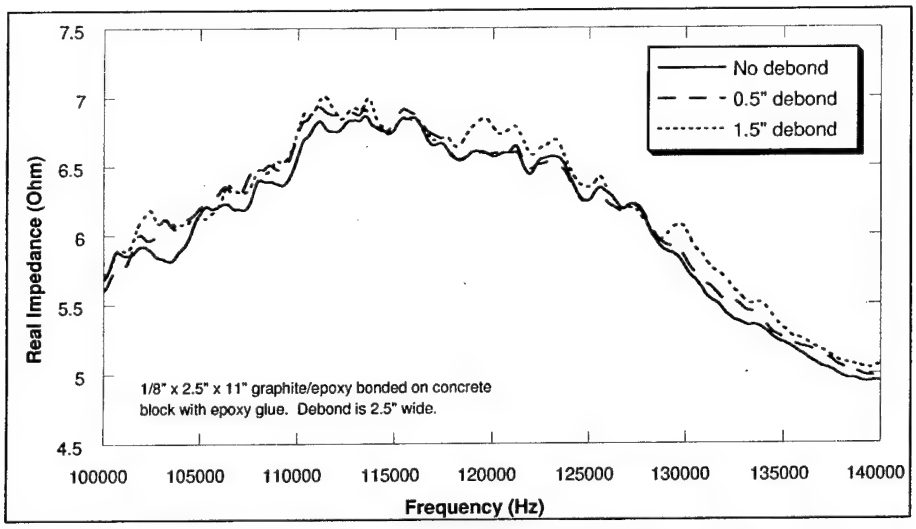


**Figure 13. Impedance measurements for debonded graphite at 100 – 140 kHz.**

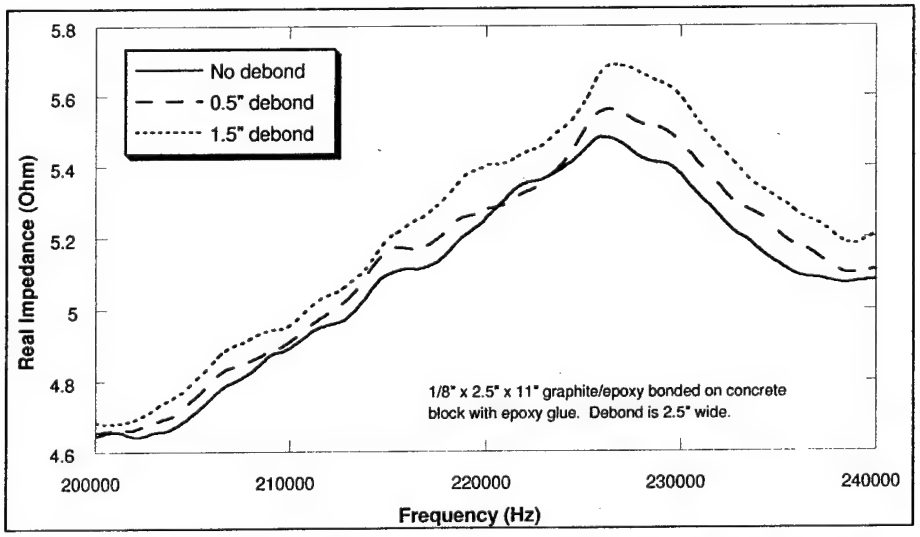


**Figure 14. Impedance measurements for debonded graphite at 200 – 240 kHz.**

A clear modification of the impedance can be observed over all frequency ranges. However, due to the higher dynamic activity, the best range for this specific application is the 30 – 40 kHz range.

These preliminary results demonstrated that a 0.5 in. debond can be detected with a PE sensor located 9 in. away. The dissipation of the propagating wave is caused only by the graphite material damping, not the concrete substrate. The effective range of the PE sensor was believed to reach up to 24 in., as predicted through the theoretical modeling noted above. However, in order to ensure the success of the Norfolk Pier 11 implementation, a conservative sensing range of 12 in. was assumed. Therefore, for the demonstration, it was decided to place the PE sensors no more than 24 in. apart.

# 4 Laboratory Tests of PE Sensors on Composite-Upgraded Masonry Wall Models

## Introduction

In this phase of the project CERL researchers conducted failure tests on nine masonry wall sections upgraded with FRP composite material. All wall sections (excluding an unreinforced baseline section) were instrumented with PE sensors in order to test the impedance-based structural monitoring technique. The objective of these tests was to incrementally load each wall sections to failure to determine whether the impedance-based technique could effectively detect crack development, upgrade debonding, and delamination within the composite fabric.

The tests were run in two series. The first series consisted of five concrete block masonry walls — one nonreinforced control section and four identical experimental sections, each reinforced with a different type of FRP composite (Quattrone, Berman, and Kamphaus, January 1998; Raju 1997). These walls were fabricated to support a separate research project whose objective was to compare the structural performance of four different types of composite reinforcement. The other test series included three specimens — two made of concrete block and one made of brick — fabricated exclusively for testing the impedance-based monitoring technique. Table 2 identifies the type of reinforcement used on each test wall and summarizes the test data for all walls, including the nonreinforced concrete masonry control wall (Figure 15).

## Vacuum-Assisted Sensor Bonding Technique

As discussed in Chapter 3, bond quality determines the quality of electromechanical coupling between the sensor patch and the structure. A high-quality bond is essential for impedance-based structural monitoring.

**Table 2. Summary of test wall composition and reinforcement.**

| Test Sample | Composite Manufacturer | Materials | Fracture Load | Remarks |
|---|---|---|---|---|
| Wall 0 | Control specimen, no upgrade | Type N mortar, no composite reinforcement | 31,000 lb (Avg of 4 walls) | Failure usually occurred in stairstep fashion along a diagonal path, following the mortar lines. |
| Wall 1 | Reichhold Chemicals, Inc. | Concrete masonry w/ E-glass / vinyl ester / *in situ* $[0/90/\pm45]_4$ | 60,000 lb | Failure along top length occurred at 50,000 lb. A centerline crack with multiple cracks at the lower corner appeared at 60,000 lb. |
| Wall 2 | Tonen Corp. | Concrete masonry w/ carbon / epoxy / *in situ* $[0/90]_2$ | 45,000 lb | A centerline crack appeared at 12,000 lb due to sudden dynamic unloading. The crack became more pronounced at 45,000 lb. |
| Wall 3 | Fyfe Co., LLC | Concrete masonry w/ E-glass / epoxy / *in situ* (woven, 2 layers) | 48,000 lb | A centerline crack appeared at 48,000 lb. Test was stopped even though the structure could carry more load. |
| Wall 4 | Owens Corning | Concrete masonry w/ S2-glass / phenolic / 1/4" premolded (woven) | 58,000 lb | A centerline crack appeared at 45,000 lb. At 55,000 lb the top corner of the structure failed. At 58,000 lb, the bottom corner of the structure failed. |
| Wall 5 | Fyfe Co., LLC | Brick w/ E-glass / epoxy / *in situ* (woven, 2 layers) | 81,000 lb | Some visible debonding occurred at 60,000 lb. Additional debonding occurred at 74,000 lb. |
| Wall 6 | Fyfe Co., LLC | Concrete masonry w/ E-glass / epoxy / *in situ* (woven, 2 layers) | 56,000 lb | Top block cracked at 30,000 lb. Other cracks appeared as load was increased. Stair step failure occurred at 46,000 lb but wall still held load. |
| Wall 7 | Clark Schwebel Tech-Fab Co. | Concrete masonry w/ E-glass structural grid $[0/90]_2$ | 56,000 lb | Crack appeared in one block at 20,000 lb. More cracks appeared as load was increased to 36,000 lb. No further cracks were noted until the wall failed. |

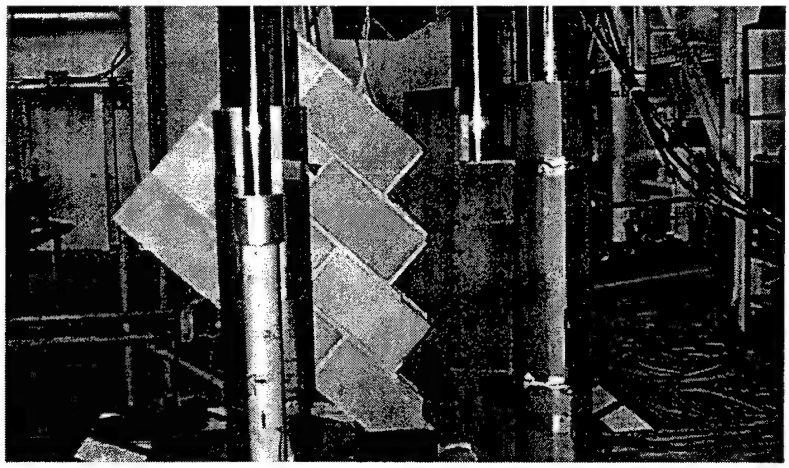

**Figure 15. Failed Wall 0 (nonreinforced control section).**

To provide the tightest possible bond while using the thinnest feasible layer of adhesive, a vacuum-assisted sensor-mounting technique was developed. First, a PE sensor, a square strip of porous release film, a square strip of 0.05 in. thick porous foam, and a nylon bagging film were stacked into a four-layer assembly. Then the mating surfaces of the PE sensor and the composite were cleaned thoroughly with acetone. A one-part cyano-acrylate epoxy was applied to the PE sensor face and the assembly was immediately placed on the composite material. A vacuum setup, comprising a compressor, tubes, and sealant tape wrapped around the PE sensor assembly, was used to establish a vacuum around the sensor. The vacuum field forces the PE sensor tightly against the composite surface. As noted in Chapter 3, this technique yields a good bond within 2 hours. Figure 16 shows the main components used in the vacuum setup, including the compressor (near upper left), tubes, and five of the layered sensor/actuator patch assemblies described above.

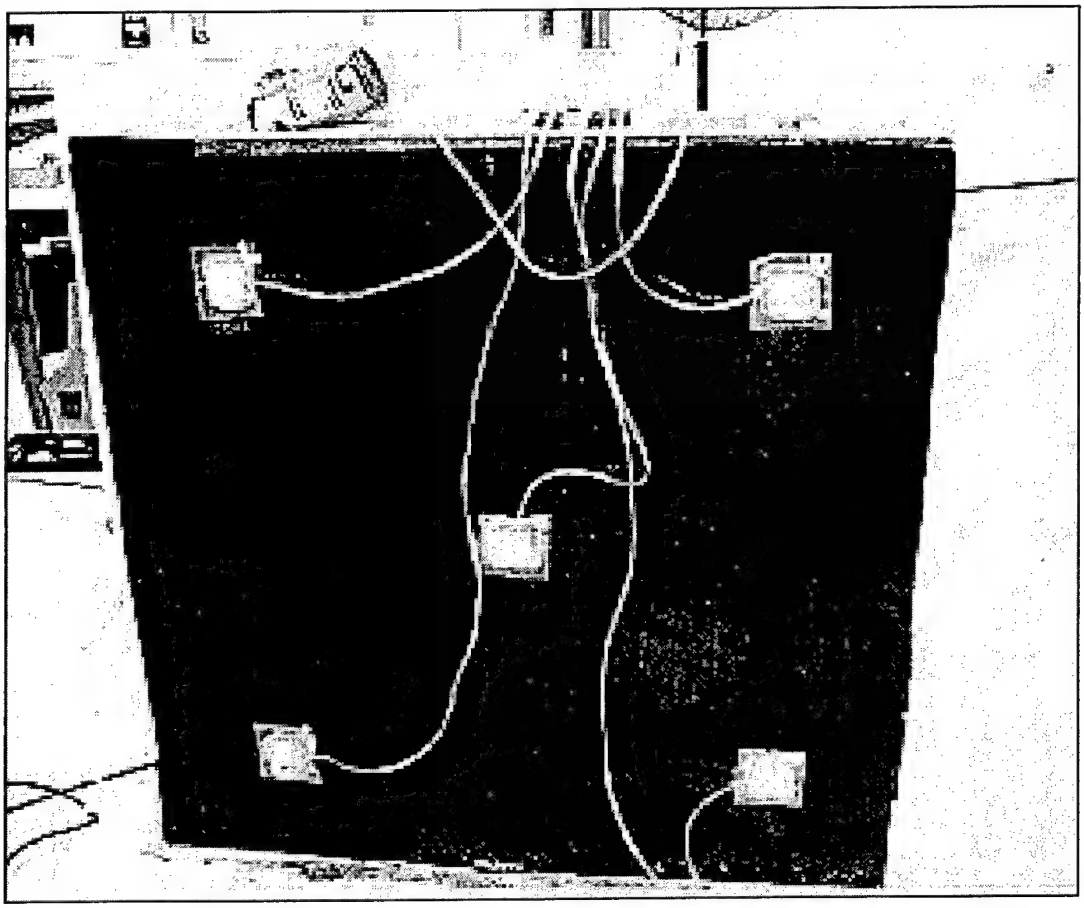

**Figure 16. Typical PE sensor patch configuration (Wall 2 shown).**

## Sensor Configuration

Based on the results of high-frequency wave propagation modeling (see Chapter 3), the sensing radius of each PE sensor was estimated to be 12 in. Therefore, the entire composite face of each wall section could be monitored using five PE sensors mounted 24 in. apart — one near each corner and one in the center (Figure 16). It should be noted that all composite reinforcement materials were thick enough to prevent wave propagation into the masonry itself — a potential technical problem that was noted and addressed in earlier work (see Chapter 3).

## Loading Procedure

Each wall section was mounted diagonally in the million-pound load test machine according to ASTM E519-81 to induce a shearing load failure (Figure 17). Each structure was loaded in steps and PE sensors were used to interrogate the structure at each constant load step to determine incipient damage (in particular, delamination effects).

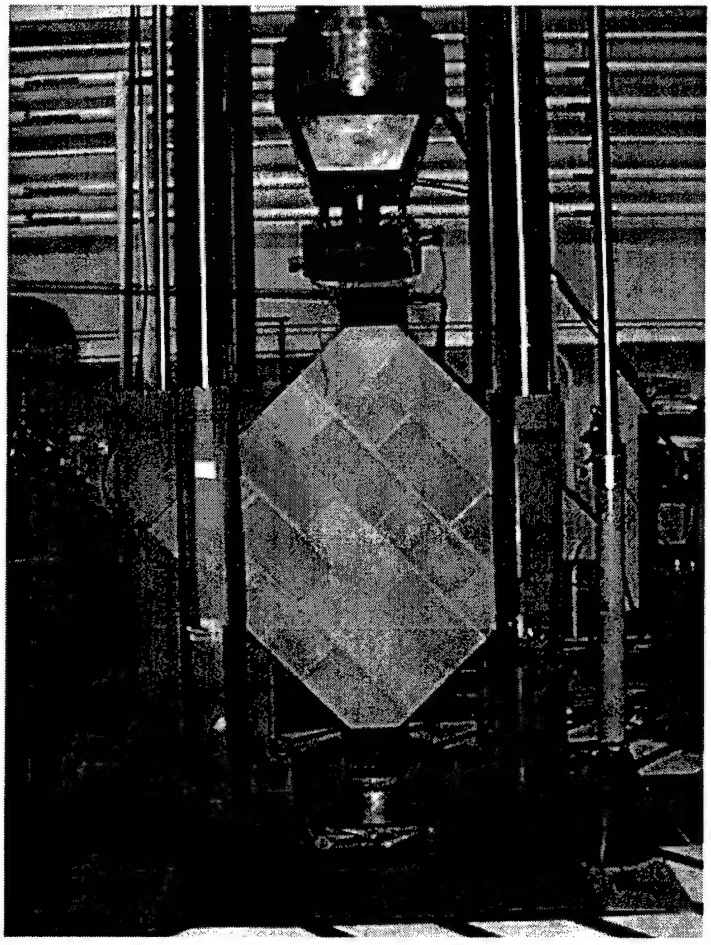

**Figure 17. Wall section mounted diagonally in CERL's million pound load test machine.**

## Data Acquisition and Processing

The hardware and software used to collect and process the data from the PE sensors are the *HP 4192A Low Frequency Impedance Analyzer* (Hewlett Packard), a laptop computer and a PCMCIA GPIB data acquisition card. The base commercial software requirements are the National Instruments (Austin, TX) *NI 488.2M* and *Measure for Windows*. The Reinforced Structure Integrity Monitoring (RSIM) software developed for this specific application at VPI & SU was used to collect and process the data.

## Wall Test Results

### *Wall 1*

Wall 1 used the composite reinforcement manufactured by Reichhold Chemicals, Inc. (E-glass / vinyl ester / *in situ* $[0/90/\pm45]_4$). The wall section was loaded in stages to 50,000 lb, at which point failure along the top line occurred. The loading was stopped at 60,000 lb, at which point a center line crack appeared (Figure 18). The Correlation Metric was used to interpret the data from all PE sensors. As discussed in Chapter 2, the damage metric provides a summary as well as a quantitative analysis of the data obtained from the frequency response curves. The Correlation Metric was used to interpret and summarize the damage data collected from PE sensors 1 – 5.

It can be seen from Figure 19 that at 50,000 lb (Damage #6), when top line fracture occurred, a large increase in damage metric values was returned by sensors 1, 2, and 5. The relative increase in damage metric (from Damage #5 to Damage #6) is the greatest for PE sensor 1 (closest to the crack, 2232.4 percent), followed by PE sensor 2 (close to the crack, 740 percent) and PE sensor 5 (crack within sensing range of the PE sensor, 182 percent). It should be noted that PE sensor 2 was being interrogated while the wall was being loaded to 50,000 lb, and it picked up the damage as it was occurring. PE sensor 3 showed a decrease while PE sensor 4 showed only a small increase because the damage was essentially out of their sensing range. The absolute numerical value of the damage metric at fracture load was highest for PE sensor 1, then for PE sensors 2, 5, 3, and 4, respectively.

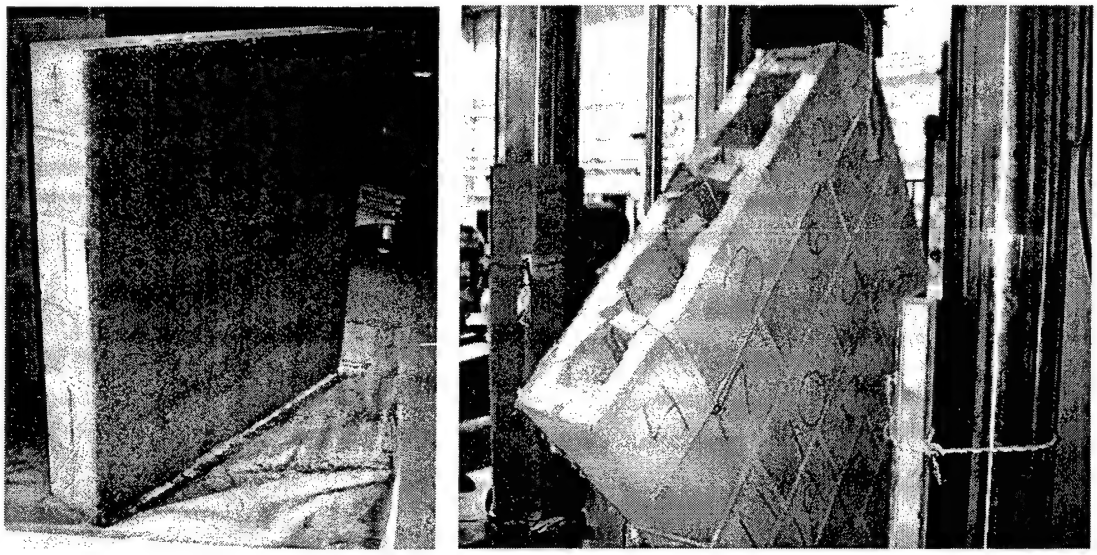

**Figure 18. Wall 1 before loading (left) and after failure (right).**

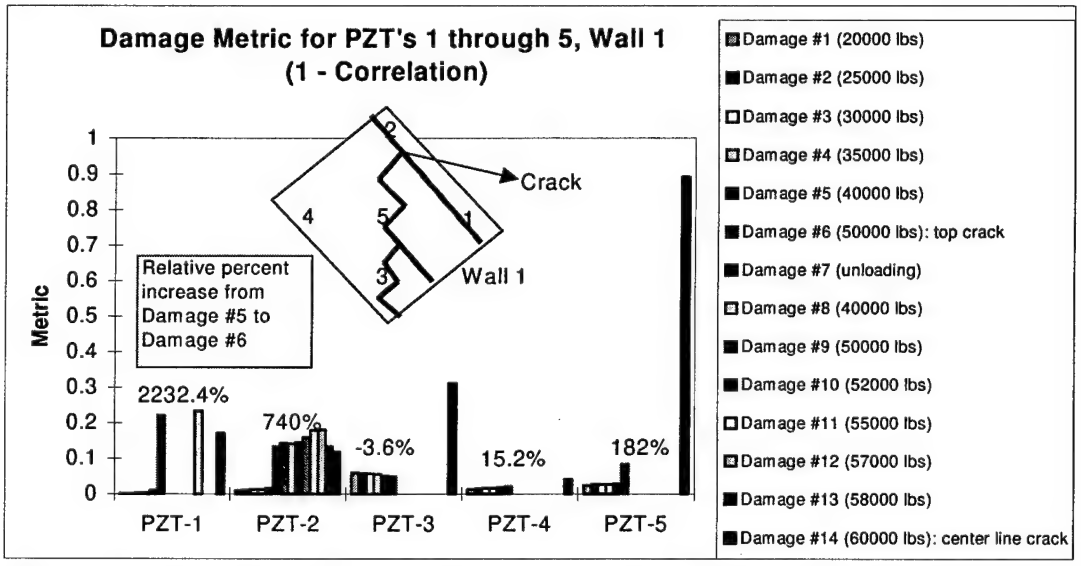


NOTE: *PZT* was an earlier abbreviation for *PE patch sensor*, but is now superseded. In this chart, PZT means PE patch sensor.

**Figure 19. Correlation Metric for Wall 1, PE sensors 1 – 5.**

At Damage #14, when the center line crack appeared, there was a large increase in the damage metric for PE sensors 5, 3, and 1. Sensors 5 and 3 were located right in the path of this center line crack and, not surprisingly, they showed a large increase in the damage metric. The increase shown by sensor 1 may indicate that debonding became more pronounced in its vicinity. PE sensor 2, however, did not show a large increase for this damage even though it was close to the crack. It should be noted that PE sensor 2 was influenced by both the top and centerline cracks. If Damage #14 is compared to Damage #1 rather than to later readings, the increase in the metric is apparent. PE sensor 4 also was distant from the damage, so it does not show a large increase in the metric.

It can be seen from the above observations and Figure 15 that damage locations can be approximately predicted using this monitoring technique. Multiple cracks in different areas at different times were picked up accurately.

### *Wall 2*

Wall 2 was upgraded with a composite reinforcement manufactured by Tonen Corp. (carbon / epoxy / *in situ* $[0/90]_2$). Wall 2 was loaded in stages to 12,000 lb, at which point an impact load was accidentally introduced to the wall and failure occurred upon unloading (Figure 20). Since the composite overlay held the fractured assembly together, the loading was continued and eventually was stopped at 45,000 lb, at which point the fracture in the structure became pronounced. The Correlation Metric was used to interpret and summarize the damage data collected from PE sensors 1 – 5.

Figure 21 shows that at 12,000 lb (Damage #6), when the initial fracture occurred, there was a large increase in the damage metric values for sensors 1, 4, and 5. The relative increase in the metric from Damage #5 to Damage #6 was greatest for PE sensor 4 (2549 percent), then PE sensor 1 (659 percent) and PE sensor 5 (423 percent). PE sensor 2 returned a large relative increase in the damage metric from Damage #5 to Damage #6, but the absolute values of the metrics are very small. PE sensor 3 showed a small relative increase (125 percent).

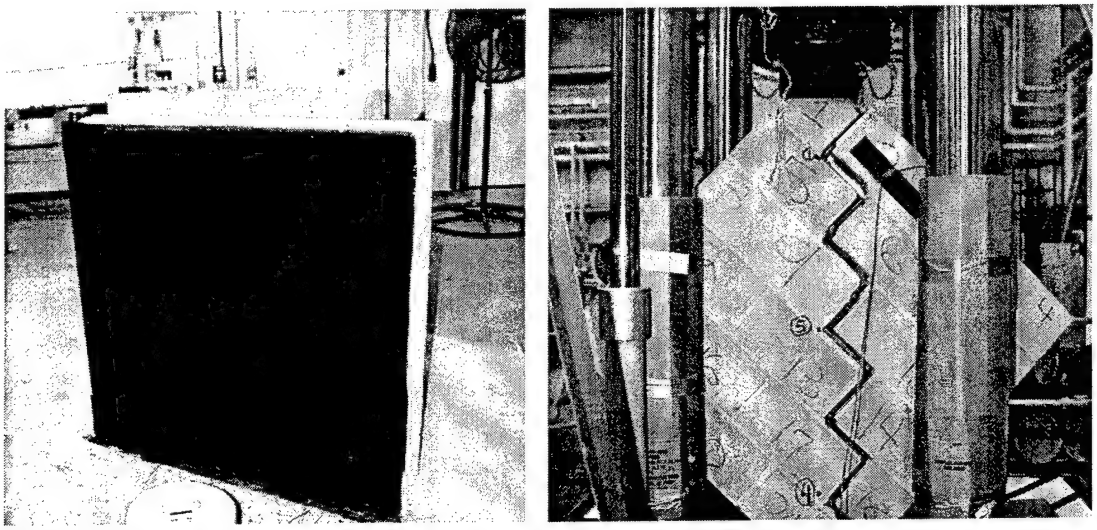

**Figure 20. Wall 2 before loading (left) and after failure (right).**

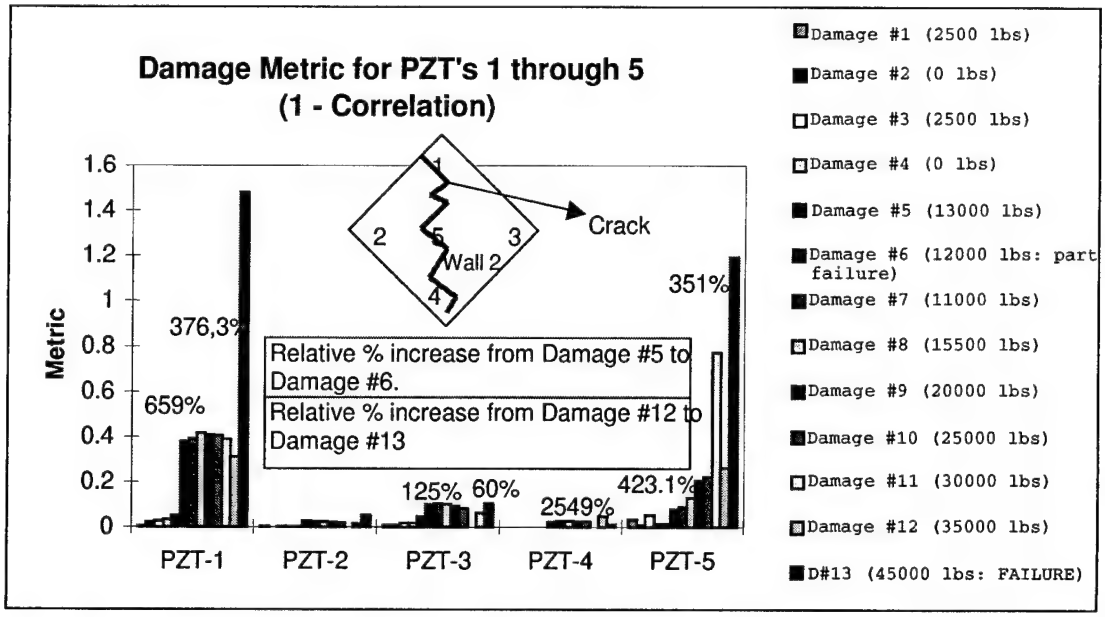


NOTE: *PZT* was an earlier abbreviation for *PE patch sensor*, but is now superseded. In this chart, PZT means PE patch sensor.

**Figure 21. Correlation Metric for Wall 2, PE sensors 1 – 5.**

The relative increase in damage metric from Damage #12 to Damage #13, at which load the fracture became more pronounced, was greatest for PE sensor 1 (376.3 percent), then for PE sensor 5 (351 percent). PE sensor 3 showed a small relative increase (60 percent).

PE sensor 1 showed the failure as it occurred. It returned the highest absolute numerical values for the damage metric, followed by PE sensor 5. It can be seen from Figure 16 that sensors 1 and 5 were very informative about imminent damage. Although PE sensor 2 had large relative increases in damage metrics, the absolute values of these metrics were very small. PE sensor 3 did not sense the damage because of its distance. While PE sensor 4 was close to the damage, it showed only small absolute values for the damage metric, possibly because debonding in the vicinity of the sensor was not severe.

### *Wall 3*

Wall 3 was upgraded with composite reinforcement called the TYFO™ S Fibrwrap System, manufactured by Fyfe Co., LLC (E-glass / epoxy / *in situ* [woven, 2 layers]). The wall was loaded in stages to 49,000 lb, at which point failure occurred (Figure 22). The Correlation Metric was used to interpret and summarize the data from PE sensors 1 – 5.

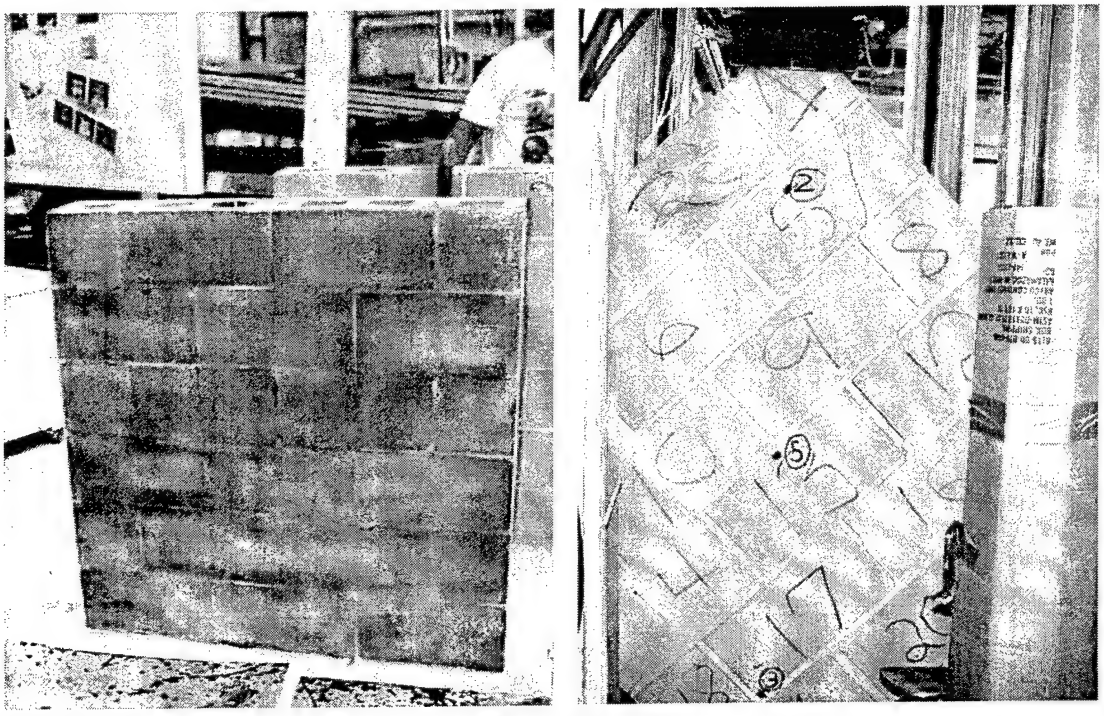

**Figure 22. Wall 3 before loading (left) and after failure (right).**

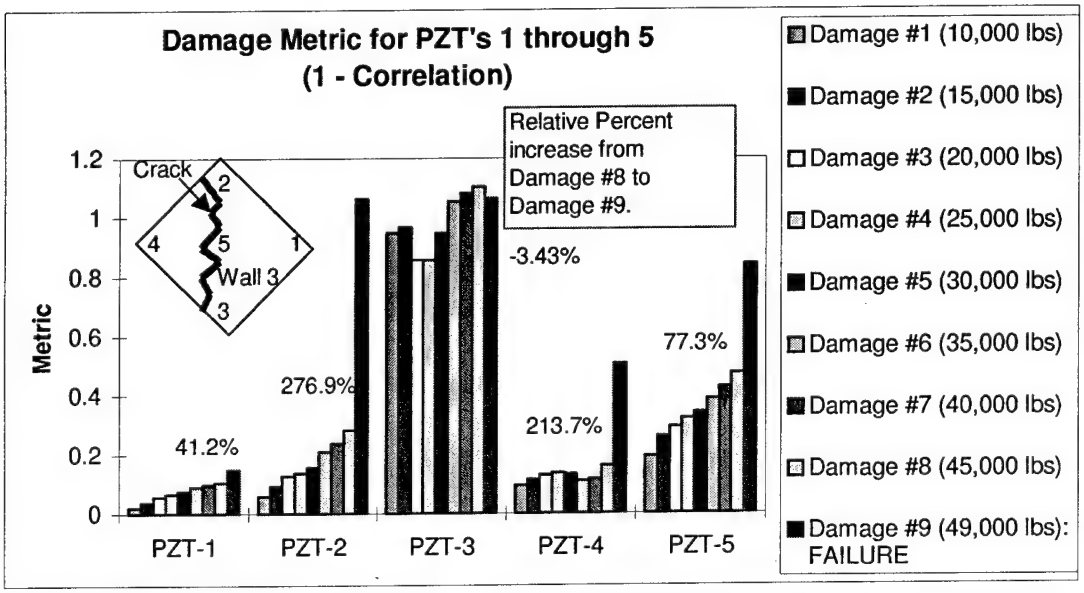


NOTE: *PZT* was an earlier abbreviation for *PE patch sensor*, but is now superseded. In this chart, PZT means PE patch sensor.

**Figure 23. Correlation Metric for Wall 3, PE sensors 1 – 5.**

It can be seen from Figure 23 that at 49,000 lb (Damage #9), when failure occurred, there was a large increase in the damage metric values for PE sensors 2, 4, and 5. The relative increase in damage metric (from Damage #8 to Damage #9) was the greatest for PE sensor 2 (closest to the crack, 276.9 percent), then for PE sensor 4 (crack within sensing range of the PE sensor, 213.7 percent) and PE sensor 5 (close to the crack, 77.3 percent). PE sensor 3 showed a decrease in

damage even though it was close to the crack, possibly because the debonding near the sensor was not very severe. PE sensor 1 showed only a small increase because it was distant from the damage. The absolute numerical value of the damage metric at fracture load was highest for PE sensor 3 then, in order, PE sensors 2, 5, 4, and 1.

The large increase in the metric at 60,000 lb (Damage #14) could be attributed either to actual damage that is not visible) or unloading effects on the structure at the end of the test.

### *Wall 4*

Wall 4 used a composite reinforcement manufactured by Owens Corning (S2-glass / phenolic / 1/4 in. premolded [woven]). The structure-composite combination was loaded in stages to 45,000 lb, at which point failure occurred (Figure 24). The loading was finally stopped at 58,000 lb. The Correlation Metric was used to interpret and summarize the data from PE sensors 1 – 5.

It can be seen from Figure 25 that at Damage #5, at which point the centerline crack appeared, there was a large increase in damage metric for PE sensors 1, 4, and 5. These sensors were along the line of the damage. PE sensor 1 showed a 71 percent increase from the previous reading, PE sensor 4 showed a 233.3 percent increase, and PE sensor 5 showed a 274.9 percent increase. PE sensors 2 and 3, which were distant from the centerline crack, showed a 2.8 percent increase and a 17.2 percent decrease, respectively.

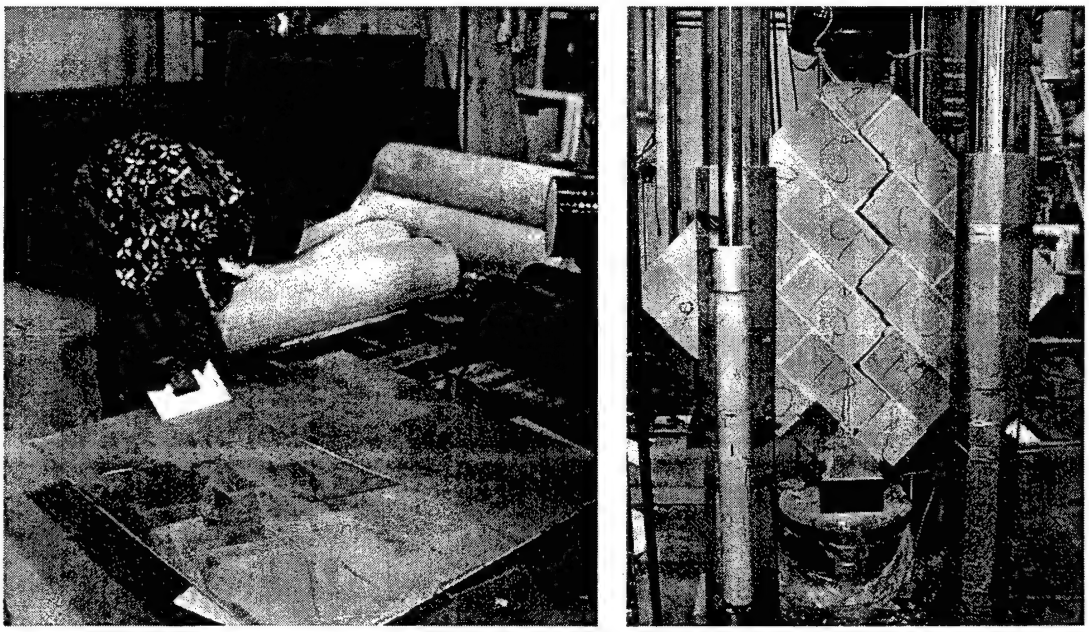

**Figure 24. Preparing composite plate for Wall 4 (left) and failed wall (right).**

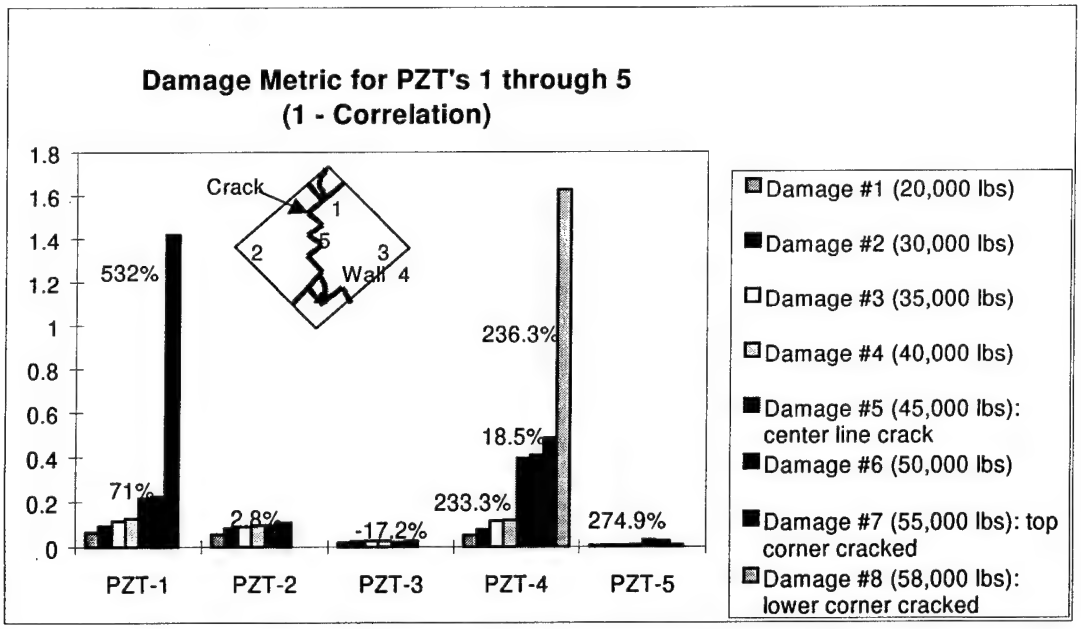


NOTE: *PZT* was an earlier abbreviation for *PE patch sensor*, but is now superseded. In this chart, PZT means PE patch sensor.

**Figure 25. Correlation Metric for Wall 4, PE sensors 1 – 5.**

At Damage #7, when the top corner of the block fractured, PE sensor 1 (which was positioned right above the damage) showed a 532 percent increase from the previous reading. PE sensor 4, although distant from this damage, showed an 18.5 percent increase.

At Damage #8, when the bottom corner of the block crumbled, PE sensor 4 (which was right above the damage) showed a 236.3 percent increase over the previous reading.

### *Wall 5*

Wall 5 was a double-wythe 4 x 4 ft structure made of standard 10-hole red brick and reinforced with the TYFO™ S Fibrwrap System by Fyfe Co. LLC (E-glass / epoxy / *in situ* [woven, 2 layers]), which was also used on Wall 3. The Correlation Metric was used to interpret the data collected from PE sensors 1 – 5.

The wall was tested by applying a load in stages until the wall failed. The rate of loading was set to 5000 lb/min. The initial steps were 20,000 lb apart. After 60,000 lb, the step size was reduced to 7000 lb.

It can be seen from Figure 26 that the damage metric increased as the load was increased. However, the magnitude of the metric is small, most values are less than 0.1. As the load was increased from 20,000 lb to 40,000 lb, some cracking noises were heard. When the load was increased from 40,000 lb to 60,000 lb, a

loud pop was heard. Upon inspection of the wall, some debonding had occurred near the upper shoe (PE sensor 2). Additional debonding at the upper shoe was noted during data collection at 74,000 lb. The wall broke at 81,000 lb load during data collection for PE sensor 1.

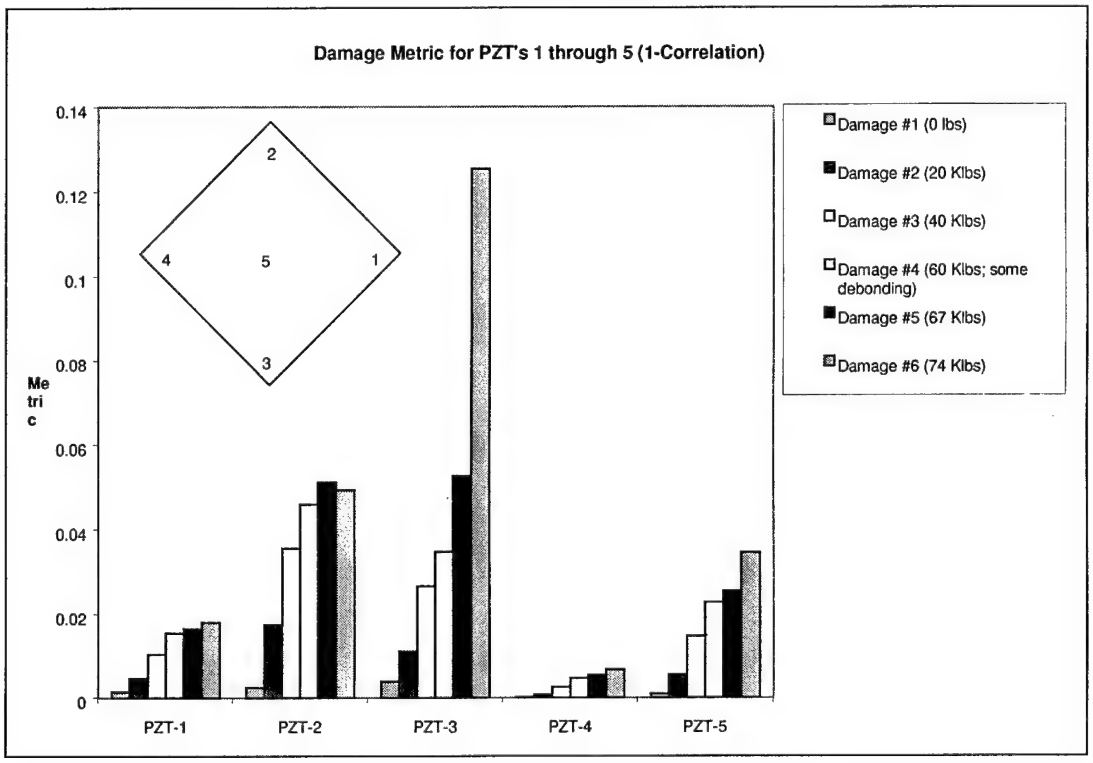


NOTE: *PZT* was an earlier abbreviation for *PE patch sensor*, but is now superseded. In this chart, PZT means PE patch sensor.

**Figure 26. Correlation Metric for Wall 5, PE sensors 1 – 5.**

Figure 26 shows that the damage metric was largest near the top and bottom corners of the wall, where the compressive load was applied. The damage metric rose even when damage was not observed visually. When the wall finally broke, the bricks near both the upper and lower load shoes were crushed. It is also seen that the damage metric was largest for PE sensor 2 and PE sensor 3, which were nearest to the load shoes. It is not clear why the damage metric for PE sensor 2 at 74,000 lb was slightly lower than for PE sensor 2 at 67,000 lb. Nevertheless, the large rise in the PE sensor 3 damage metric was a good indicator for structural impending failure.

### *Wall 6*

Wall 6 was a 4 x 4 ft concrete masonry block wall reinforced with the same Fyfe Co. composite reinforcement that was used for Walls 3 and 5. The wall was tested by applying a load in stages until the wall failed. The rate of loading was

set to 2500 lb/min. The initial steps were 10,000 lb apart. After 30,000 lb, the step size was reduced to 2000 lb. The Correlation Metric was used to interpret the information from PE sensors 1 – 5.

Wall 6 had a number of partial failures at various loads, making it possible to see the effects of failure in the PE sensor readings. Each time debonding or cracking was detected visually, the damage metric would change.

It can be seen in Figure 27 that the damage metric was greatest at the top of the wall. The damage metric for PE sensor 2 was small at the beginning, but suddenly jumped at 30,000 lb. This large change was due to cracks occurring in the block, both externally (Figure 28) and internally (Figure 29). The cracks were circled in Figure 21 because they were difficult to see. Parts of the cracks are obscured by the top load shoe. Cracks also appeared in the block mounted in the bottom load shoe. They were much smaller than the cracks in the top blocks, however, and did not photograph well, so no figure is provided.

The damage metric for PE sensor 3 also showed a large increase as a result of the lower block cracking. PE sensor 5 (center) also showed a jump in its damage metric, but not as large as the ones at top and bottom. PE sensors 1 and 4 show little response because they are distant from the damaged blocks.

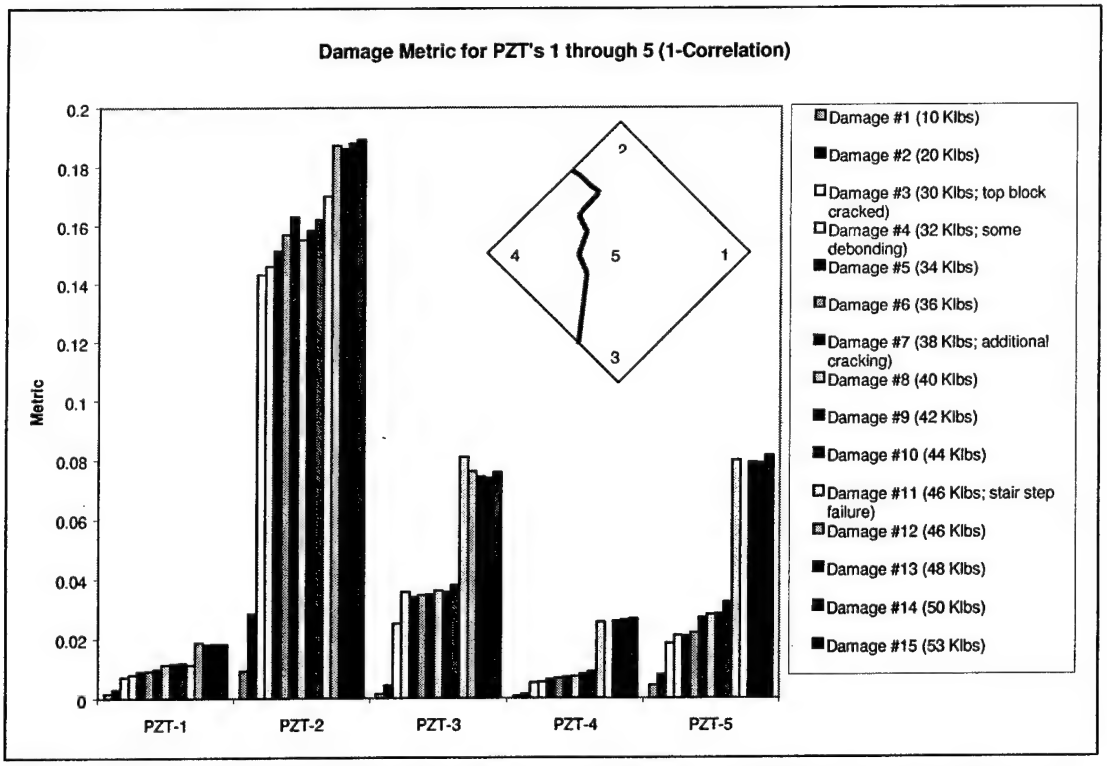


NOTE: *PZT* was an earlier abbreviation for *PE patch sensor*, but is now superseded. In this chart, PZT means PE patch sensor.

**Figure 27. Correlation Metric for Wall 6, PE sensors 1 – 5.**

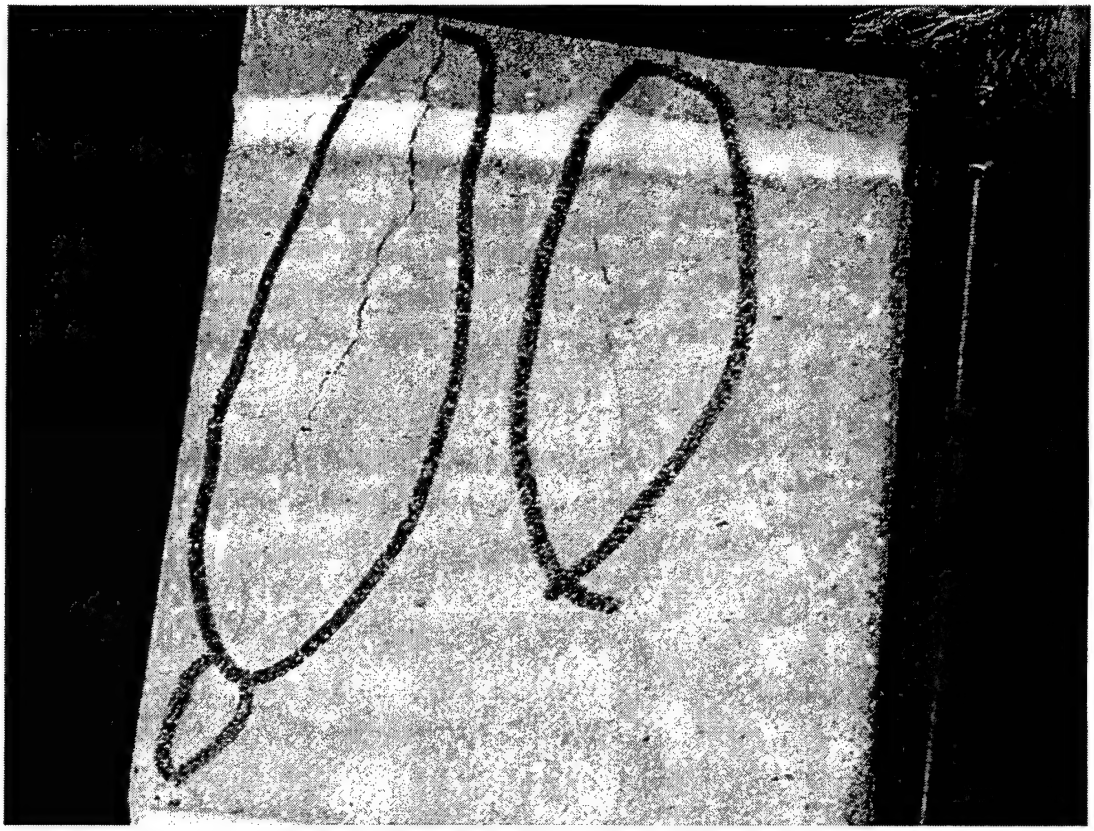

Figure 28. A side view of the top of Wall 2 showing the cracks that appeared at 30,000 lb load.

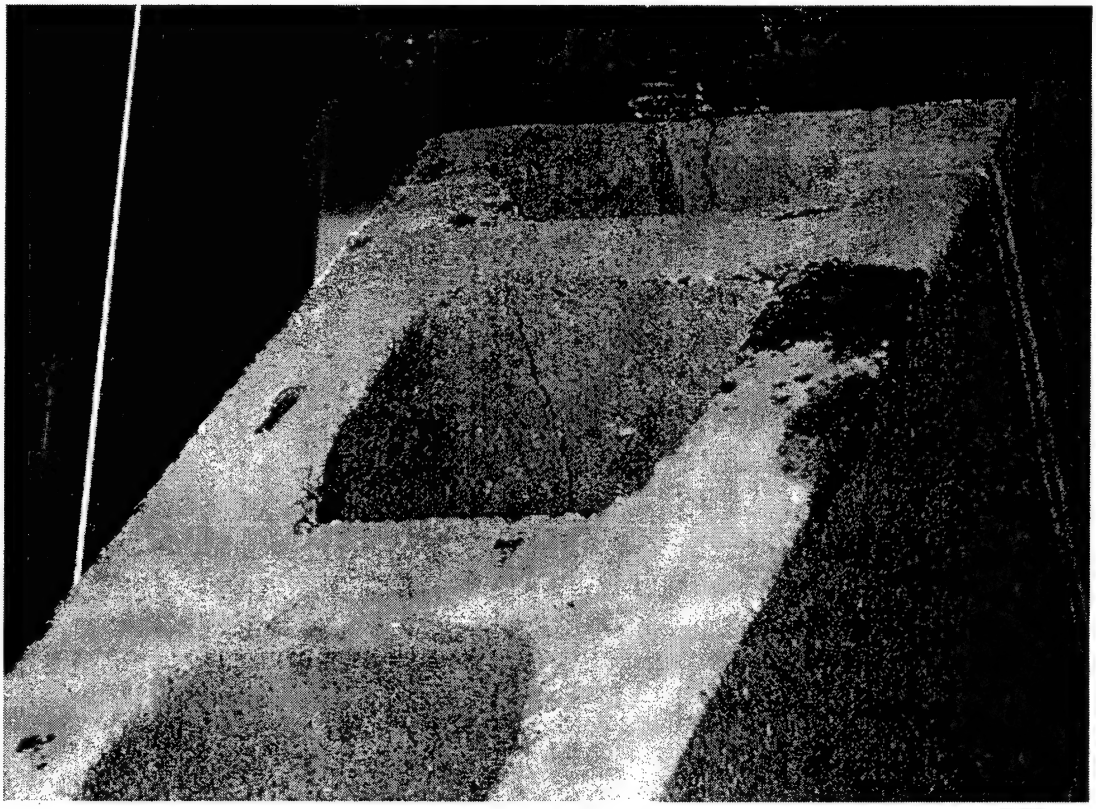

Figure 29. Oblique view of concrete block from Wall 6 showing internal cracks that appeared at 30,000 lb load.

As the load was increased to 38,000 lb, cracking was heard. Examination of the wall showed that the cracks in the top blocks had grown. The damage metric for PE sensor 2 went down slightly at this point. When the load reached 44,000 lb, some of the composite debonded from along mortar joints about halfway between PE sensors 3 and 4. At this point, the damage metrics jumped to double their previous value.

The wall broke at 46,000 lb but continued to hold the load. A stairstep crack appeared in the wall (see inset diagram in Figure 27). The break occurred while measuring PE sensor 4, so the data for PE sensors 4 and 5 are missing from the chart. The wall continued to hold the load until it failed at 56,000 lb. When the wall broke, the damage metrics for all PE sensors jumped. The composite material held the wall together, however, enabling the wall to continue holding the load. When the wall finally failed completely, the composite layer sheared off the bottom blocks and the lower blocks collapsed (see Figure 30).

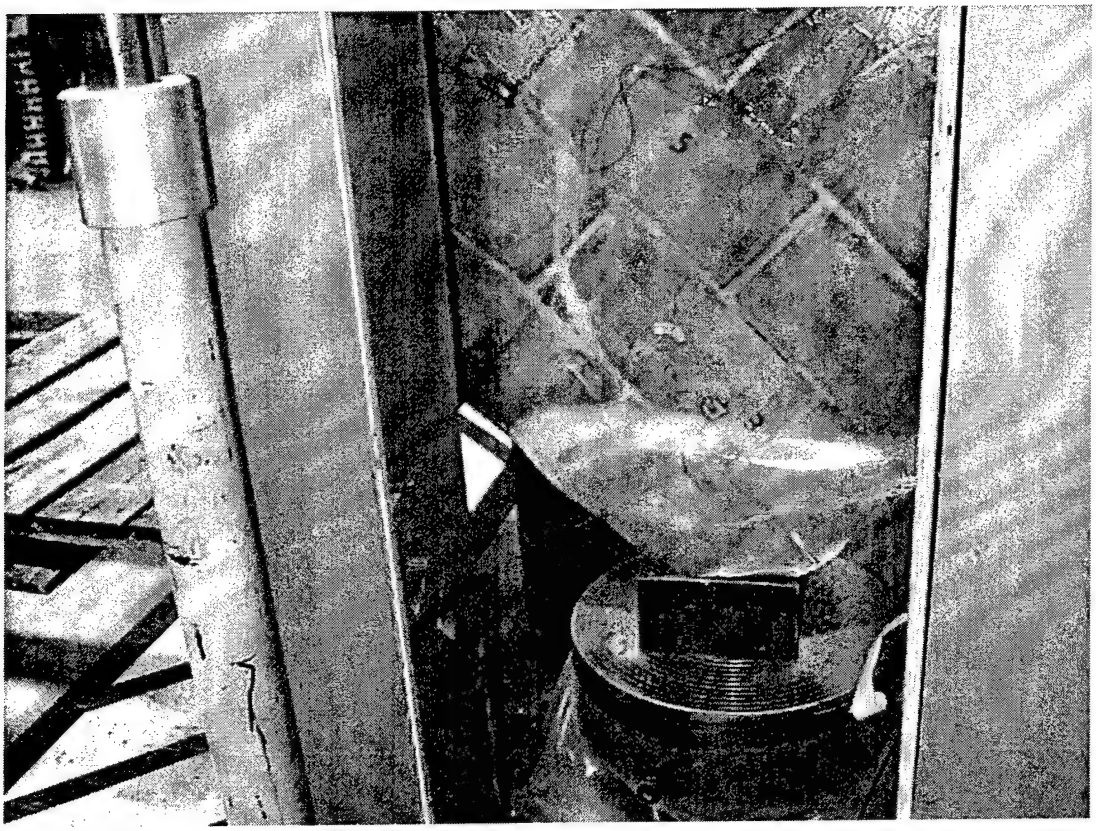

**Figure 30. Wall 6 after failure. Note the large section of composite layer that has debonded near the bottom load shoe. The top to bottom failure in the wall can be seen as a lighter gray zigzag on the left of the picture.**

### *Wall 7*

Wall 7 was a 4 x 4 ft concrete masonry block wall reinforced with composite reinforcement manufactured by Clark Schwebel Tech-Fab Co., Anderson, SC. The material used was T-1012 glass reinforced epoxy structural grid consisting of two layers oriented at 90 degrees to each other and covered with epoxy.

The wall was tested by applying a load in stages until the wall failed. The rate of loading was set to 2500 lb/min. The initial steps were 10,000 lb apart. After 30,000 lb, the step size was reduced to 3000 lb. The Correlation Metric was used to interpret the information from PE sensors 1 – 5.

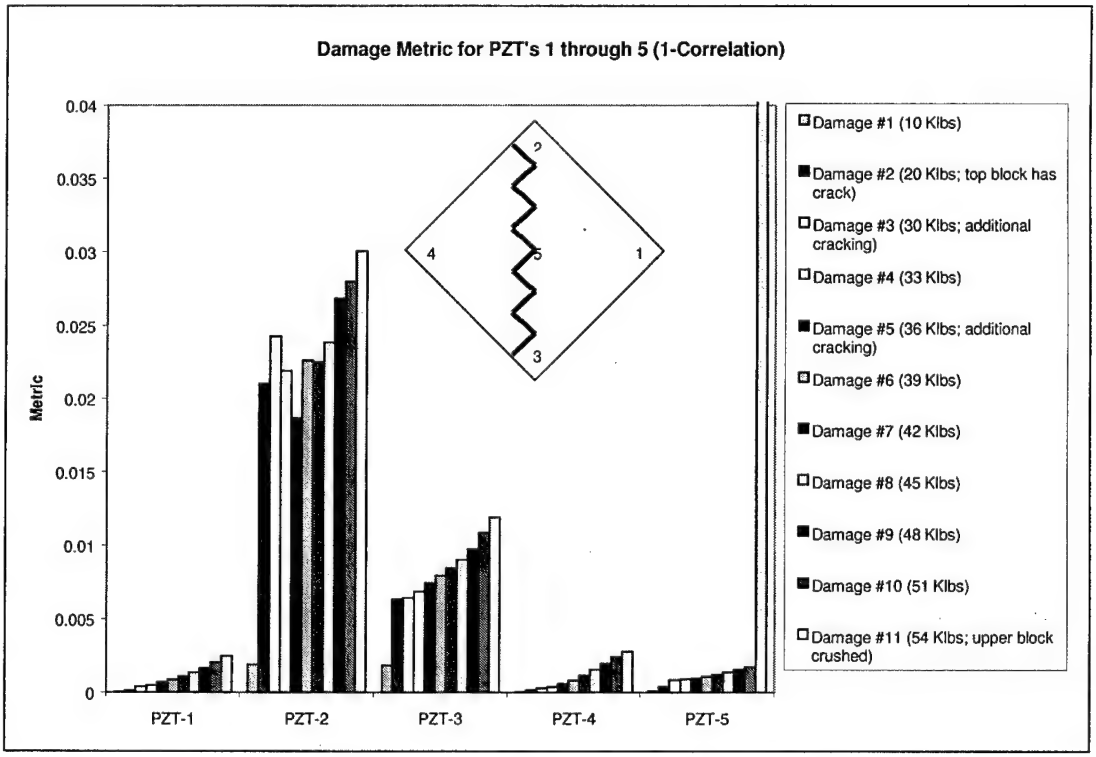


NOTE: *PZT* was an earlier abbreviation for *PE patch sensor*, but is now superseded. In this chart, PZT means PE patch sensor.

**Figure 31. Correlation Metric for Wall 7, PE sensors 1 – 5. The data for Damage 11, PE sensor 5 is off the chart. Its value is 0.27.**

It can be seen in Figure 31 that the damage metric was greatest at the top of the wall. The damage metric for PE sensor 2 was small at the beginning, but jumped when the load reached 20,000 lb. Cracking was heard while approaching this load and, upon inspection, it was found that the top block had cracked. As the load increased, noises were heard at 30,000, 33,000 and 36,000 lb. The cracks in the top block grew during this time. Figure 32 shows the resultant cracks. The damage metric first grew, then it fell at loads of 33,000 and 36,000 lb. After that, the metric rose until the wall failed.

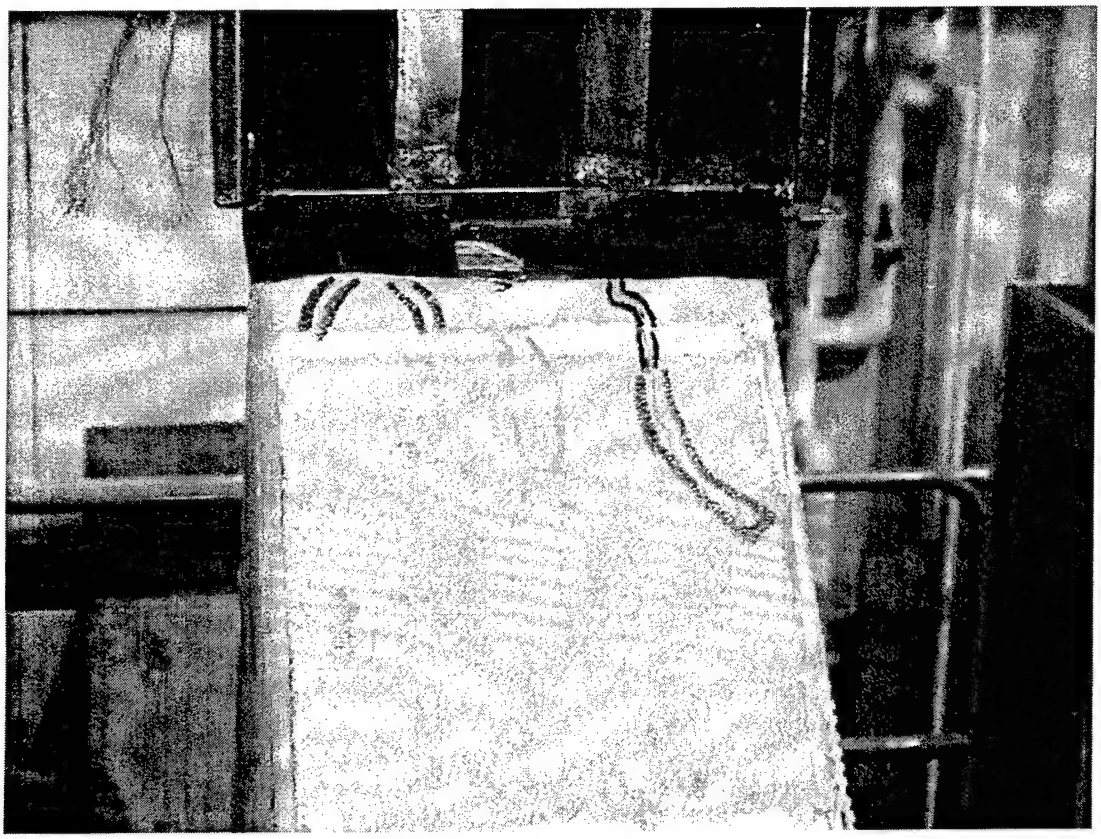

**Figure 32. A side view of the top of Wall 7 showing cracks that were present at 36,000 lb load. The original crack which appeared at 20,000 lb load only reached as far down as the first mortar line. The cracks are very thin and are outlined with a marker pen to aid in visualization.**

During this time, the damage metric for PE sensor 3 jumped at 20,000 lb but showed only normal growth after that. The implication here is that no further cracking occurred in the lower block until the wall failed. PE sensors 1 and 4 show only regular growth with load.

There was no further cracking from 36,000 to 51,000 lb. At 54,000 lb, we again heard a noise. Upon inspection, the bottom block had crushed slightly (see Figure 33. That damage was not reflected in the damage metric for PE sensor 3. That PE sensor only showed normal growth with load. On the other hand, PE sensor 5, in the center of the wall, damage metric increased dramatically. The value is off the graph in Figure 31 and had a value of 0.27 — 10 times the largest value of any other PE sensor. Finally, at 56,000 lb, the wall failed with a large stair step pattern along the mortar lines. In addition, several blocks along that line were shattered.

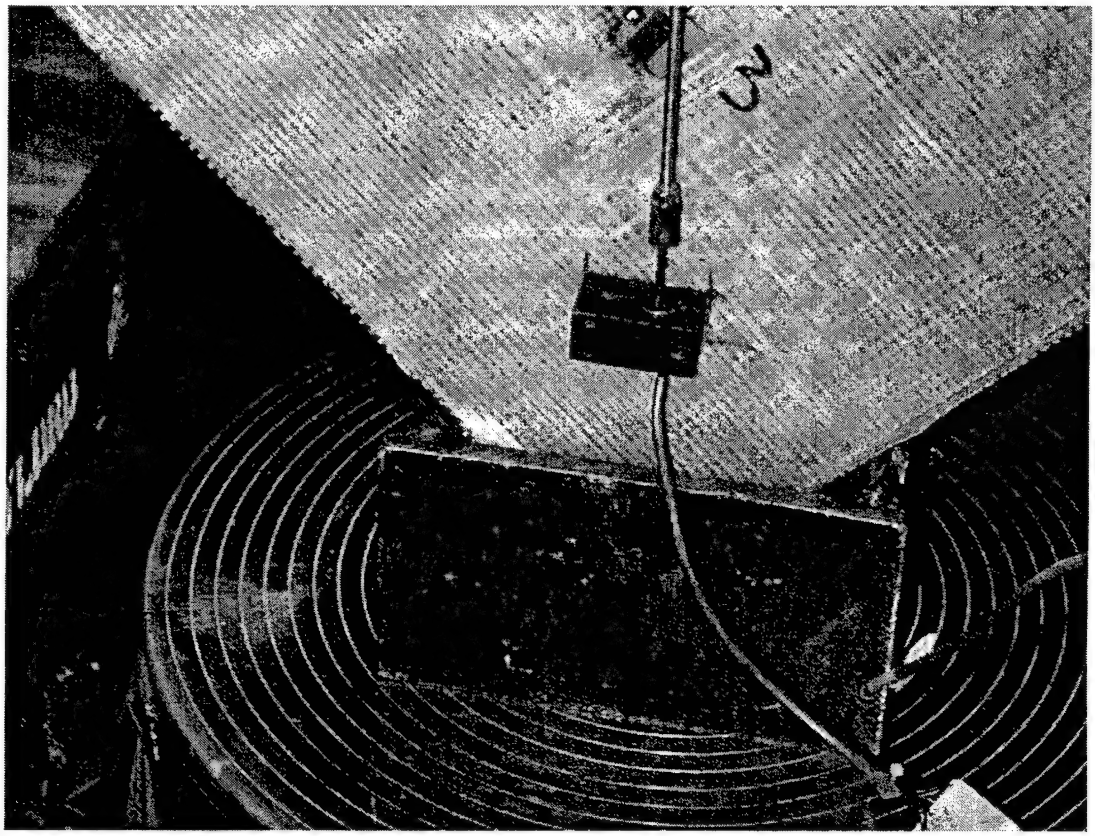

**Figure 33. A view of the bottom shoe at 54,000 lb. The concrete masonry block had given way and a small portion of the composite was crushed. The crushed portion is visible at the left edge of the shoe. PE sensor 3, visible at the top of the picture, only recorded a slight increase in damage metric.**

The very large damage metric for PE sensor 5 at 54,000 lb was investigated further. It is possible that debonding of the reinforcement layer occurred under that PE sensor. However, because the reinforcement layer is opaque, if there was any debonding it could not be seen. It is also possible that some other type of hidden damage occurred near PE sensor 5. When the wall failed, the stair step failure passed directly underneath PE sensor 5.

To test the hypothesis that the large reading may have been due to failure of the PE sensor or its wiring, the raw data for Wall 7 (shown in Figure 34) were reviewed The data show that the peaks in the response were greatly reduced for just this one load, which accounts for the large change in the damage metric. The other parts of the impedance curve follow closely the curves for the other loads. Therefore, it was concluded that the PE sensor was working correctly.

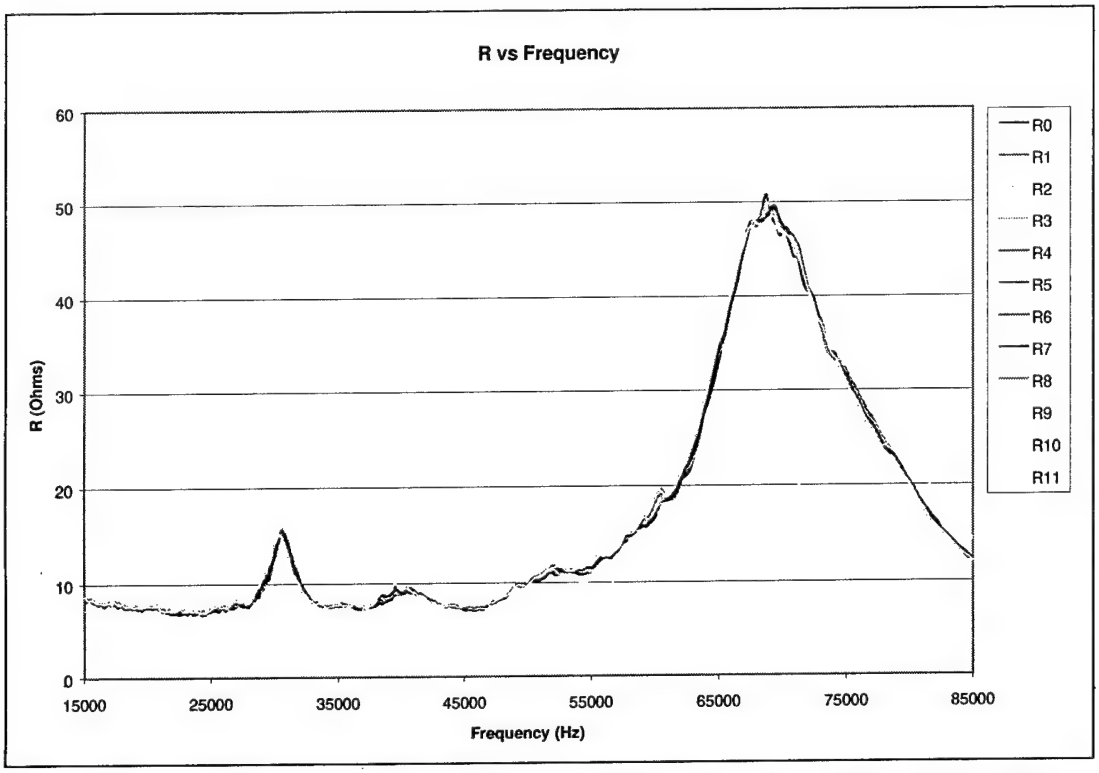


**Figure 34. The resistive portion of the impedance for Wall 3, PE sensor 5. The real part of the impedance for the 53,000 lb load has its peaks quite reduced compared to other loads, but the rest of the curve follows the earlier runs. It is unlikely, therefore, that the PE sensor had failed.**

## Discussion of Results

The data collected from PE sensors on the eight test walls generally reflected structural damage as it occurred. However, two factors made it difficult to predict damage before it was visible to an observer. The main reason was that the loading was carried out in discrete blocks. Hence, if damage occurred while the load was increased from one step to the next, it was often detected after the crack was physically visible. The reason contributing to this effect was that the data acquisition system had a minimum time requirement to obtain a set of readings from all the attached PE sensors. The time needed to acquire a complete set of data from all sensors was longer than the time taken to increase the load from one step to the next. The load was normally increased in steps of 5000 lb. However, if the load had been increased in much smaller steps (maybe 800 to 1000 lb per step), and time had been available to make a complete set of readings from all sensors at each load step, there is little doubt that damage prediction of damage would have improved dramatically.

Twice during the testing a PE sensor picked up damage to the structure while the load was being increased. The damage metric chart on the computer screen

clearly indicated debonding, which in turn indicated that cracking was imminent in the wall due to failure of the composite upgrade to provide shear transfer to the wall. In these cases, a new crack became visible seconds later. This result strongly indicates that, if loads had been increased in smaller steps (as would probably happen in real life applications), this technology would be very successful in detecting debonding of composite reinforcement well in advance of cracks appearing in the masonry.

It should be noted that the PE sensors are much more sensitive to debonding effects than to cracks in the concrete block. If cracks appeared in the concrete block without debonding at the composite/concrete interface, the PE sensors will not show significant change. However, it was observed that debonding was the first stage of crack propagation.

The Correlation Metric charts were found to be very useful in providing a quick graphical indication of the extent of structural damage in the test walls. Using the damage metric values, a numerical comparison of the damage between successive tests could be made to quantify the extent of damage.

# 5 Structural Monitoring Demonstration Using PE Sensors

## Introduction

The Naval Facilities Engineering Service Center (NFESC, Port Hueneme, CA) reinforced the underside of a section of Norfolk Pier 11 with a carbon-fiber composite reinforcement grid in order to upgrade its maximum loading capacity by 10 percent. The bond between the concrete pier and the composite reinforcement must be maintained at all times to ensure proper performance. The impedance-based qualitative structural integrity monitoring technique is well suited for such an application because no analytical modeling is necessary and the PE sensors can be retrofitted nondestructively.

## Technical Objective

The main objective of this phase of the work was to adapt the impedance-based technique to monitor the structural integrity of Pier 11 after being reinforced with carbon-fiber composites. This work focused on the two types of damage most likely to occur in this application: (1) edge debonding of the composite from the concrete substrate and (2) delamination within the composite in the area of maximum loading. Another important issue considered was the effects of a harsh marine environment on installation and operation of the PE sensors.

## Grid Layout and Instrumentation

The carbon-fiber composite material was applied to Pier 11 in a grid pattern [0/90] using strips approximately 12 in. wide. The reinforced area measured approximately 19 x 14 ft, and the grid comprised 12 strips by 9 strips, respectively. Each strip was separated from adjacent parallel strips by 6 in. The PE sensors were installed on areas of the test section most likely to degrade under real-world operating conditions:

- each of the four corners
- the middle of the test section, which is subject to the highest loading.

With each 1.25 x 1.25 x 0.01 in. PE sensor having a sensing radius of 12 in. (i.e., the width of each composite strip), it was determined that the test section could be monitored effectively with 24 sensors — 5 in each of the four corners and 4 in the center. A diagram of the grid, the sensor locations, and sensor tracking numbers is shown in Figure 35. In this configuration the corner sensors were capable of monitoring the areas in Figure 36 shaded medium gray.

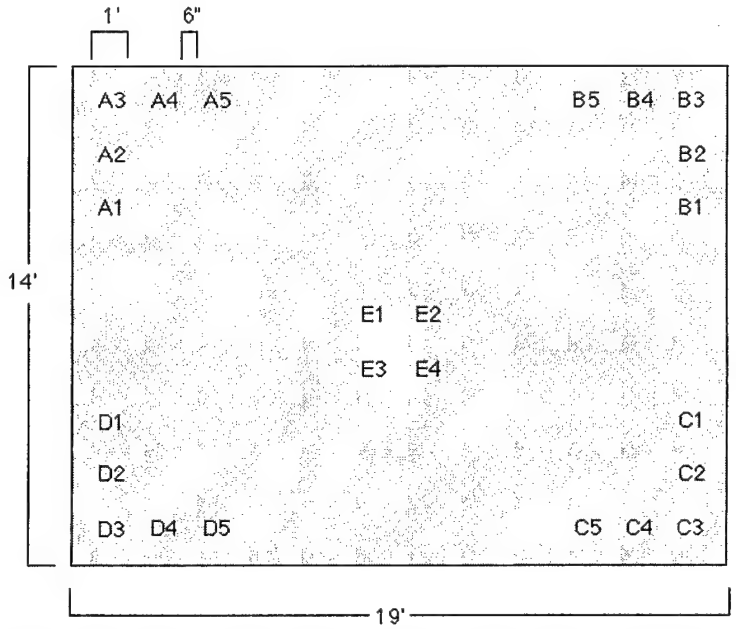


**Figure 35. Diagram of sensor locations and tracking numbers on Pier 11.**

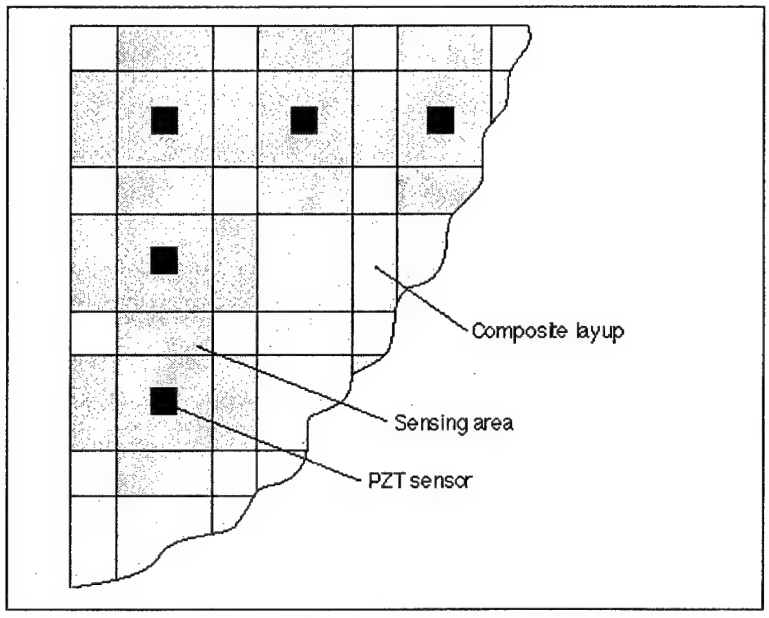


**Figure 36. Schematic of edge sensors bonded at the middle of composite strip intersections.**

The PE sensors were located on the composite reinforcement measuring approximately 14 x 19 ft. For the corner debonds, a total of 5 PE sensors located 18 in. apart monitored the edge up to 48 in. from the corner. Each PE sensor was bonded 12 in. from the edge. For the monitoring of the high-load region, 4 PE sensors located 18 in. apart monitored an area of 42 x 42 in.

### *Sensor Installation Issues*

Based on the results of preliminary laboratory experiments described in Chapter 3, a detailed protocol was developed for bonding PE sensors to the composite reinforcement under the concrete pier. The protocol not only incorporated lessons learned in the laboratory experiments but also addressed site-specific issues for Norfolk Pier 11 and similar applications. One such issue was the need to protect all sensors and wiring from pier traffic and the marine environment. Another issue was the need to ensure the quality of the bond in relatively inaccessible locations.

For many applications it would be easy to clamp the PE sensor to the substrate during bonding, or to apply pressure through some other simple means. However, because the PE sensors were applied under Pier 11 to an overhanging surface, pressure during bonding was applied using the vacuum bag technique described in Chapter 4 (see Figure 37). Epoxy and silicone sealants were used to weatherproof all PE sensors and exposed electrical connections. A junction box was bolted to a conveniently located site on the pier, serving as a convergence point for the leads from all installed sensors (Figure 38). By connecting a computer-controlled impedance analyzer to the wires in this junction box, a technician can easily collect data for the entire test section of the pier.

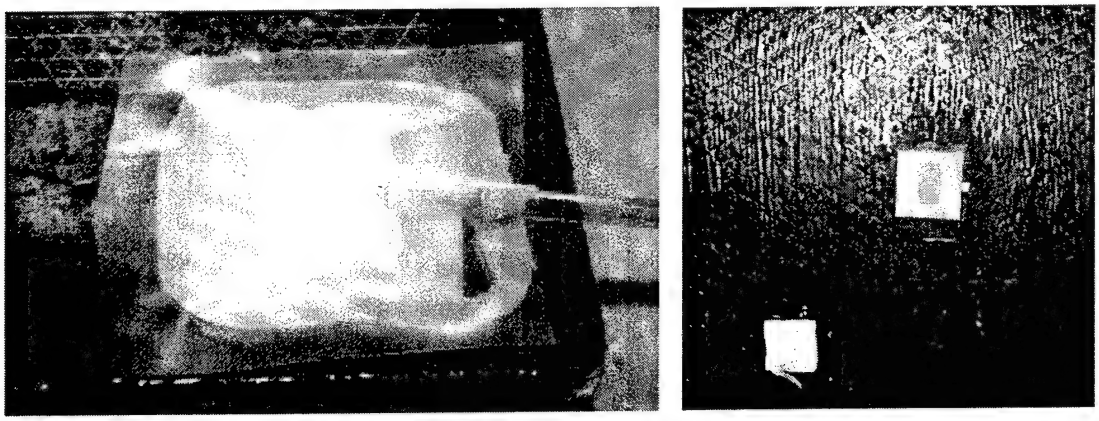

**Figure 37. Laboratory-tested vacuum bag procedure (left) was used to install the PE sensors on the underside of Norfolk Pier 11 (right).**

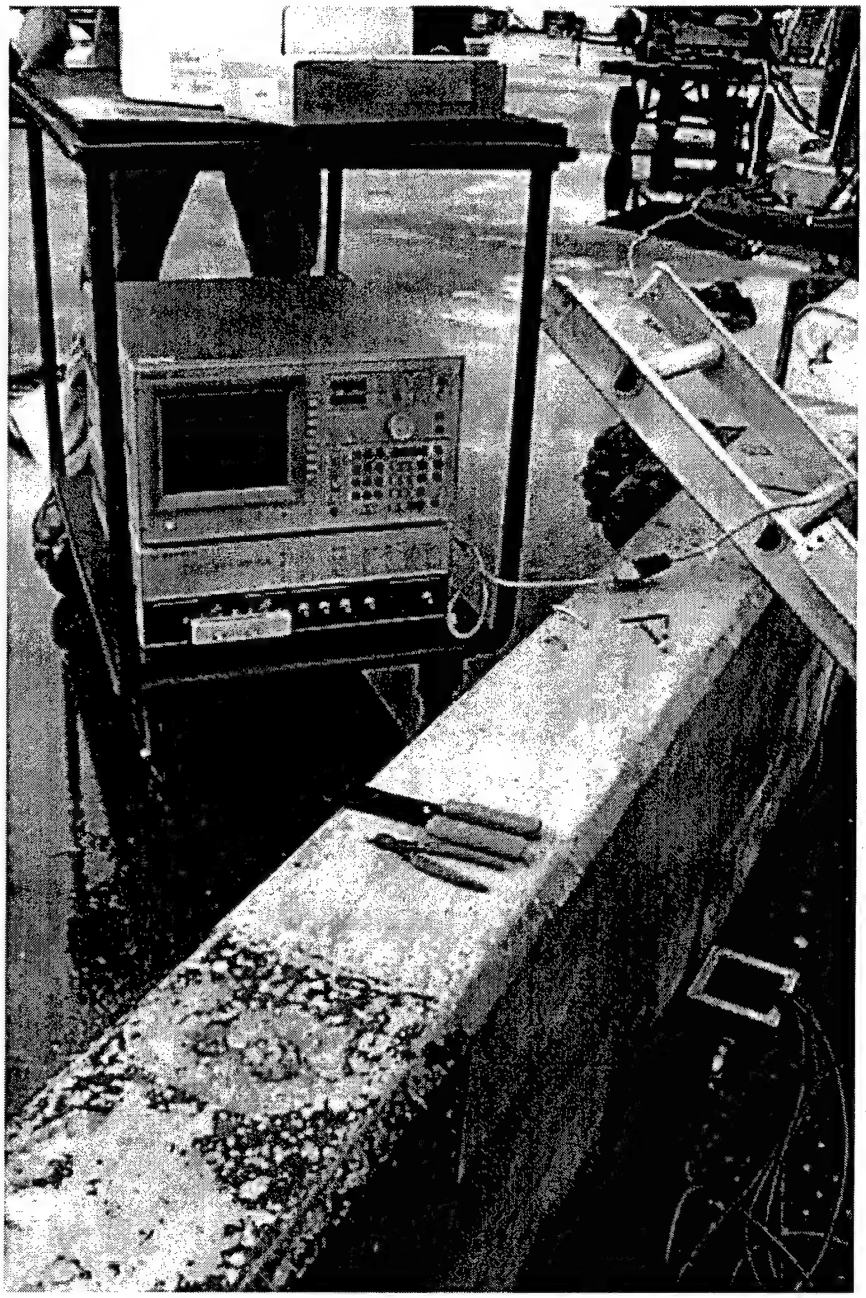

Figure 38. Impedance analyzer setup showing junction box at lower right.

### *Bonding Procedure*

The sensor installation procedure used at Norfolk Pier 11 is listed below:

1. Make sure that the graphite composite reinforcement has fully cured.
2. Mark the locations of all PE sensors (see Figure 35).
3. At each PE sensor location, sand the fiberglass mesh facing off the composite surface taking great care not to damage the reinforcement material underneath.
4. Clean the surface of the reinforcement material with acetone and dry it.

5. Clean the surface of the PE sensor with acetone and dry it.
6. Install each sensor at its prepared location using the vacuum bag technique as follows:

    a. Install the air dam.
    b. Embed the vacuum line in the air dam.
    c. Apply cyano-acrylate adhesive to the layered sensor assemblies ( consisting of plastic, foam, Teflon, double-sided tape, and PE sensor, prepared in advance).
    d. Apply the layered assemblies to the graphite reinforcement.
    e. Apply vacuum and check for leaks.
    f. Let cyano-acrylate adhesive cure for 2 hours under vacuum.

7. Bond all sensors using the procedure described in step 5.
8. Bolt the weatherproof junction box to the waler.
9. Install protective steel wire conduit from the junction box to the pier edge.
10. Run a weatherproof 10-conductor, 24 gauge shielded cable from the junction box underneath the pier to each selected measurement area on the graphite reinforcement (i.e., the four corners and the center).
11. Attach the weatherproof cables to the pier using self-adhesive wire clamps.
12. Solder the leads to each PE sensor.
13. Weatherproof all PE sensors with epoxy.
14. Weatherproof all wire ends with silicone.
15. Connect every wire to a terminal in the junction box.
16. Weatherproof the junction box.
17. Make impedance measurements to verify all connections and sensor responses.

Under favorable working conditions, and with experienced installers, a two-person crew could have completed the Pier 11 sensor installation in three 10-hour days (60 man-hours total) with little or no sensor failure. Subsequent visits to make impedance measurements would require an estimated 3 man-hours.

#### Difficulties Encountered During Sensor Installation (November 1996)

Difficult work conditions were encountered during sensor installation on 25 – 27 November 1996. First, problems arose due to the condition of the composite reinforcement at the time of sensor installation. The epoxy resin in the reinforcement grid was still tacky in several areas when the sensor installation crew arrived, and this made it difficult to prepare a good bonding surface for the sensors. The uncured resin also presented another problem: baseline impedance values taken from uncured composite material might be expected to differ significantly from later measurements taken after the resin had fully cured. In other words, impedance values taken from partially cured composite material

could provide false baseline data which would, when compared to later measurements taken from the cured composite, falsely indicate damage.

The initial impedance measurements made during this visit indicated that six sensors — 25 percent of the total — were not working properly. On the final day of the visit the surf was too rough to allow safe access to the floating platform under the pier, from which the workers were installing the PE sensors and wiring. Consequently, a second visit (on 9 January 1997) was required to complete the installation and make a full, valid baseline set of impedance measurements. However, these initial impedance measurements proved to be valuable for system diagnostic purposes and for comparison with the full baseline data set made during the subsequent January visit.

Tasks remaining for completion during the follow-up visit were as follows:

- Sensor A1 needed to be connected.
- Sensors A1, B2, B3, B4, B5, E1, E2, E3, and E4 needed to be weatherproofed with epoxy.
- Sensors E1, E2, E3, and E4 required examination for possible faulty connections.
- A second coating of silicone sealant was needed for the wires in corners C and D of the composite grid.

#### Follow-up Field Work (January 1997)

First, the work performed during the November 1996 visit was inspected. It was found that, overall, the installed sensors had effectively withstood the harsh winter marine environment. The following observations were noted:

- The junction box remained well sealed, and no signs of moisture or degradation were observed inside the box.
- The wires connecting the PE sensors in corners C and D were hanging loosely. Although the electrical connections remained intact, the single coating of silicone had not been sufficient to hold the wires in place. However, the wires for sensor groups A, B, and E, to which two coats of silicone were applied, remained well protected and held in place.
- The epoxy protection applied to the PE sensors worked very well, and no degradation was observed.
- The PE sensors to which no protective epoxy had been applied (A1, B2, B3, B4, B5, E1, E2, E3, E4) showed significant corrosion at the copper connection tab and on the solder. A white corrosion residue accumulated only at the sol-

der locations, leaving the bodies of the PE sensors with no apparent corrosion.

- While attempting to wipe the corrosion residue from the unprotected PE sensors, small portions of the nickel-plating came off the electrode near the solder connection.

After the inspection, the unfinished work from the November visit was completed where possible:

- The wiring connection to sensor A1 was made.
- The unprotected PE sensors giving questionable results were reconnected.
- All unprotected PE sensors (A1, B2, B3, B4, B5, E1, E2, E3, E4) were sealed with epoxy.
- The problems measuring the impedance of sensors E1, E2, E3, and E4 were traced to a defective switch in the junction box. Direct connections were made to bypass the defective switch and make impedance measurements of sensor group E.

The hanging wires in corners C and D could not be re-affixed because the floating platform used during the first visit was not available. Access to these wires was blocked by sewer pipes running under the pier, and they could not be reached from the boat that was available during this visit. As noted above, however, all connections to these sensors were functional despite the hanging wires.

### *Completing the Baseline Impedance Measurements*

As noted previously, impedance measurements were made during the November 1996 visit, but technical difficulties prevented the collection of a full, valid baseline data set. During the January 1997 visit, two sets of impedance measurements were made in conjunction with the follow-up work. First, measurements were made for all installed sensors known to be connected and functional (A2, A3, A5, B3, B4, C1, C3, C4, C5, D1, D2, D4, and D5). After the follow-up work (described above) was completed, a set of measurements was taken from the affected sensors (A1, A4, B1, B2, B3, B4, B5, C2, D3, E1, E2, E3, and E4). All of these impedance measurements were made using the same procedure that was employed during the first visit.

The impedance measurements for all 24 sensors were taken across a wide frequency range. These measurements comprise the baseline data set for Norfolk Pier 11, and they were stored for reference during future inspections. Subsequent readings can be made at a scheduled interval to monitor the structural in-

tegrity of the reinforced pier section, and these measurements also will be stored in the database for long-term validation of the impedance-based technique.

The impedance measurements were made over the 10 kHz to 270 kHz frequency range in four subintervals, as listed in Table 3. The first subinterval uses a smaller frequency step to account for the large dynamic activity found at lower frequencies. In this initial test 3800 data points per PE sensor were recorded.

**Table 3. Frequency ranges used in the impedance measurements.**

| Frequency range (kHz) | No. of frequency samplings |
|---|---|
| 10 – 50 | 1600 (25 Hz step) |
| 50 – 90 | 800 (50 Hz step) |
| 90 – 190 | 1000 (100 Hz step) |
| 190 – 270 | 400 (200 Hz step) |

The anticipated time required for the installation of all the PE sensors, wiring, and junction box was estimated to be 2 days. After installation, another day was expected to be necessary for data acquisition to ensure proper sensor operation. Subsequent data acquisition required access only to the junction box, not the floating platform.

## Analysis of Impedance Measurements

### *Initial Impedance Data (November 1996)*

As noted previously, the initial impedance measurements, made during the first visit, do not include results for sensor group E due to the defective switch in the junction box. Both the real and imaginary parts of the impedance measurements are presented, even though only the real impedance measurements are to be used for structural integrity monitoring purposes. Figure 39 – Figure 42 show the real impedance for sensor groups A, B, C, and D, respectively, while Figure 43 – Figure 46 show the imaginary impedance for sensor groups A, B, C, and D, respectively. On all graphs, the data in the 30 kHz to 40 kHz frequency range are missing due to an error made during the measurements.

In terms of real impedance for all sensor groups, it can be seen that there is low dynamic activity (i.e., few peaks and valleys) over the large frequency range. This result was expected due to the high stiffness of the structure and the damping characteristics of the composite material, and it is helpful when monitoring debonds and delaminations since the new dynamic activity induced by such defects will show up very readily.

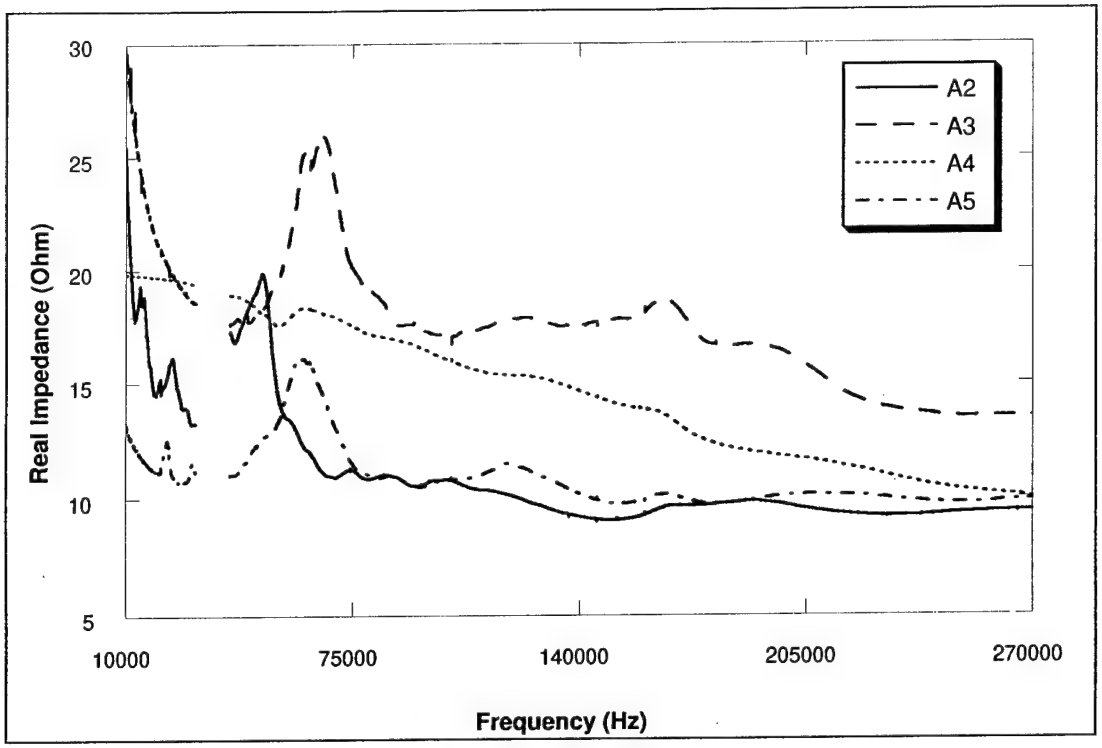


Figure 39. Real impedance first measurements of the PE sensors in group A.

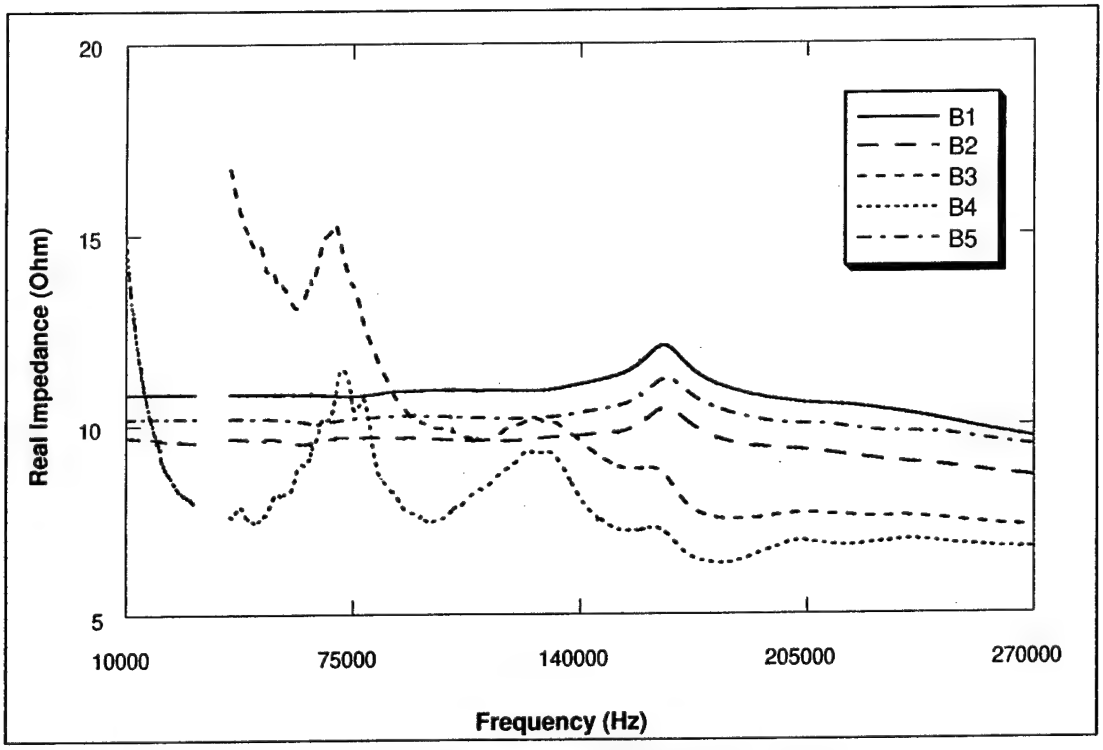


Figure 40. Real impedance first measurements of the PE sensors in group B.

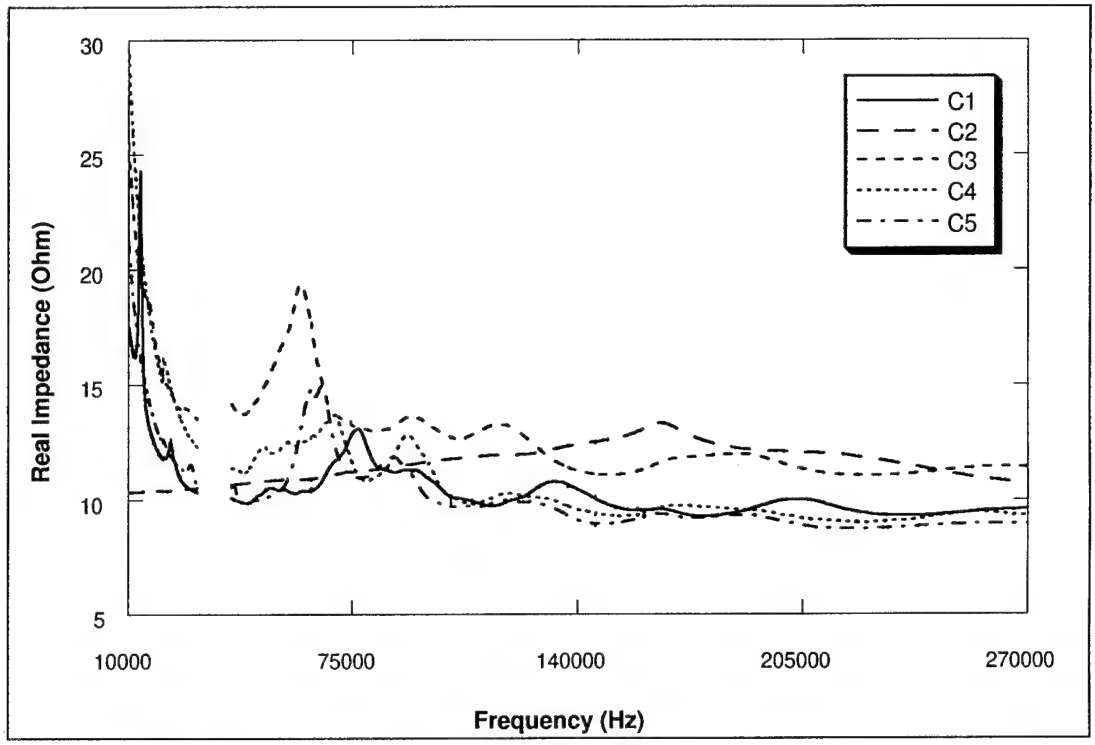


Figure 41. Real impedance first measurements of the PE sensors in group C.

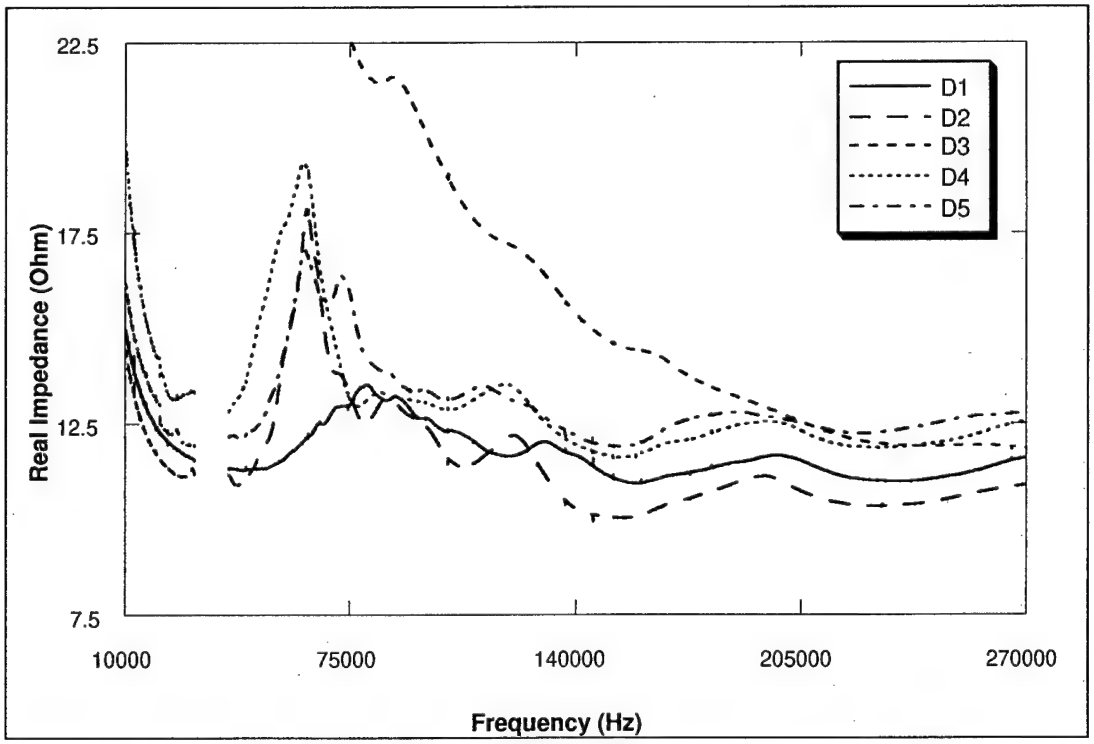


Figure 42. Real impedance first measurements of the PE sensors in group D.

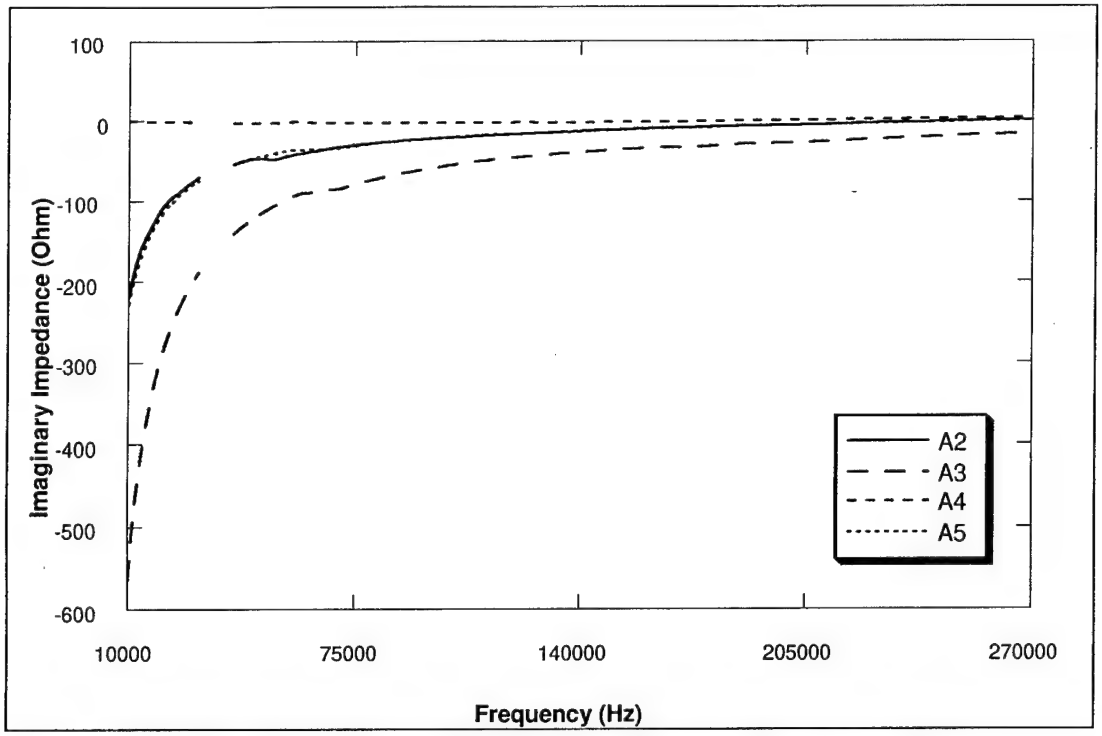


**Figure 43. Imaginary impedance first measurements of the PE sensors in group A.**

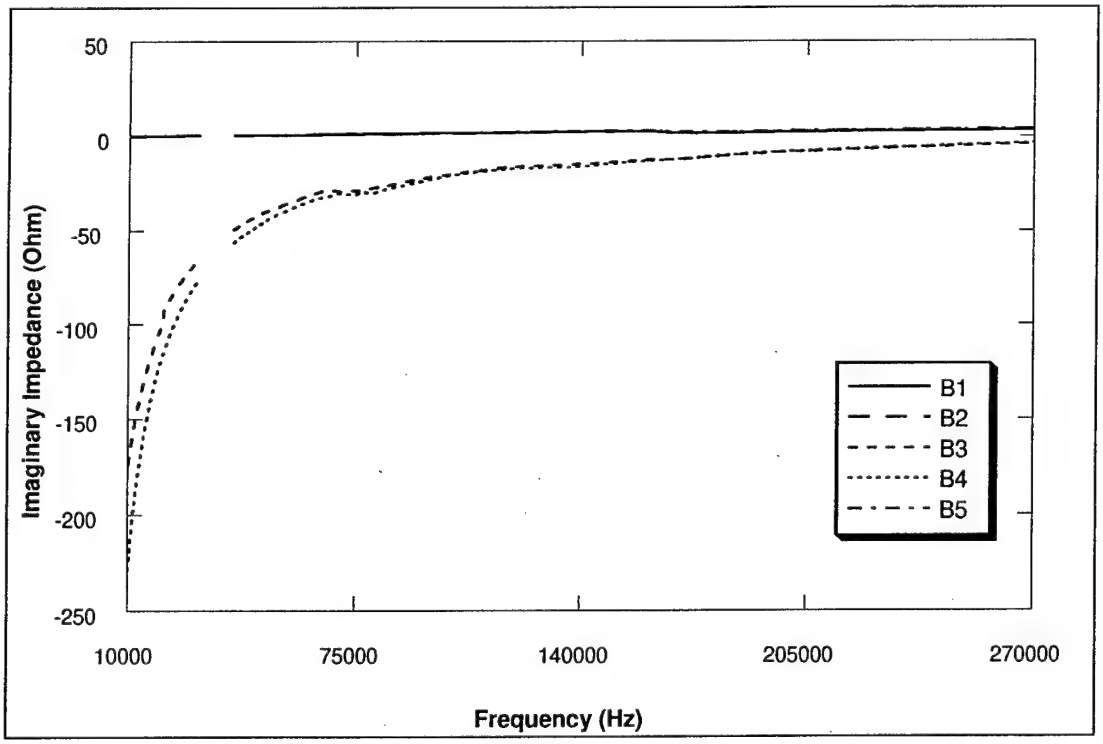


**Figure 44. Imaginary impedance first measurements of the PE sensors in group B.**

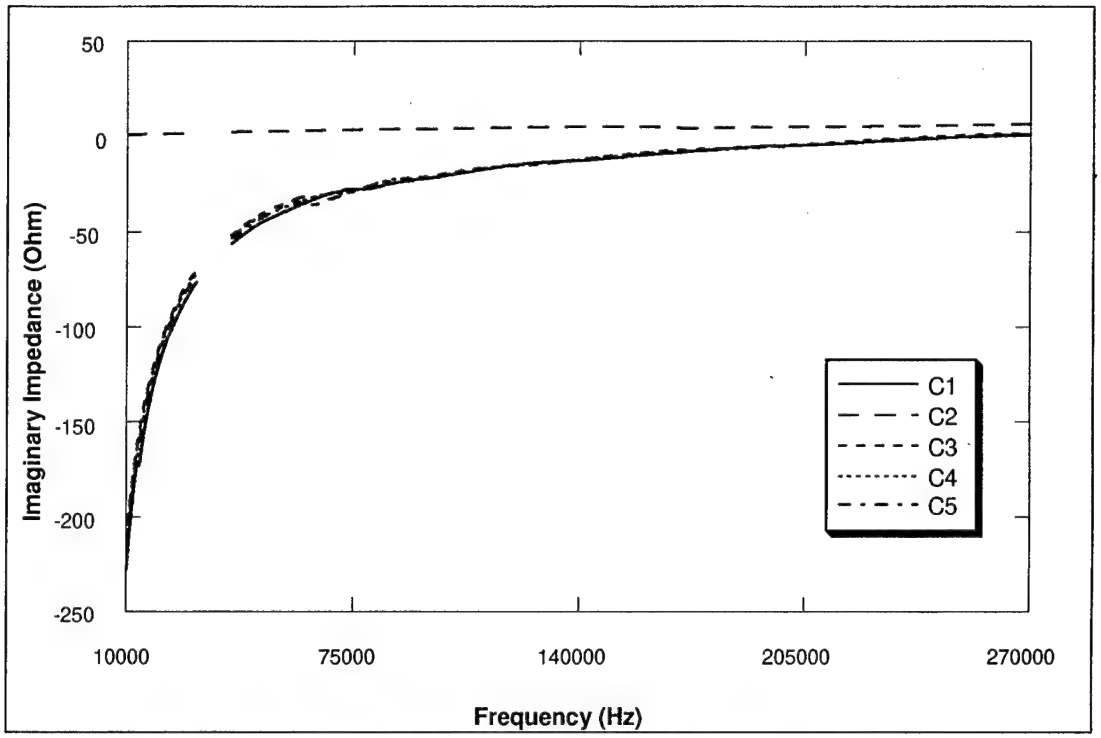


Figure 45. Imaginary impedance first measurements of the PE sensors in group C.

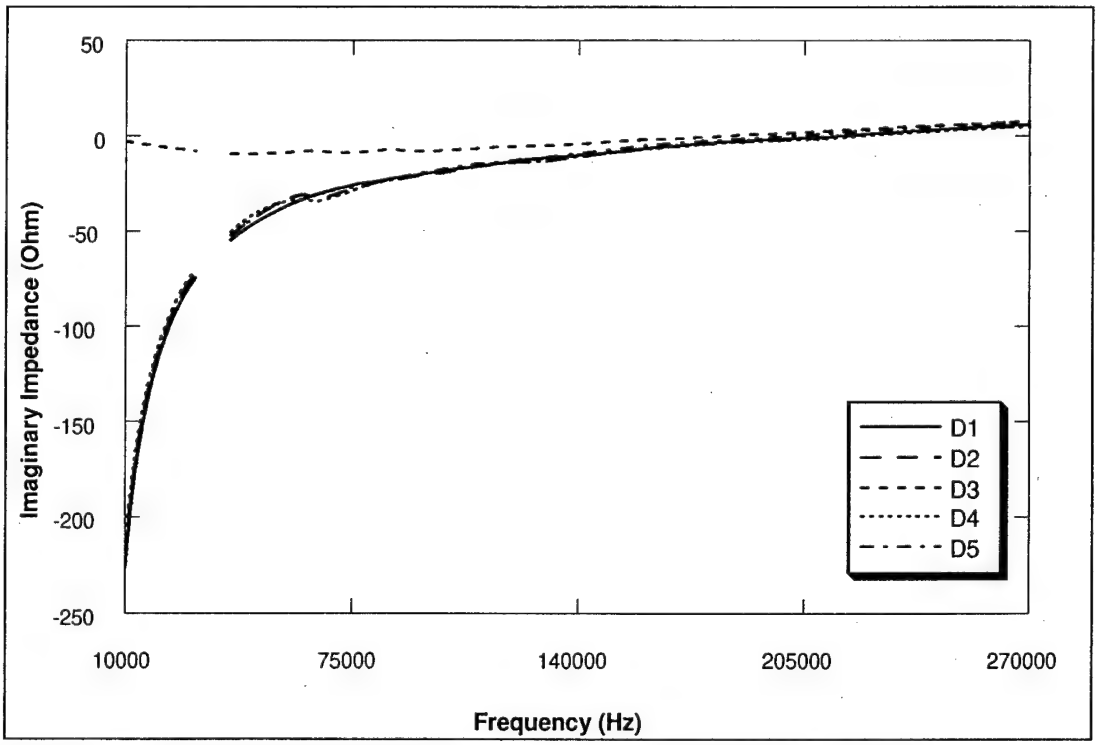


Figure 46. Imaginary impedance first measurements of the PE sensors in group D.

In the imaginary impedance graphs, very few peaks and valleys can be observed because the imaginary impedance has a high dependency on the frequency. The small variations due to the dynamic interaction between the PE sensor and the structure are obscured by the impedance uniform variation due to this frequency dependency. Because impedance variations caused by structural damage occur in the dynamic interaction, they will not be observable on the imaginary impedance graphs. This is one reason why imaginary impedance is not used in monitoring of structural damage.

Analyzing the real and imaginary impedance results, a few sensors (A4, B1, B2, B5, C2, and D3) gave unexpected results. Indeed, in all cases, the imaginary impedance is very stable over the frequency range, almost frequency independent, whereas the other sensors have a strong frequency dependency, as it should be. Furthermore, the real impedance of these sensors also gave unexpected results: the real impedance does not increase significantly at lower frequencies. In short, a close attention should be given to sensors A4, B1, B2, B5, C2, and D3 since they give unexpected, thus questionable, results.

The ambient temperature at which the impedance measurements were varied between 39 °F and 42 °F.

### *Full Baseline Impedance Data (January 1997)*

Figure 47 – Figure 51 show the real impedance for sensor groups A, B, C, D, and E, respectively, based on the January 1997 impedance measurements. These impedance measurements produced results very similar to the first ones. As in the November 1996 set, some questionable results were obtained. Sensors A4, B1, B5, C2, and D3 still gave flat real and imaginary impedance responses over the frequency range. However, sensor B2 gave results that vary with frequency. It is unclear why this change occurred between the first and second set of impedance measurements.

The ambient temperature at which the impedance measurements were made varied between 39 °F and 43 °F.

The next section presents a more detailed comparison between the first and second sets of measurements.

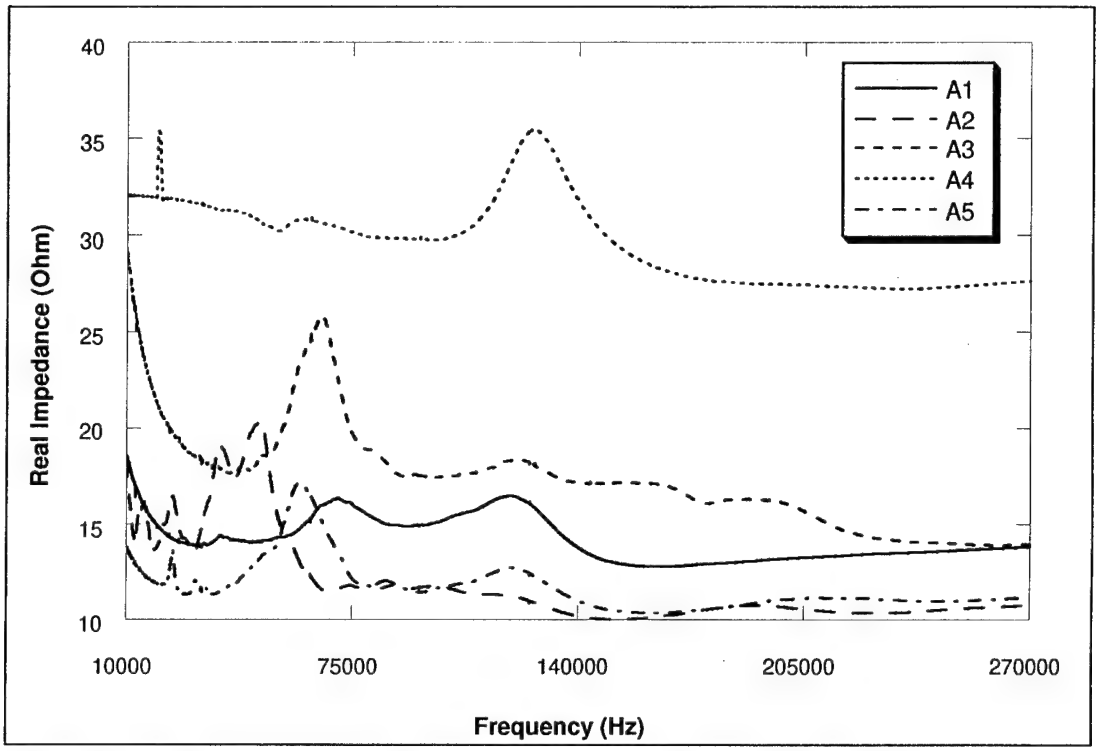


Figure 47. Real impedance second measurements of the PE sensors in group A.

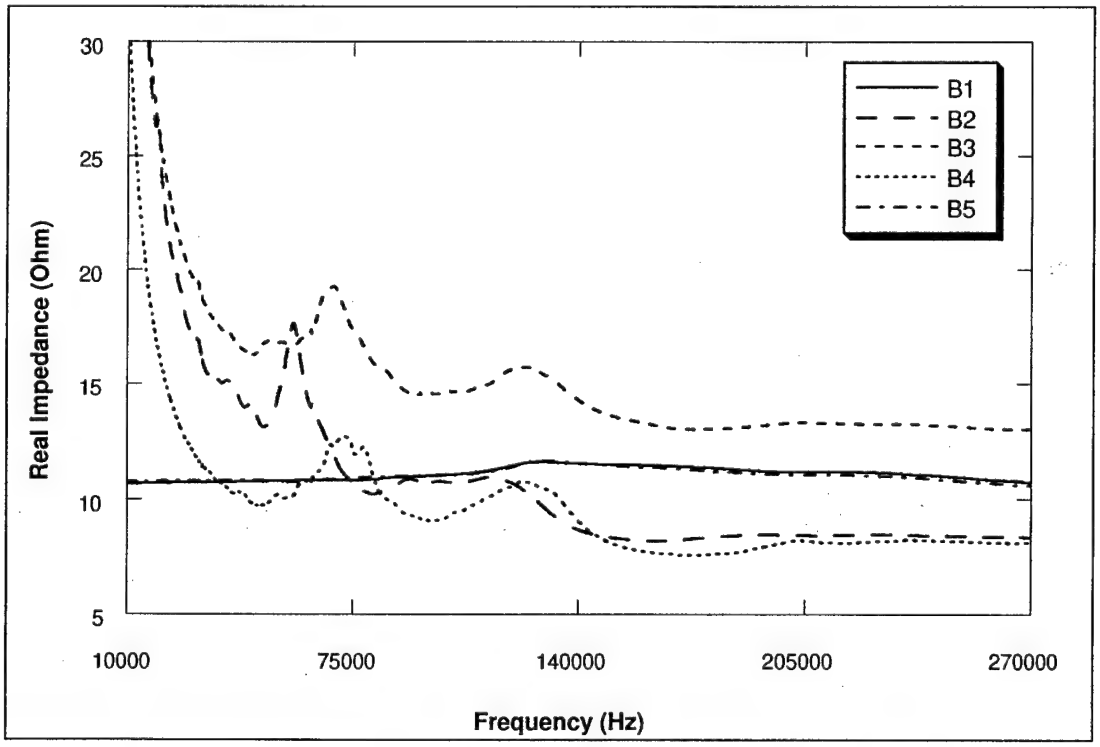


Figure 48. Real impedance second measurements of the PE sensors in group B.

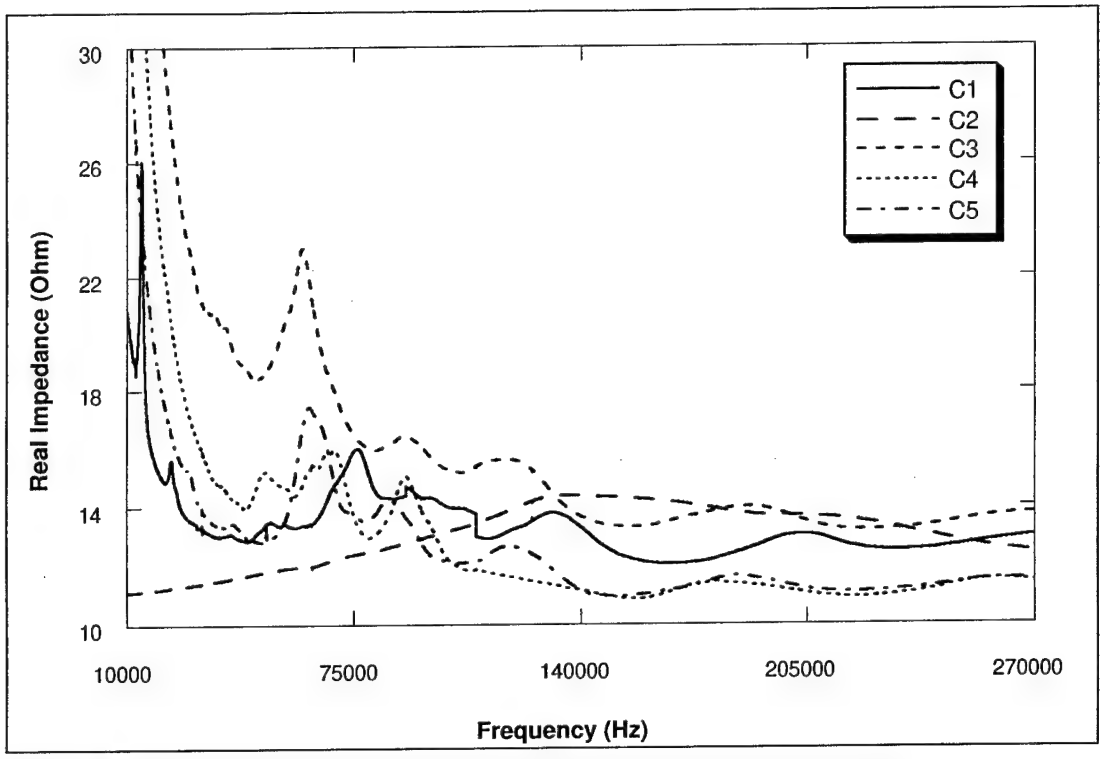


Figure 49. Real impedance second measurements of the PE sensors in group C.

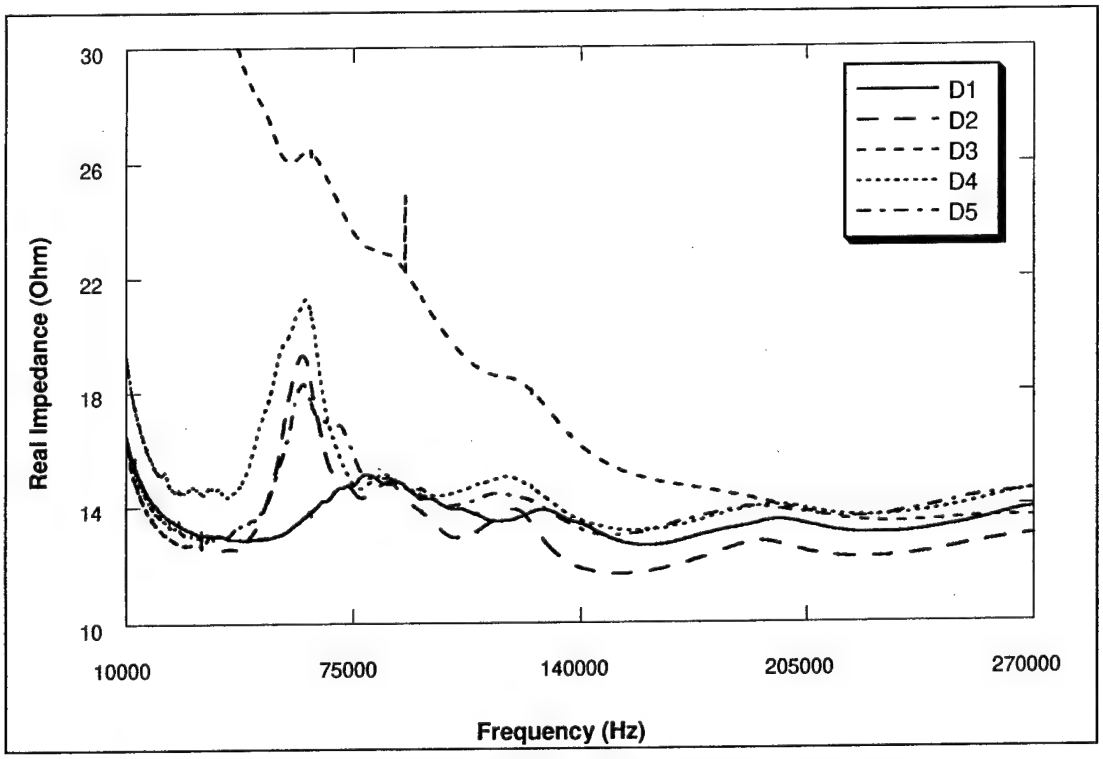


Figure 50. Real impedance second measurements of the PE sensors in group D.

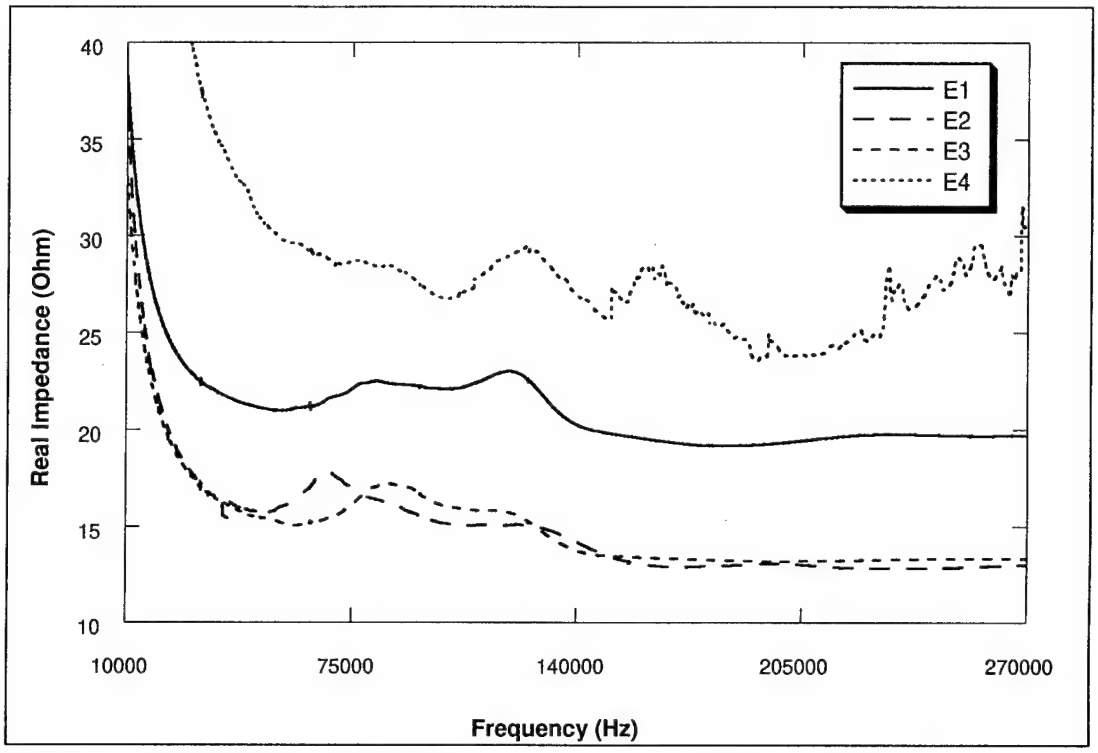


**Figure 51. Real impedance second measurements of the PE sensors in group E.**

### *Comparison of Initial Data Set With Full Baseline Impedance Data*

This section compares the November 1996 real impedance data with the January 1997 real impedance data. No comparison of the imaginary impedance measurements is made because, as noted previously, the variations were minimal and did not provide any relevant information.

Comparisons of the first and second real impedance measurements for sensor groups A, B, C, and D are shown in Figure 52 – Figure 55, respectively. The thick lines represent the first set of measurements while the thin lines represent the second set. Because sensors A1, E1, E2, E3, and E4 provided no data during the first round of measurements, these sensors are not included in the comparison graphs. Furthermore, sensors A4, B1, B2, B5, C2, and D3 were excluded from the comparison graphs because of the questionable results they returned.

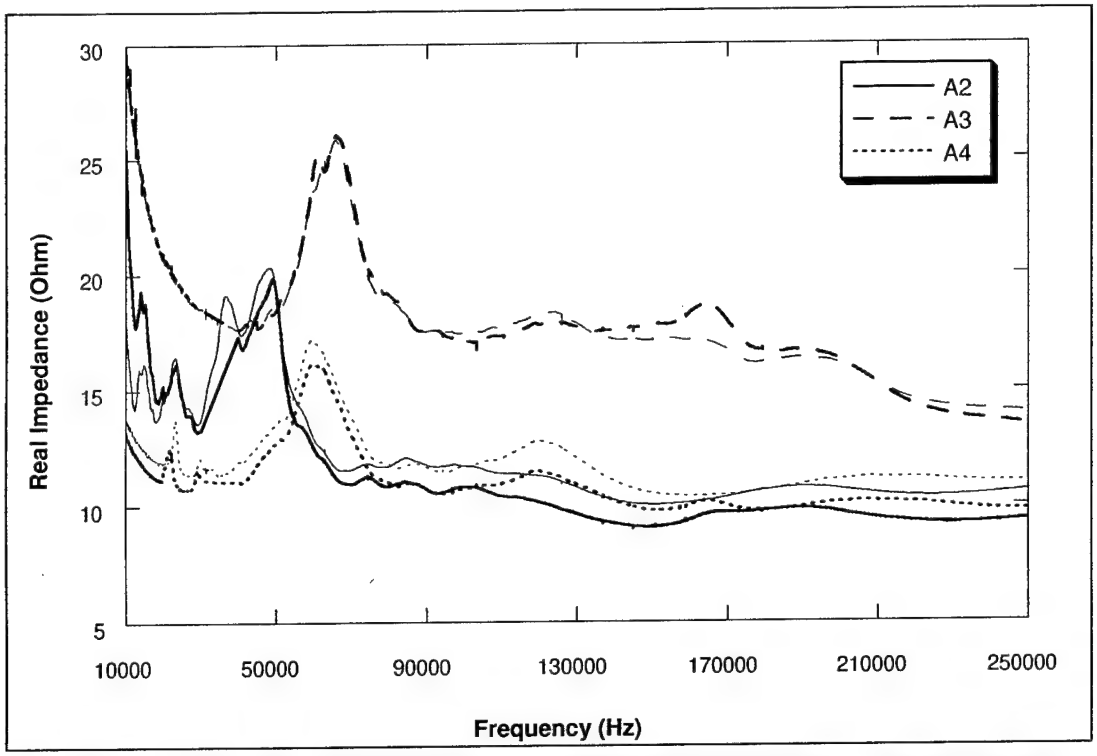


**Figure 52. Comparison the first and second real impedance measurements of sensor group A.**

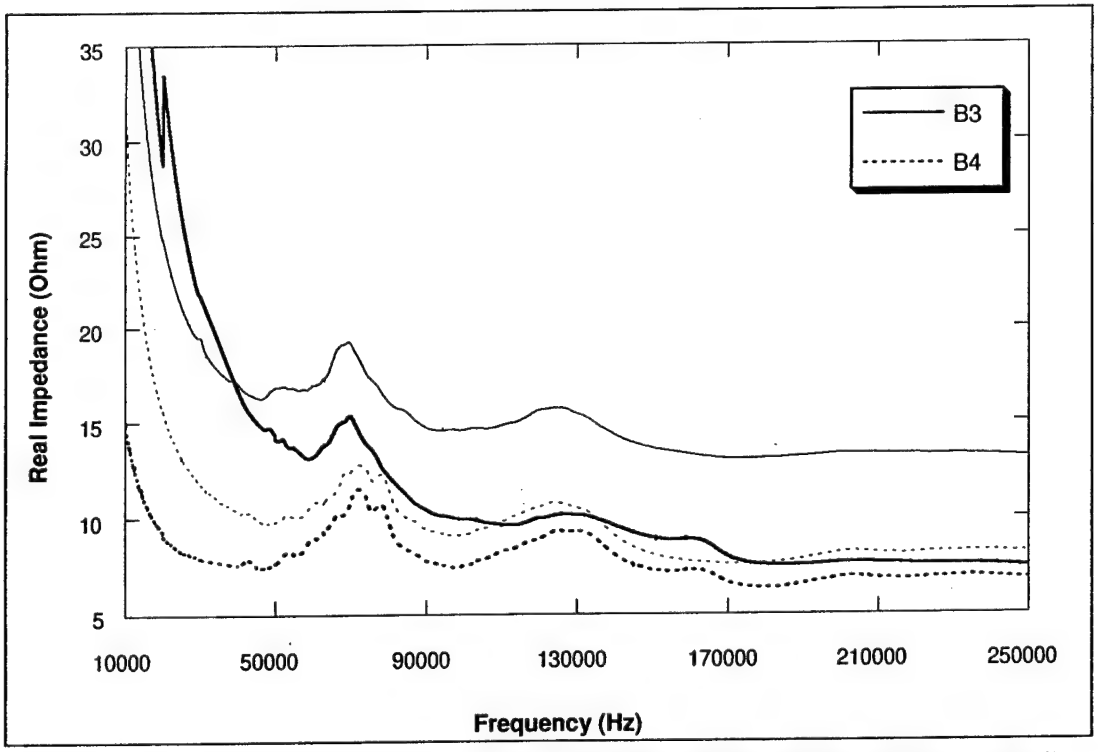


**Figure 53. Comparison the first and second real impedance measurements of sensor group B.**

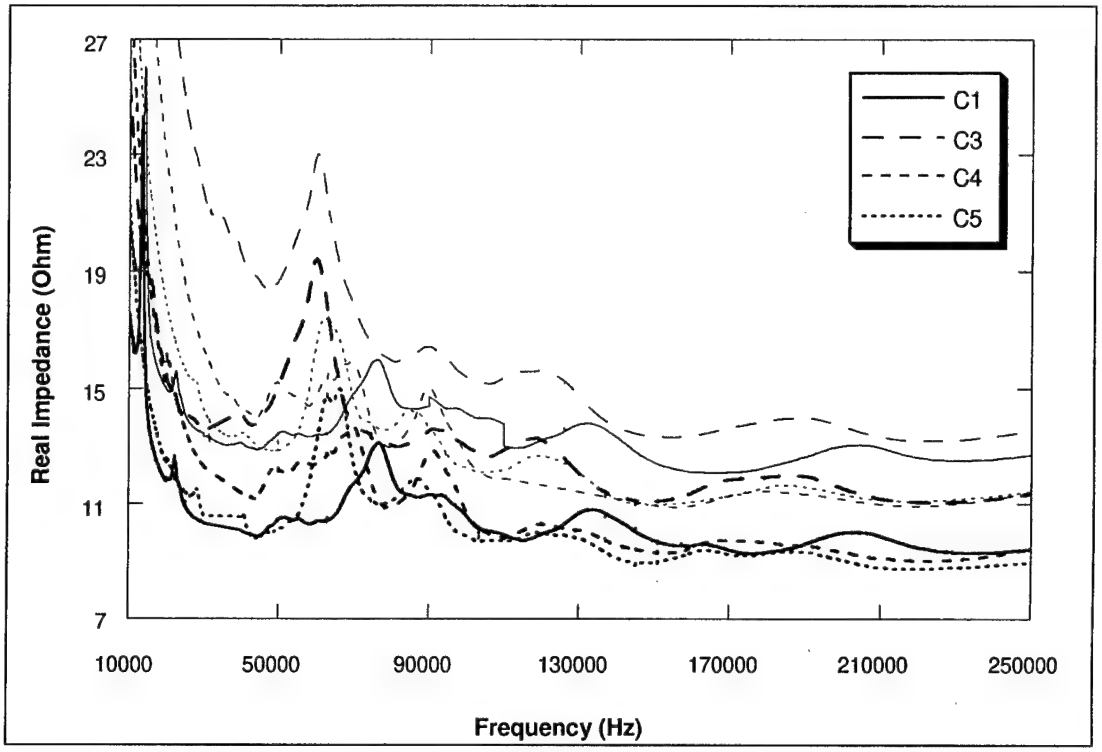


**Figure 54. Comparison the first and second real impedance measurements of sensor group C.**

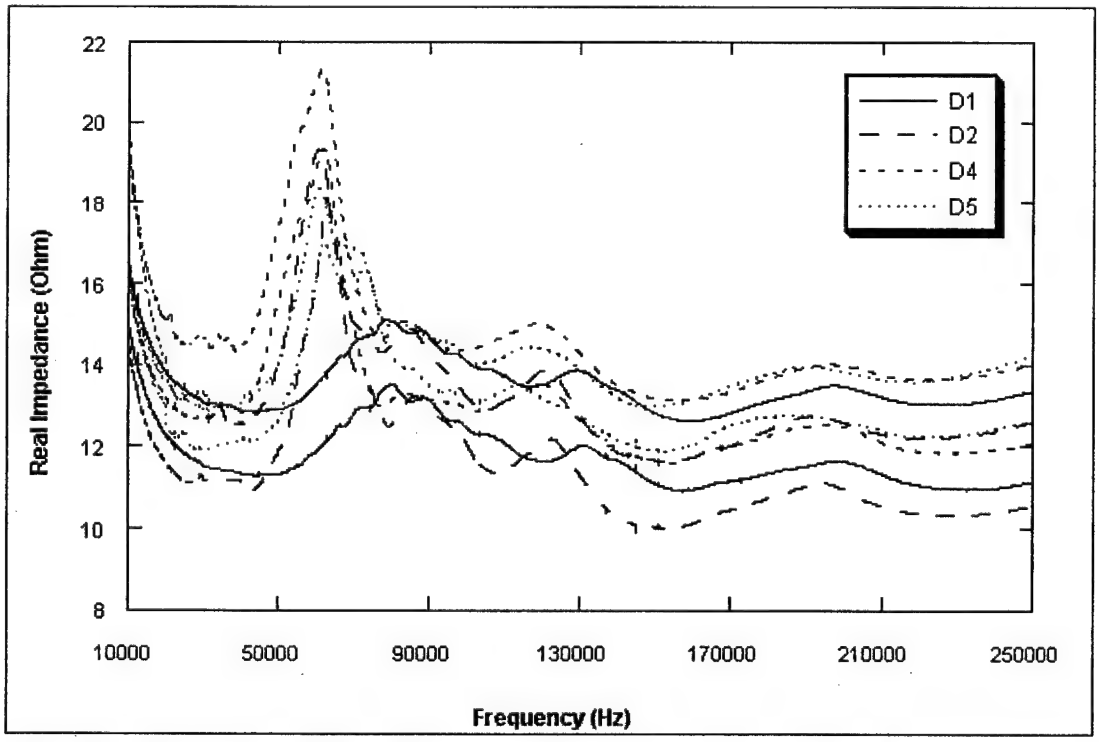


**Figure 55. Comparison the first and second real impedance measurements of sensor group D.**

In the comparison graphs, a common feature for most sensors is the presence of a global vertical shift between the first and second real impedance measurements. This global vertical shift is not an indication of damage; it is attributable to factors other than structural damage, such as temperature/moisture effects and loading. The presence of damage in the structure would be indicated by local variations (i.e., not global shifts) in the real impedance graphs. Thus, the global vertical shift between the first and second measurements can be removed with a correction factor that will shift uniformly the second measurements over the frequency range. This procedure promotes a more meaningful analysis of impedance measurements over time by filtering out the global shifts and focusing on the local variations. The comparison of the first and corrected second impedance measurements for sensor groups A, B, C, and D are shown in Figure 56 – Figure 59, respectively.

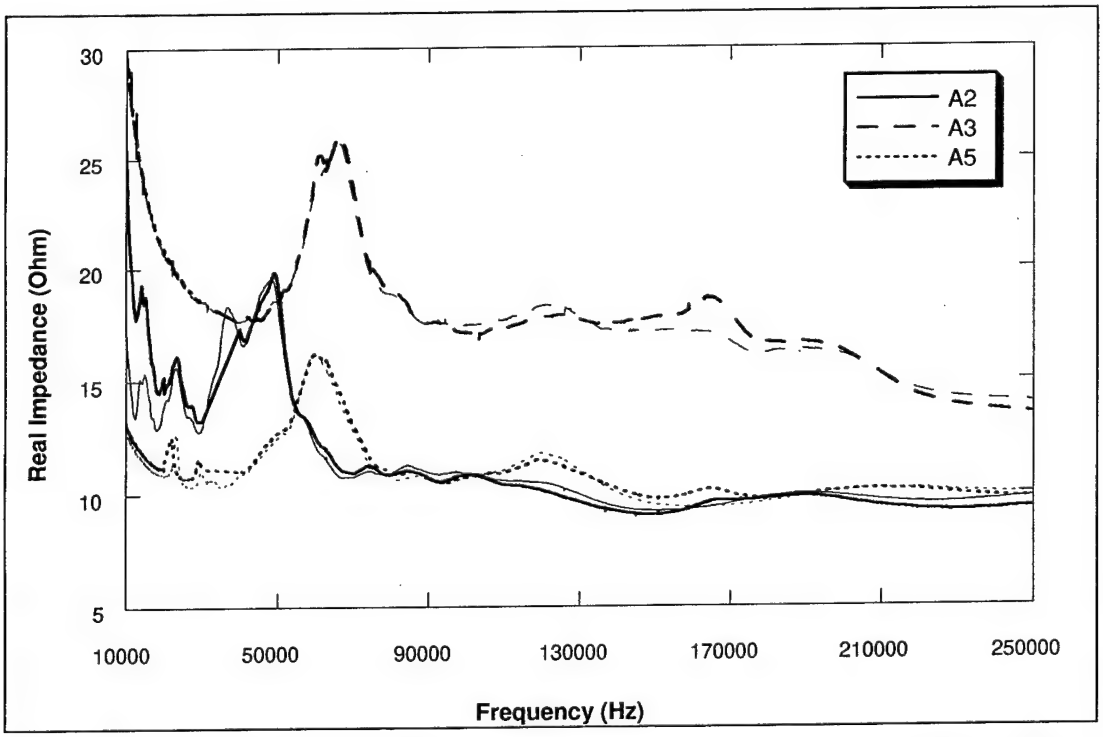


**Figure 56. Comparison the first and corrected second real impedance measurements of sensor group A.**

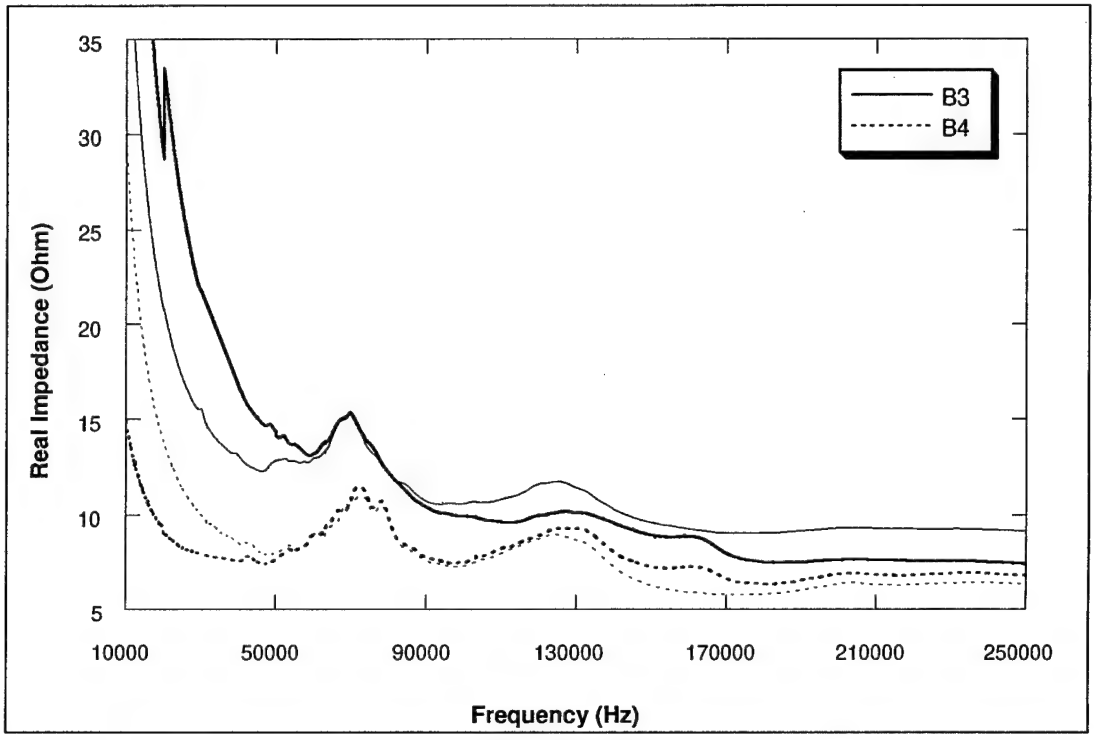


**Figure 57. Comparison the first and corrected second real impedance measurements of sensor group B.**

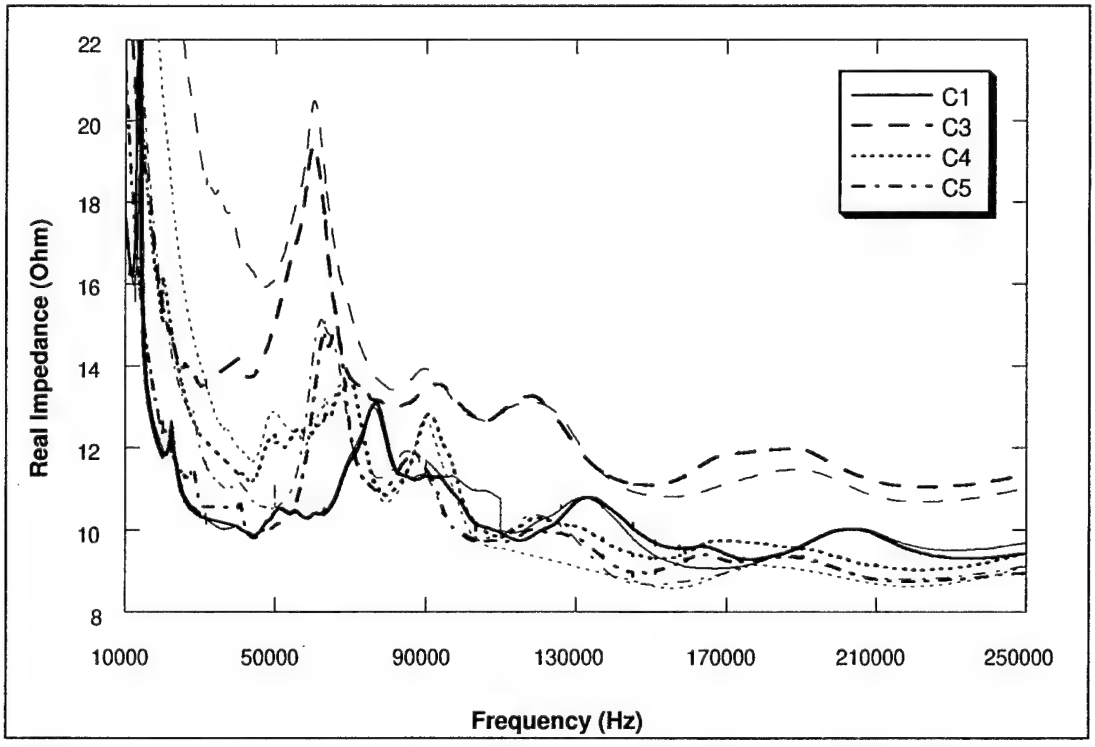


**Figure 58. Comparison the first and corrected second real impedance measurements of sensor group C.**

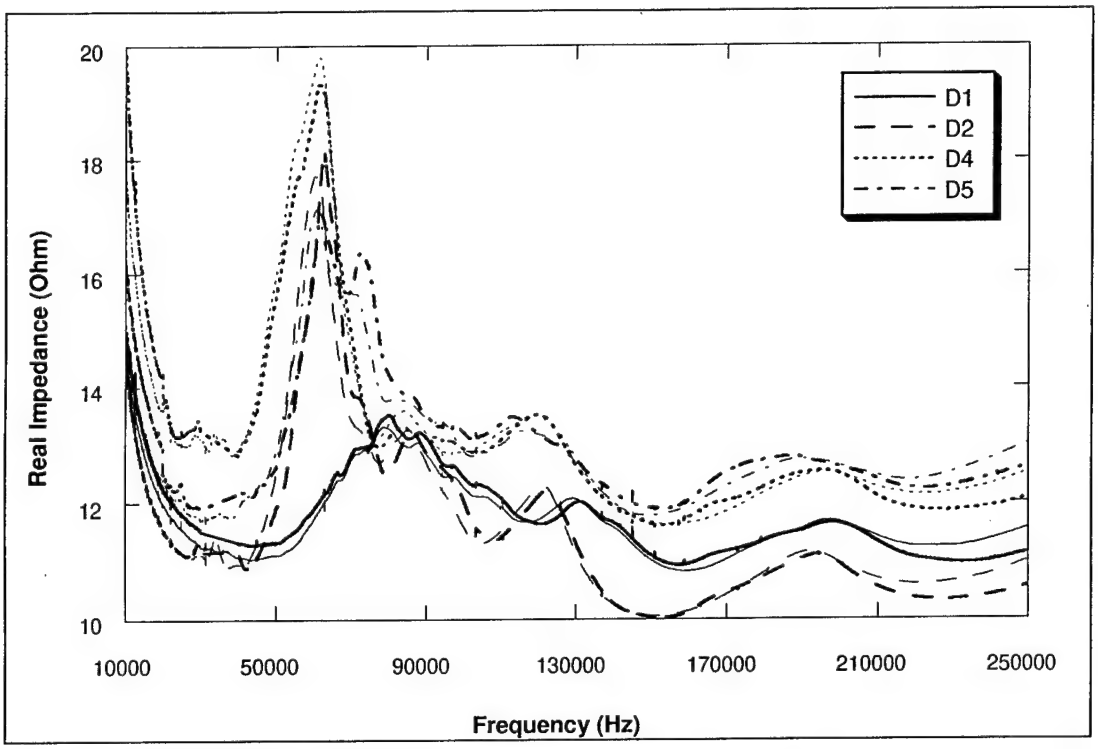


**Figure 59. Comparison the first and corrected second real impedance measurements of sensor group D.**

The analysis of the corrected graphs shows only small variations between the first and second impedance measurements. Even though these variations are evident, none of the sensors showed new peaks or valleys in the impedance graphs. The presence of damage is most often associated not with local variations of the type shown in the comparison graphs but rather with *new* peaks and valleys in real impedance, which signify a significant change in structural impedance. Thus, since there were no significant new peaks or valleys in the second set of real impedance measurements, it can be concluded that no damage had occurred in the composite reinforcement.

# 6 Conclusions and Recommendations

## Conclusions

A practical real-time, impedance-based structural integrity monitoring technology using piezoelectric patch sensors has been developed, tested, and demonstrated. The technology includes a set of damage metrics that simplify the interpretation of raw structural integrity data collected by the system. The series of studies reported here focused on the detection of debonding and delamination in structures reinforced with fiber-reinforced composite materials, but the monitoring technique may be applicable to many kinds of materials systems. Additionally, because the technique is not based on any model it can readily be applied to complex structures.

### *The Preliminary Experiments*

Based on the results of the developmental studies (see Chapter 3), it is concluded that:

- The actuator/sensors are small, light, and can be installed nondestructively.
- The structural monitoring technique is unaffected by changes in boundary conditions, loading, or operational vibration.
- The actuator/sensors are sensitive only within a 1 or 2 ft radius of the sensor, and this limitation enables the monitoring technique to pinpoint the location of damage on large or complex structures.
- The use of high frequencies for structural interrogation enables the detection of imminent damage or minor changes in structural integrity, such as loose bolts in a bridge joint and the debonding of composite reinforcement material from a structural element.
- A high-quality bond between the PE sensor and the target surface — a composite reinforcement fabric, in the current studies — is essential to ensure proper electromechanical coupling between the sensor and the structure.

### *The Wall-Loading Tests*

Based on the results of structural loading studies in the laboratory (see Chapter 4), it is concluded that:

- Data collected from the PE sensors was generally indicative of damage when it occurred.
- The technology can reliably detect imminent damage.

Twice during the testing a PE sensor picked up damage to the structure while the load was being increased, and the data were reported before a crack became visible. In these cases the damage metric chart on the computer screen clearly indicated that debonding had occurred and, therefore, that cracking was imminent. In both cases a crack appeared seconds after the damage report. This is ample proof that if the load were increased in smaller steps (as would probably happen in real life applications) this technology would be very successful in picking up debonding between the composite material and the concrete surface, well in advance of cracks appearing in the wall.

In these tests the technology's ability to predict damage before it was physically visible was limited by two factors. First, the loading was carried out in discrete, relatively large increments. Since sensor measurements were taken at the conclusion of each loading step, damage that occurred during the load increase often would not be registered by the data acquisition system until after the crack had already appeared. Second, the time required by the data acquisition system to obtain a set of readings from all PE sensors was longer than the time needed to increase the load from one step to the next. In effect, then, there was a data processing bottleneck that interfered with real-time data reporting. It is believed that this bottleneck would vanish in real-world applications because (1) structures are generally subject to smaller loading increments over time and (2) structural damage usually develops and manifests itself over much longer time frames than were available for these experiments.

### *The Norfolk Pier Demonstration*

Based on results from the Norfolk Pier 11 demonstration that are available to date, it is concluded that:

- The installation procedures and bonding methods used in the demonstration were appropriate for the application and feasible for real-world use.
- The structural monitoring sensors and wiring generally performed as intended.
- Onsite impedance measurements were successfully taken and processed on two separate occasions.

A comparison of the two data sets indicated that, after correction factors were applied for differences in ambient conditions, there was virtually a perfect cor-

relation between impedance curves over time. Therefore, the demonstration structural monitoring system indicates that there has been no degradation in the pier's composite reinforcement to date.

## Recommendations

One recommendation arising from this work was that the damage metric algorithm be modified to account for changes in load, temperature, and other environmental stresses. This work is currently being accomplished, and the results will be published in a follow-up report.

It is also recommended that:

- PE sensors should be applied to critical locations in structures using FRP composite upgrades where debonding of the FRP composite from the substrate is of great concern.
- PE sensors should be applied to structures using FRP composite upgrades where the upgrades are not easily accessible for visual inspection and where nondestructive evaluation techniques are preferred.
- At this time, PE sensors should be applied only in structures that are subjected to constant loads and temperatures for a long enough time to allow impedance data to be collected at constant load and temperature.

# 7 References

## Cited

Crawley, E.F. and E.H. Anderson, "Detailed Models of Piezoceramic Actuation of Beams," *Journal of Intelligent Material Systems and Structures*, vol 1, no. 1 (January 1990).

GangaRao, Hota V.S., S.V. Kumar, H.K. Thippeswamy, and J.C. Trovillion, "Connection of a Jointless Bridge with FRP Bars in Concrete Deck," *International Conference on Fiber Reinforced Structural Plastics in Civil Engineering*, December 1995, Madras, India.

Hewlett Packard, *Operation and Service Manual, Model 4192A LF Impedance Analyzer*, Manual part number 04192-90001 (Yokogawa-Hewlett-Packard, LTD., 1983).

Lampo, R.G., A. Maher, J.P. Busel, and R. Odello, "Design and Development of FRP Composite Piling Systems," *Proceedings of International Composites Exposition and Symposium*, January 1997, Nashville, TN.

Lampo, R.G., T. Nosker, P.K. Dutta, and R. Odello, "FRP Composite Piling Systems for Waterfront Applications," *Proceedings of American Society of Civil Engineers, Ports '98*, March 1998, Long Beach, CA.

Liang, C., F.P. Sun and C.A. Rogers, "An Impedance Method for Dynamic Analysis of Active Materials Systems," *Proceedings of the 34th Structures, Structural Dynamics and Materials Conference* (American Institute of Aeronautics and Astronautics [AIAA], April 1993).

Marshall, O.S., Jr., S.C. Sweeney, and J.C. Trovillion. 1998. "Seismic Rehabilitation of Unreinforced Masonry Walls," *Proceedings of the 1998 ACI Fall Convention*, October 1998, Los Angeles, CA.

Quattrone, R., J.B. Berman and J. Kamphaus., "Upgrade and Monitoring of Unreinforced Masonry Structures using Fiber Reinforced Polymers," *Proceedings of the 1998 Composites Expo* (Composites Institute [CI], January 1998), pp 13C1-13C7.

Quattrone, R., J.B. Berman and S.R. White,. "Self-Monitoring Structures Containing Magnetostrictive Composites," *Proceedings from the 21st Army Science Conference*, June 1998, Norfolk, VA, pp 21-26.

Raju, V., "Implementing Impedance-Based Health Monitoring," Masters Thesis in Mechanical Engineering (Virginia Polytechnic Institute and State University [VPISU], November 1997).

"Summary of Findings," *Inland Navigation and Flood Damage Reduction CW/R&D Vision Workshop* (Pentagon City, VA, 6-7 May 1996), pp 2-1.

"Summary of Findings," *Coastal Navigation and Storm Damage Reduction R&D Vision Workshop*, (Dallas, TX, 12 April 1996), pp 1-4.

Sun, F.P., Z. Chaudhry, C. Liang and C.A. Rogers, "Truss Structure Integrity Identification Using PE sensor Sensor-Actuator," *Proceedings of the 2nd International Conference on Intelligent Materials* (International Society for Optical Engineering [SPIE], June 1994), pp 1210-1222.

## Uncited

Chaudhry, Z., F.P. Sun, and C.A. Rogers, "Health Monitoring of Space Structures Using Impedance Measurements," *Proceedings of the 5th International Conference on Adaptive Structures* (International Society for Optical Engineering [SPIE], 1994).

Chaudhry, Z., T. Joseph, F.P. Sun and C.A. Rogers, "Local-area Health Monitoring of Aircraft via Piezoelectric Actuator/Sensor Patches," *Proceedings of the 1995 SPIE Conference on Smart Structures and Materials* (International Society for Optical Engineering [SPIE], February 1995).

Chaudhry, Z., F. Lalande, A. Ganino and C.A. Rogers, "Monitoring the Integrity of Composite Patch Structural Repair via Piezoelectric Actuators/Sensors," *Proceedings of the 36th Structures, Structural Dynamics and Materials Conference* (American Institute of Aeronautics and Astronautics [AIAA], 1995).

Esteban, J., F. Lalande and C.A. Rogers, "A Theoretical Modeling of Wave Localization Due to Material Damping," *Proceedings of the 1996 SPIE Conference on Smart Structures and Materials* (International Society for Optical Engineering [SPIE], February 1996).

Giurgiutiu, V., and C.A. Rogers., "Recent Advancements in the Electro-Mechanical (E/M) Impedance Method for Structural Health Monitoring and NDE," *Proceedings of the 1998 SPIE Conference on Smart Structures and Materials* (International Society for Optical Engineering [SPIE], March 1998).

Krishnamurthy, K., F. Lalande and C.A. Rogers, "Effects of Temperature on the Electrical Impedance of Piezoelectric Sensors," *Proceedings of the 1996 SPIE Conference on Smart Structures and Materials* (International Society for Optical Engineering [SPIE], February 1996).

Liang, C., F. P. Sun and C.A. Rogers, "Dynamic Output Characteristics of Piezoelectric Actuators," *Proceedings of the 1993 SPIE Conference on Smart Structures and Materials* (International Society for Optical Engineering [SPIE], February 1993).

Pardo de Vera, C., and J.A. Guemes., "Embedded Self-Sensing Piezoelectrics for Damage Detection," *Proceedings of the International Workshop on Structural Health Monitoring,* (September 1997), pp 445-455.

Rogers, C.A., and F. Lalande, "Solid-State Active Sensing for In-Situ Health Monitoring," *Proceedings Society for Machine Failure Prevention Technology*, 1996).

Sun, F.P., C. Liang and C.A. Rogers, "Experimental Modal Testing using Piezoceramic Patches as Collocated Sensor-Actuators," *Proceedings of the SEM Spring Conference and Exhibits* (Society for Experimental Mechanics [SEM], 1994).

Sun, F.P., Z. Chaudhry, C.A. Rogers and M. Majmundar, "Automated Real-time Structural Health Monitoring via Signature Pattern Recognition," *Proceedings of the 1995 SPIE Conference on Smart Structures and Materials* (International Society for Optical Engineering [SPIE], February 1995).

Woon, C.E., and L.D. Mitchell, "Variations in Structural Dynamic Characteristics Caused by Changes in Ambient Temperature: I. Experimental," *Proceedings of the 14th International Modal Analysis Conference* (Society for Experimental Mechanics [SEM], February 1996).

Woon, C.E., and L.D. Mitchell, "Variations in Structural Dynamic Characteristics Caused by Changes in Ambient Temperature: II. Analytical," *Proceedings of the 14th International Modal Analysis Conference* (Society for Experimental Mechanics [SEM], February 1996).

Zhou, S.W., and C.A. Rogers, "Temperature Rise and Thermal Stress of Piezoelectric Elements in Active Structures," *Proceedings of the International Mechanical Engineering Congress and Exposition* (American Society of Mechanical Engineers [ASME], November 1994).

# CERL DISTRIBUTION

Chief of Engineers
ATTN: CEHEC-IM-LH (2)
ATTN: CEHEC-IM-LP (2)
ATTN: CECC-R
ATTN: CERD-L
ATTN: CERD-M
ATTN: CEMP-ED

Defense Tech Info Center 22304
ATTN: DTIC-O (2)

10
11/98

☆U.S. GOVERNMENT PRINTING OFFICE: 1999 - 746-070/80070

# REPORT DOCUMENTATION PAGE

Form Approved
OMB No. 0704-0188



| 1. AGENCY USE ONLY (Leave Blank) | 2. REPORT DATE | 3. REPORT TYPE AND DATES COVERED |
|---|---|---|
| | August 1999 | Final |

**4. TITLE AND SUBTITLE**
Piezoelectric Patch Sensors for Structural Integrity Monitoring of Composite-Upgraded Masonry and Concrete Structures

**5. FUNDING NUMBERS**
62784
AT41
FM-CM9

**6. AUTHOR(S)**
J. Berman, R. Quattrone, A. Averbuch, F. Lalande, H. Cudney, V. Raju, and G.L. Cohen

**7. PERFORMING ORGANIZATION NAME(S) AND ADDRESS(ES)**
U.S. Army Construction Engineering Research Laboratory (CERL)
P.O. Box 9005
Champaign, IL 61826-9005

**8. PEFORMING ORGANIZATION REPORT NUMBER**
TR 99/72

**9. SPONSORING / MONITORING AGENCY NAME(S) AND ADDRESS(ES)**
Headquarters, U.S. Army Corps of Enginers
20 Massachusetts Avenue NW
Washington, DC 20314-1000

**10. SPONSORING / MONITORING AGENCY REPORT NUMBER**

**9. SUPPLEMENTARY NOTES**
Copies are available from the National Technical Information Service, 5385 Port Royal Road, Springfield, VA 22161

**12a. DISTRIBUTION / AVAILABILITY STATEMENT**
Approved for public release; distribution is unlimited.

**12b. DISTRIBUTION CODE**

**13. ABSTRACT** *(Maximum 200 words)*

An acoustical impedance-based structural integrity monitoring technique employing piezoelectric (PE) patch sensor/actuators was used to detect real-time damage introduced to composite-upgraded wall test specimens. Concrete and brick masonry wall sections externally upgraded with fiber-reinforced polymer (FRP) composite materials were subjected to various stresses in a load test machine. During the tests, the wall sections were periodically interrogated via the PE sensor/actuators and electrical impedance measurements were made at various frequencies. When damage was present, the impedance vs frequency signature changed. Furthermore, there was a marked difference between the signature pattern for loading and for debonding of the composite upgrade or cracking of the concrete/masonry substrate.

This report includes details on the development of the impedance-based technique and documents a demonstration of the technology on a composite-upgraded pier at Norfolk, VA.

**14. SUBJECT TERMS**
concrete
composite materials
piezoelectric (PE)
fiber-reinforced polymer (FRP)
masonry

**15. NUMBER OF PAGES**
80

**16. PRICE CODE**

| 17. SECURITY CLASSIFICATION OF REPORT | 18. SECURITY CLASSIFICATION OF THIS PAGE | 19. SECURITY CLASSIFICATION OF ASTRACT | 20. LIMITATION OF ABSTRACT |
|---|---|---|---|
| Unclassified | Unclassified | Unclassified | SAR |